Géomorphologie : relief, processus, environnement

vol. 32 - n° 1 | 2026
torrents et torrentialités n°2

When geomorphological field data and systemic analysis help refine the uncertainties of numerical hydrometeorological models in extreme values. Case study: The catastrophic flood event of October 14-15, 2018, in the Aude watershed (southern France)

Quand les données de terrain géomorphologiques et l'analyse systémique permettent d'affiner les incertitudes des modèles hydrométéorologiques numériques dans les valeurs extrêmes. Étude de cas : la crue catastrophique des 14-15 octobre 2018 dans le bassin de l'Aude (France du Sud)

Gilles Arnaud-Fassetta, Mathieu Brun, Mathieu Dupuis, Typhaine Bellon, Léa Perrine, Guillaume Brousse and Monique Fort

Electronic version
URL: https://journals.openedition.org/geomorphologie/21382
DOI: 10.4000/15rpd
ISSN: 1957-777X

Publisher
Groupe français de géomorphologie

Printed version
Date of publication: July 1, 2026
ISSN: 1266-5304

Provided by Université Paris Cité

Electronic reference
Gilles Arnaud-Fassetta, Mathieu Brun, Mathieu Dupuis, Typhaine Bellon, Léa Perrine, Guillaume Brousse and Monique Fort, "When geomorphological field data and systemic analysis help refine the uncertainties of numerical hydrometeorological models in extreme values. Case study: The catastrophic flood event of October 14-15, 2018, in the Aude watershed (southern France) ", *Géomorphologie : relief, processus, environnement* [Online], vol. 32 - n° 1 | 2026, Online since 27 February 2026, connection on 03 March 2026. URL: http://journals.openedition.org/geomorphologie/21382 ; DOI: https://doi.org/10.4000/15rpd

revue en ligne : https://journals.openedition.org/geomorphologie/

Géomorphologie : Relief, Processus, Environnement

vol. 32, n° 1 (2026), p. 41-74
Mise en ligne le 26 février 2026 sur journals.openedition.org
http://journals.openedition.org/geomorphologie/21382
https://doi.org/10.4000/15rpd

https://gfg.cnrs.fr/

When geomorphological field data and systemic analysis help refine the uncertainties of numerical hydrometeorological models in extreme values. Case study: The catastrophic flood event of October 14-15, 2018, in the Aude watershed (southern France)

Quand les données de terrain géomorphologiques et l'analyse systémique permettent d'affiner les incertitudes des modèles hydrométéorologiques numériques dans les valeurs extrêmes. Étude de cas : la crue catastrophique des 14-15 octobre 2018 dans le bassin de l'Aude (France du Sud)

Gilles Arnaud-Fassetta [a*], Mathieu Brun [a], Mathieu Dupuis [b], Typhaine Bellon [a], Léa Perrine [a], Guillaume Brousse [a], Monique Fort [a]

[a] UMR 8586 PRODIG, Université Paris Cité, 8, rue Albert Einstein, 75013 Paris, France.
[b] Syndicat mixte des milieux aquatiques et des rivières (SMMAR), Av. Claude Bernard, 11000 Carcassonne, France.

ABSTRACT

A detailed systemic analysis of the hydrometeorological event of Oct. 14-15, 2018, made it possible to identify, for the first time, all the predisposing, triggering, and aggravating/mitigating factors that explain the genesis, impacts, and management of the event in the Aude watershed. Attention then focused on one of the parts of the watershed that received the highest cumulative rainfall, namely the Rieu Sec watershed, a right-bank tributary of the Orbiel River in the Minervois. It has been shown that the Oct. 2018 event was extraordinary in several respects (meteorology; hydrology; geomorphology; sediment budget; specific degradation rate; impact on riparian vegetation; recurrence interval estimated at 204-378 yrs). A model of small, mountainous watersheds (< 40 km²) functioning is proposed, in which high-magnitude/low-frequency flood events play a key role. The significant variability in precipitation observed from one sub-watershed to another complicates the management of rainfall and floods. The challenge for the future lies in improving flood forecasting, and the effective dissemination of these forecasts.

Keywords: Mediterranean, Aude watershed, extreme flash flood, systemic analysis, sediment budget, radiocarbon dating, riparian forest.

RÉSUMÉ

L'analyse systémique fine de l'événement hydrométéorologique des 14-15 octobre 2018 a permis d'identifier, pour la première fois, tous les facteurs de prédisposition, de déclenchement et d'aggravation/atténuation qui expliquent la genèse, les impacts et la gestion de l'événement dans le bassin-versant de l'Aude. L'attention s'est ensuite concentrée sur l'une des parties du bassin-versant qui a reçu les plus forts cumuls de précipitations, à savoir le bassin-versant du Rieu Sec, un affluent de rive droite de l'Orbiel dans le Minervois. Il est démontré que l'événement d'octobre 2018 a été extraordinaire à plusieurs égards (météorologie ; hydrologie ; géomorphologie ; budget sédimentaire ; taux de dégradation spécifique ; impact sur la ripisylve ; intervalle de récurrence estimé à 204-378 ans). Un modèle de fonctionnement des petits bassins-versants montagnards (< 40 km²) est proposé dans lequel les événements de crue de haute magnitude/basse fréquence jouent un rôle clé. La variabilité significative des précipitations observées d'un sous-bassin-versant à l'autre complexifie la gestion des pluies et des crues. Le défi pour l'avenir réside dans l'amélioration des prévisions d'inondation et la diffusion effective de ces prévisions.

Mots-clés : *Méditerranée, bassin-versant de l'Aude, crue-éclair extrême, analyse systémique, budget sédimentaire, datation radiocarbone, ripisylve.*

ARTICLE INFORMATION
Received March 3, 2025.
Accepted February 9, 2026.

*Corresponding author.
ORCID: 0000-0001-9238-0773
E-mail adresses:
gilles.arnaud-fassetta@u-paris.fr
mathieu.brun31@gmail.com
mathieu.dupuis@smmar.fr
bellon.typhaine@gmail.com
leaperrine@bbox.fr
guillaume.brousse@edf.fr
fort.monique@gmail.com

1. Introduction

Each year, an average of 3 to 6 heavy-precipitation events (HPEs) occur around the Mediterranean Sea, with a higher concentration in the northwestern region. These HPEs, which are typically defined as events with daily rainfall exceeding 150 mm (Ricard et al., 2012), often lead to flash floods and significant geomorphological and societal impacts (*e.g.*, Tricart, 1958; Stuckmann, 1970; Guigo, 1973; Chardon, 1990; Pech, 1990; Arnaud-Fassetta et al., 1993; Soutadé, 1993; Lajournade et al., 1998; Arnaud-Fassetta et al., 2002; Menad et al., 2012; Rinaldi et al., 2016; Lorenzo-Lacruz et al., 2019; Liébault et al., 2024; Normand and Heggy, 2024). The significant rainfall observed over durations ranging from a few hours to several days during these HPEs is due to intense convection concentrated in specific areas. The development of powerful convective systems,

such as Mediterranean HPEs, is facilitated by three factors: (*i*) The orographic effect, which causes rising air masses; (*ii*) Thermal energy accumulated over the summer; and (*iii*) The presence of a cut-off low, an isolated mass of cold air at high altitude that separates from the main jet stream and remains stationary over a region for several days. This phenomenon acts as a catalyst for HPEs, increasing atmospheric instability and amplifying rainfall. Mediterranean HPEs #9, #15, #29, #34, #40, #43, #50, and #51 (fig. 1) are examples of disasters associated with a synoptic cut-off low. Forecasting these Mediterranean HPEs is challenging. Currently, fine-scale weather forecasting systems like MétéoFrance's AROME model can only predict their onset at best 2 or 3 days in advance. In reality, the 'correct' scenario often emerges from the model just a few hours before the phenomenon begins (Kreitz et al., 2020). Figure 1 highlights the most notable HPEs (and the floods induced by these events), which have predominantly occurred in autumn (89 % of cases) over the last 150 yrs. Southern France is particularly impacted by Mediterranean HPEs and flash floods, both in terms of the number of deaths and the number of occurrences. In the Aude department, the most recent HPE occurred on Oct. 14-15, 2018, resulting in 15 deaths, and is the focus of this paper.

The Mediterranean HPEs currently present several challenges for the scientific community.

(*i*) Establishing correlations between the magnitude and frequency of events. Rainfall intensity is measured by the amount of precipitation in millimeters per unit of time (fig. 1B). The recurrence interval (RI) of rainfall is a statistical probability that tends to become imprecise when assessing the extreme values of exceptional events, primarily due to the limited historical data available.

(*ii*) Comparing probabilistic models with real-world observations. A flood event can be analyzed through the lens of hydro-meteorology and/or geomorphology. Hydro-meteorological models that provide return frequencies are essentially probabilistic models. In contrast, field data, such as hydrogeomorphology and chrono-stratigraphy, provide concrete descriptions of the impact of floods at specific points within a watershed (WS) at particular times. This field data is instrumental in capturing the complexity of geomorphological systems and the non-linearity of processes through the concept of 'critical thresholds' (Tricart, 1962; Schumm, 1973; fig. 2). For example, G. Arnaud-Fassetta (1997) shows that in the Rhône delta, the channel of the Petit Rhône R. aggraded after the Oct. 1993 flood event (RI. 30 yrs), whereas the floods of Jan. and Nov. 1994, despite being in the same RI range (70 yrs and 20 yrs, respectively), were erosive. In the Upper Guil valley (French southern Alps), G. Arnaud-Fassetta et al. (2005) demonstrate that the Jun. 2000 flood (RI. 30 yrs) may have had more significant local impacts in the valley floor compared to those highlighted in Jun. 1957 (RI > 100 yrs), linked to the destabilization of slopes in 1957, and the subsequent channelization of the Guil R., which amplified the specific stream power at certain sectors of the floodplain. This concept of 'critical thresholds' clearly indicates that the magnitude of flood events and their impacts on the valley floor do not follow a linear function. The morphological impacts of flood events in riverbeds do not simply increase proportionally with the rise in discharge and specific stream power. Instead, flood impacts, such as bed aggradation or incision, bed widening or contraction, changes in energy gradient, sediment storage or removal in the valley floor, and varying levels of driftwood production, respond to instability threshold effects influenced by the boundary conditions of the WS and the impact of human activities (Chorley, 1969; Brierley and Fryirs, 2005). In the Aude department, the flood event that occurred on Oct. 14-15, 2018, had varied hydro-bio-morphological impacts depending on the WS. This suggests that a HPE predicted by numerical models may have had only minor local effects, while extreme rainfall cells in certain areas might have gone undetected by radar due to the grid's coarse resolution (Calvet and Lemartinel, 2002).

(*iii*) Going beyond current hydro-meteorological uncertainties. Following the hydro-meteorological event that occurred in the Aude department on Oct. 14-15, 2018, studies have failed to reach a consensus on the event's RI, with estimates varying significantly depending on the authors. In order of publication, H. Ayphassorho (2019) first suggested that the available observations for the Oct. 14-15, 2018, event in the Aude department are insufficient for accurately determining the rainfall RI. The authors speculate, without supporting evidence, that the rainfall RI could be on the order of 200 yrs or more, highlighting a limitation of meteorological models. They also discuss flood RIs in the Clamoux, Orbiel, Lauquet, and Sals WSs, which correspond to exceptional frequencies estimated between 1/100 and 1/250 yrs. The margin of uncertainty in hydrological models appears to be quite high. Subsequently, M. Kreitz et al. (2020) concluded that the RI of rainfall over 6 h on Oct. 14-15, 2018, is of a centennial order in the Middle Aude WS, where the observed rainfall intensities are comparable to the historic event of 1891 and significantly higher than the Nov. 1999 event. They further note that if intraday data were available for the Conques-sur-Orbiel or Cuxac-Cabardès stations, the 100-yr RI would likely be exceeded. Unfortunately, this cannot be demonstrated, as such meteorological data do not exist. Moreover, S. Benaksas and G. Piton (2023) estimate that the extreme flood of Oct. 14-15, 2018, in the Rieu Sec WS (the study area) may have reached a peak flow (245-251 m^3/s) exceeding the two-millennial flow, estimated at 124 m^3/s by the SHYREG method (Arnaud et al., 2014). Finally, the DDTM (2024) employs the 'Aude method' (Lang et al., 2014) to calculate a peak flow of 350 m^3/s, which was observed at the Rieu Sec brook on Oct. 14-15, 2018. This peak flow is 1.32 times higher than the estimated centennial discharge of 265 m^3/s. As a result, the literature presents highly variable estimates of rainfall and flash-flood return frequencies for Oct. 14-15, 2018, in the Aude department, ranging from 100 yrs to 2000 yrs. This paper will demonstrate, using geomorphological and stratigraphic data, that the hydro-meteorological event on Oct. 14-15, 2018, in the Aude WS has a local RI exceeding 204-378 yrs. Beyond that, the aim of the article is to provide a feedback on what happened in the Aude WS on Oct. 14-15, 2018, using a systemic approach, to quantify the impacts of the flood by set up a sediment budget, and to highlight the role of riparian vegetation and uprooted trees in controlling river flows in the floodplain.

2. Study area

The Aude River (Strahler order. 7) is 225.6 km long, originating in the Carlit massif at an altitude of 2172 m, and it flows into the Mediterranean Sea through the Grau de Vendres (fig. 3). Its riverbed, which has an average width at bankfull stage ranging

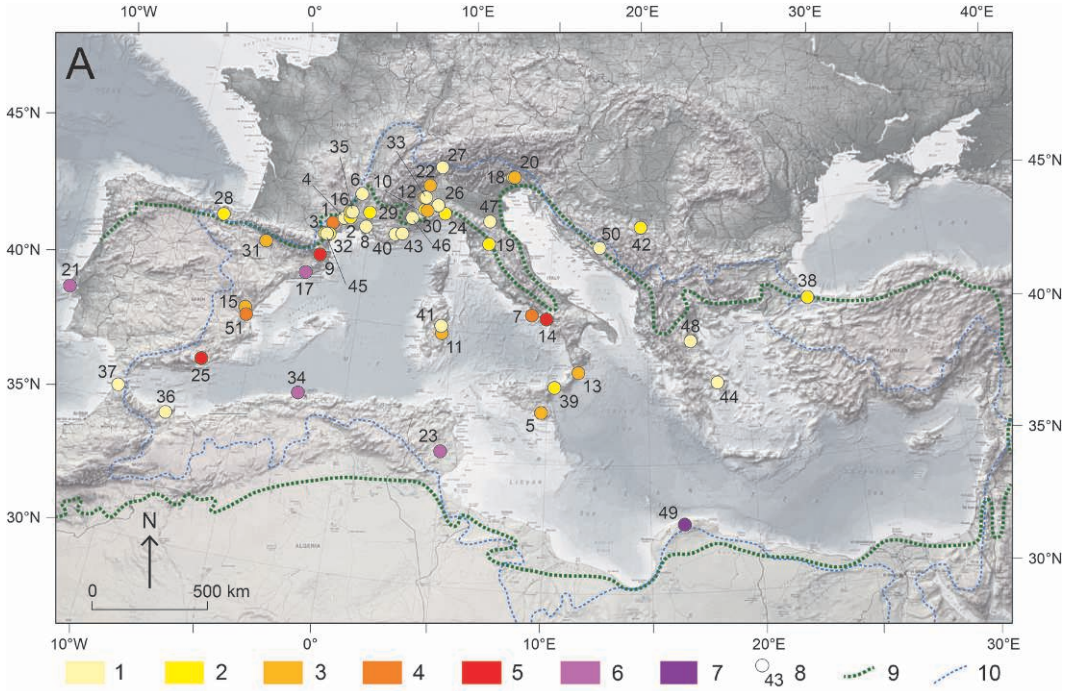

B

Event	Year	Month, day	Geographical location	Number of deaths (greater than or equal to 15)	Missing persons count	Maximum rainfall intensity (> 150 mm / 24 h)	Rain gauge station	Reference
# 51	2024	Oct., 29	Spain (Province of Valencia)	240		772 mm / 24 h	Turís	AEMET data
# 50	2024	Oct., 3-4	Bosnia-Herzegovina	27		250 mm / 12 h	Grude	Hadžić et al. (2022)
# 49	2023	Sept., 10	Libya	5898	8000	414 mm / 25 h	Al-Bayda	Normand & Heggy (2024)
# 48	2023	Sept., 3-8	Greece	17		762 mm / 24 h	Portaria	He et al. (2024)
# 47	2023	May, 17	Italy (Emilia-Romagna)	15		250 mm / 24 h	At the foot of the Apennines	Local media and internet data
# 46	2020	Oct., 2-3	France (Alpes-Maritimes department)	18		663 mm / 24 h	Les Mesches	Carrega & Michelot (2021)
# 45	2018	Oct., 14-15	France (Aude)	15		244 mm / 6 h	Trèbes	This paper
# 44	2017	Nov., 15	Grèce (Western Attica)	24		280 mm / 13 h	Mandra	Speis et al. (2019)
# 43	2015	Oct., 3	France (Côte d'Azur)	20		175 mm / 2 h	Cannes	MétéoFrance data
# 42	2014	May, 20	Bosnia-Herzegovina, Serbia, Croatia, Slovakia	60		205 mm / 24 h	Belgrade	Zorn & Zrc Sazu (2014)
# 41	2013	Nov., 18	Italy (Sardinia)	19		470 mm / 24 h	Monte Novo	Local media and internet data
# 40	2010	June, 15	France (Var department)	27		461 mm / 24 h	Lorgues	MétéoFrance data
# 39	2009	Oct., 1-2	Italy (Sicily, Province of Messina)	37		160 mm / 24 h	Fiumedinisi	Ortolano & Spizuoco (2009)
# 38	2009	Sept., 8-9	Turkey (Istambul)	32		253 mm / 24 h	Istambul	Local media and internet data
# 37	2008	Oct., 23-24	Morocco	28		176 mm / 6 h	Tangier	Local media and internet data
# 36	2003	Nov., 17-18	Morocco	16		150 mm / 24 h	Nador / Al Hoceima region	Local media and internet data
# 35	2002	Sept., 8-9	France (Gard department)	23		683 mm / 24 h	Anduze	MétéoFrance data
# 34	2001	Nov., 9-10	Algeria (Bab-el-Oued, Algiers)	781	115	262 mm / 24 h	Bouzaréah	Menad et al. (2012)
# 33	2000	Oct., 13-16	North-western Italy	23	11	216 mm / 24 h	Almese	Local media and internet data
# 32	1999	Nov., 12-13	France (Aude, Pyrénées-Orientales, Tarn and Hérault departments)	36		551 mm / 24 h	Lézignan-Corbières	Arnaud-Fassetta et al. (2002)
# 31	1996	August, 7	Spain (Biescas region)	87		160 mm / 2 h	Biescas	Lajournade et al. (1998)
# 30	1994	Nov., 4-6	Italy (Piemonte)	68		265 mm / 24 h	Levice	Luino (1999)
# 29	1992	Sept., 22	France (Ouvèze watershed)	47		300 mm / 6 h	Entrechaux	Arnaud-Fassetta et al. (1993)
# 28	1983	August, 26	Basque Country (Province of Bizkai)	41		500 mm / 24 h	Bilbao	Local media and internet data
# 27	1978	August, 7	Italy (Val d'Ossola)	19		265 mm / 24 h	Agarina	Pech (1990)
# 26	1977	Oct., 7-8	Italy (Piemonte and Valle d'Aosta)	15		480 mm / 12 h	Upper Orba valley	Local media and internet data
# 25	1973	Oct., 20	Spain (Andalusia)	300		600 mm / 24 h	Zurgena	Molina (1974)
# 24	1970	Oct., 7-8	Northern Italy (Genoa region)	35	8	749 mm / 24 h	Bolzaneto	Guigo (173)
# 23	1969	Sept., 26-28; Oct., 6-8, 22-29	Tunisia	542		800 mm / 1 h	Oued El Kebir	Stuckmann (1970)
# 22	1968	Nov., 2-3	Italy (Province of Biella)	72		395 mm / 24 h	Trivero	Cat Berro & Mercalli (2018)
# 21	1967	Nov., 25-26	Portugal	700		170 mm / 24 h	Oeiras, Sassoeiros	Amaral (1968)
# 20	1966	Nov., 4	Northeast Italy	87		376 mm / 24 h	Barcis	Malguzzi et al. (2006)
# 19	1966	Nov., 3-5	Italy (Tuscany)	47		339 mm / 24 h	Badia Agnano	Malguzzi et al. (2006)
# 18	1965	Sept., 2	Northern Italy	55		414 mm / 24 h	Barcis	Pacini (2023)
# 17	1962	Sept., 25	Spain (Catalonia, Riera de les Arenes)	815		212 mm / 3 h	Terrassa	Llasat (2004)
# 16	1958	Sept., 29-30	France (Gard department)	35		279 mm / 8 h	Saint-Jean-du-Gard	Pardé (1963)
# 15	1957	Oct., 13-14	Spain (Valencia, Turia River)	82		361 mm / 24 h	Bejís	Local media and internet data
# 14	1954	Oct., 25-26	Italy (Amalfi Coast)	318	250	500 mm / 24 h	Salerno	Local media and internet data
# 13	1953	Oct., 21-22	Italy (Calabria)	101		362 mm / 24 h	Badolato	Caloiero & Mercury (1980)
# 12	1951	Nov., 7-14	Italy (Polesine)	100		280 mm / 12 h	Turin	Valle (1953)
# 11	1951	Oct., 14-19	Italy (Calabria, Sardinia)	68		544 mm / 24 h	Sicca d'Erba	Pinna & Grava (2016)
# 10	1948	Sept., 4	Italy (Piemonte)	49		164 mm / 6 h	Verduno	Regione Piemonte (1994)
# 9	1940	Oct., 16-20	France, Spain ("Aiguat" event)	350		1000 mm / 24 h	Saint-Laurent-de-Cerdans	Pardé (1941)
# 8	1933	Sept., 24-30	France (Bouches-du-Rhône, Vaucluse and Hérault departments)	15		305 mm / 24 h	Entressen (Istres)	Pardé (1934)
# 7	1910	Oct., 24	Italy (Campania)	200		250 mm / 4 h	Ischia	Rosso (2017)
# 6	1907	From Sept., 12 to Nov., 12	South of France	25	Many missing people	519 mm / 24 h	Privas	MétéoFrance data
# 5	1902	Sept., 26	Italy (Sicily)	112		250 mm / 24 h	Modica	Modica Scala (1969)
# 4	1900	Sept., 28-29	France (Cévennes massif)	20		950 mm / 10 h	Valleraugue	Pardé (1941)
# 3	1891	Oct., 24-25	France (Aude and Pyrénées-Orientales departments)	34		281 mm / 20 h	Carcassonne	MétéoFrance data
# 2	1890	Sept., 19-23	France (Languedoc-Roussillon and Rhône-Alpes regions)	50		390 mm / 24 h	Saint-Jean-du-Gard	MétéoFrance data
# 1	1875	Sept., 12	France (Cévennes massif, upper Tarn watershed)	139		400 mm / 6 h	Vernazobres watershed	Antoine et al. (2001)

Fig. 1 – Non-exhaustive mapping of major hydro-meteorological events (rainfall intensity > 150 mm/24 h; at least 15 fatalities) regarding the "Mediterranean" type events that have occurred over the last 150 years in the Mediterranean basin (A), and characteristics of these events (B).

1. 15-30 fatalities; 2. 31-60 fatalities; 3. 61-120 fatalities; 4. 121-240 fatalities; 5. 241-480 fatalities; 6. 481-960 fatalities; 7. More than 960 fatalities; 8. Hydro-meteorological event (numbered in chronological order, see fig. 1B) – The Libyan disaster of 2023 was primarily technological (failure of two dams) rather than natural (Storm Daniel); 9. Bioclimatic boundary of the Mediterranean basin; 10. Hydrographic boundary of the Mediterranean basin.

Fig. 1 – Cartographie non exhaustive des événements hydrométéorologiques majeurs (intensité de pluie > 150 mm/24 h ; au moins 15 morts) de type « méditerranéen » survenus depuis 150 ans sur le pourtour du bassin méditerranéen (A) et caractéristiques de ces événements.

1. 15-30 morts ; 2. 31-60 morts ; 3. 61-120 morts ; 4. 121-240 morts ; 5. 241-480 morts ; 6. 481-960 morts ; 7. > 960 morts ; 8. Événement hydrométéorologique (numérotation par ordre chronologique, cf. fig. 1B) – La catastrophe de Libye de 2023 est plus de type technologique (rupture de deux barrages) que de type naturelle (tempête Daniel) ; 9. Limite bioclimatique du bassin méditerranéen ; 10. Limite hydrographique du bassin méditerranéen.

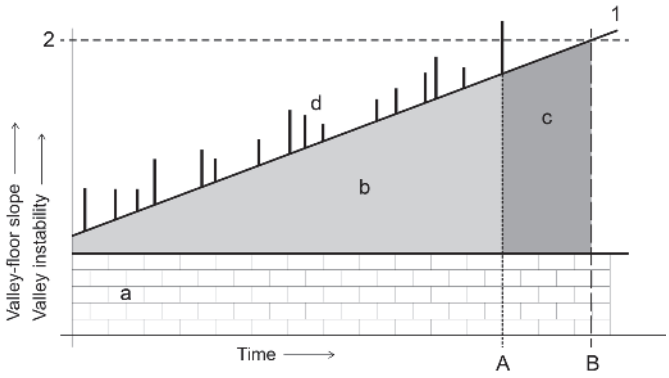

Fig. 2 – Relationship between sediment yield available for transport in the watershed, riverbed gradient, and valley-floor instability with time. Superimposed on line 1, representing an increase of sediment storage (and gradient), are vertical lines (d) representing instability of the valley floor as related to flood events. When the ascending line 1 intersects line 2, which represents the maximum sediment storage (and gradient) at which the valley is stable, failure or trenching of the valley alluvium will occur at time B. However, failure may occur earlier, at time A as the result of a major flood event. a. Physical properties of the WS; b and c. Volume of sediment accumulated in the system (b) and transported when the stability threshold is exceeded (c) (adapted from Tricart, 1962 and Schumm, 1973).

Fig. 2 – Relation entre la charge sédimentaire disponible pour le transport dans le bassin-versant, la pente du lit de la rivière et l'instabilité du fond de vallée en fonction du temps. *Les bâtonnets verticaux (d), qui représentent l'instabilité du fond de vallée face aux crues, sont superposés à la ligne 1, qui représente l'augmentation du stockage sédimentaire (et de la pente). Le creusement et le transport alluvial dans le fond de vallée se produisent au moment B, lorsque la ligne 1 croise la ligne 2 représentant le stockage sédimentaire (et la pente) maximum nécessaire à la stabilité de la vallée. Toutefois, l'instabilité du fond de vallée (creusement, transport sédimentaire) peut se produire plus tôt, au moment A, à la suite d'une crue majeure. a. Propriétés physiques du bassin-versant ; b et c. Volume de sédiments accumulés dans le système (b) et transportés lors du dépassement du seuil de stabilité (c) (adapté de Tricart, 1962 et Schumm, 1973).*

between 21 and 58 m, gradually widens as it moves downstream. The Aude WS (6074 km^2) is situated between the Montagne Noire to the north and the Pyrenees and Corbières to the south. The river drains the Aquitaine (Atlantic) basin to the west and the Languedoc (Mediterranean) basin to the east.

The Upper Aude R. flows from south to north down steep slopes (averaging 1.61 %), crossing ancient geological formations then the limestone strata of the pre-Pyrenees, while also supplying several reservoirs (Matemale, Puyvalador). Its bed-material load is predominantly coarse (D_{50} 60-80 cm), in line with high specific stream power (W_{bs} 2354-565 W/m^2), although the proportion of sand is not negligible (Astrade et al., 1999). From Carcassonne onwards, the Aude R. turns eastward, following a significant tectonic furrow that separates the Pyrenees (Corbières) from the Massif Central (Montagne Noire) and is largely filled with Tertiary molasse. The average gradient gradually declines until it reaches the mouth (from 0.13 % to 0.02 %), but its energy (W_{bs} 1942-11 W/m^2) is sustained by contributions from powerful tributaries (W_{bs} 2225-556 W/m^2). The most significant tributaries on the left bank of the Middle Aude R. flow down from the Montagne Noire. On the right bank, the Middle Aude R. also receives highly contributory tributaries from the Corbières massif (Calvet and Lemartinel, 2002). The Aude R. is bordered by the Canal du Midi, which intersects many left-bank tributaries. The hydrological regime of the Aude R. shifts to a Mediterranean pluvio-nival type, characterized by significant low-flow periods in summer. Heavy autumn rains, when they occur, can lead to rapid increases in average discharge, peaking in Feb. and remaining high in spring due to snowmelt from the Pyrenees. The tributaries reflect a Mediterranean pluvial regime with highly variable flows; their average discharge rarely exceeds a few cubic meters, and most of them have no flow at all for several months (summer, autumn). However, they can also produce flash floods of rare intensity, resulting in discharges of several hundred cubic meters in just a few hours (Gaume et al., 2009).

The Aude WS consists of 48.51 % agricultural land, 48.29 % forests and semi-natural environments, 2.52 % artificial land, 0.52 % wetlands, and 0.16 % water surfaces. Forests are found in mountainous slopes or in linear formations along watercourses. The riparian forests present significant challenges regarding logjam management. Additionally, villages situated along the tributaries of the Aude R. face a high risk of flooding (Fort et al., 2001; Arnaud-Fassetta et al., 2002; Arnaud-Fassetta and Fort, 2011). The Aude department is primarily rural and has a dense network of busy departmental roads, which heightens human vulnerability to flood hazard. One of the major managers of the Aude WS is the SMMAR (Syndicat mixte des milieux aquatiques et des rivières), established in 2002 following the catastrophic flood event of Nov. 1999. The SMMAR was created to address the need for coordinated water management and flood prevention on a WS scale, with a particular focus on river restoration, an area of study pursued for nearly 25 yrs with its primary scientific partner, Université Paris Cité-UMR 8586 PRODIG.

3. Methodological approach

The research methodology developed in this paper incorporates multiple approaches and levels of analysis across various timeframes and spatial scales.

3.1. Field missions

Following the flood event of Oct. 14-15, 2018, we conducted eighteen scientific missions, totaling 64 effective field days from Oct. 22-26, 2018 and Mar. 7-9, 2025. These field missions allowed us to (*i*) observe and analyze the (dys)functioning of rivers within their WSs and the related processes, (*ii*) capture diachronic photographs of phenomena that exemplified what took place during the flood event, (*iii*) conduct high-resolution cartographic surveys (*e.g.*, fig. 14B), (*iv*) carry out field surveys and sampling, and (*v*) engage with local stakeholders (residents, WS managers, river technicians, and politicians).

3.2. At the Aude-watershed scale

The systemic analysis of the Oct. 2018 flood is founded on both physical and societal observations and measurements, utilizing the frameworks of cindynics, spatial and temporal analysis in geography, and a comprehensive understanding of concepts and processes in physical geography. At the WS scale, we incorporated information from a bibliographic review, in addition to our own observations outlined below. A total of 40 references were used, including official

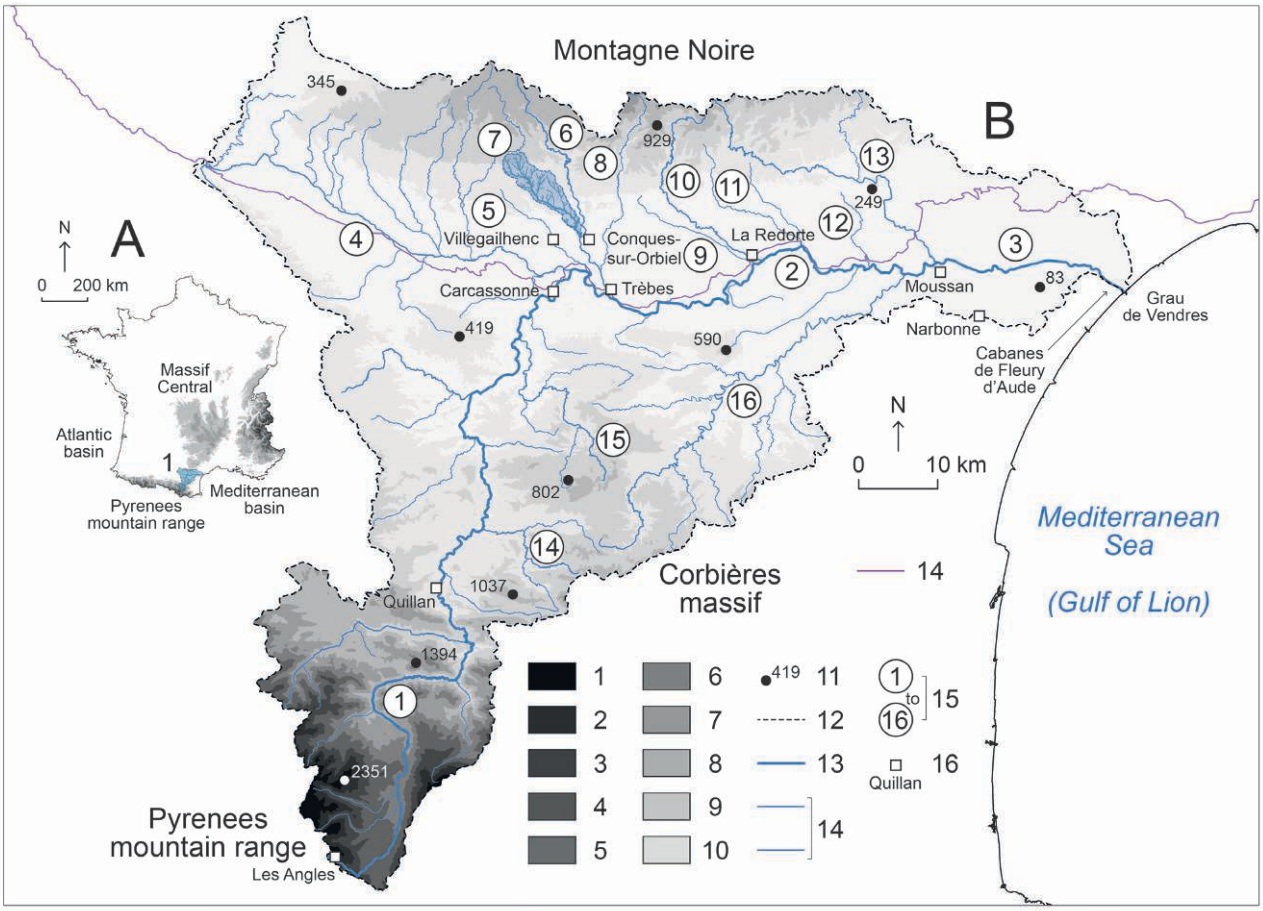

C	Aude River			Left-bank tributaries										Right-bank tributaries		
	1. Upper Aude River (Source - Carcassonne)	2. Middle Aude River (Carcassonne - Moussan)	3. Lower Aude River (Moussan - Mouth)	4. Fresquel River	5. Trapel River	6. Orbiel River	7. Rieu Sec brook	8. Clamoux River	9. Rivassel River	10. Argent Double River	11. Ognon River	12. Répudre River	13. Cesse River	14. Sals River	15. Lauquet River	16. Orbieu River
Watershed area (in km²)	1839	4838	6074	933	53	252	33.6	89	31	144	123	48	269	145	173	780
Strahler order	6	6	7	5	4	5	4	4	4	5	5	4	5	5	5	6
Number of major tributaries	14	9	0	22	10	17	6	20	4	16	9	13	35	8	14	55
Upstream elevation of riverbed (in m a.s.l.)	2172	100	6	272	480	866	545	1126	700	936	652	300	800	710	712	696
Downstream elevation of riverbed (in m a.s.l.)	100	6	0	83	80	67	123	93	38	35	24	25	8	220	115	6
River length (in km)	129	70.3	26.3	63	19.2	40.9	17.1	32.4	18.3	37.4	23.2	13.3	53.5	19.9	36.6	84.1
Channel width at bankfull stage (in m)	21 (min. 3 - max. 74)	54 (min. 26 - max. 93)	58 (min. 32 - max. 173)	12 (2-60)												
Average discharge (in m³/s)	14.6	31.5	50	5.32	0.38	2.61	0.1	0.89	0.5	0.95	0.5	0.5	2.9	1.09	0.4	4.64
Ten-year flow (in m³/s)	742	1270		260	73	192	-	140	-	94	-	-	253	200	140	563
Hundred-year flow (in m³/s)	1960	2220		679	268	984	265	514	150	727	-	247	485	-	600	1697
Discharge in October, 14-15, 2018 (in m³/s)	950	1660-3000		278	**420***	770	**350***	243	-	154	-	-	-	-	**880***	650
Gradient (in %) - Rieu Sec brook not included	1.61	0.13	0.02	0.29	2.08	1.95	-	3.19	3.62	2.41	2.71	2.07	1.48	2.46	1.63	0.82
D_{50} (in cm)	60-8	30-0.5	5-0.05	20-2												
Specific stream power at bankfull stage (in W/m²) - Rieu Sec brook not included	565-2354	324-1942	11-324	556-2225												
Number of municipalities crossed by the river	75	35	11	24	12	14	3	10	8	8	7	8	16	5	10	22

* Values in bold: reference flow at gauging station

Fig. 3 – Location of study area. A: the Aude WS (1) in France; B: main sub-WSs in the Aude WS. Elevation (in m a.s.l.); C: hydro-geomorphological characteristics of riverbeds and societal stakes.

1. > 2250; 2. 2250-2000; 3. 2000-1750; 4. 1750-1500; 5. 1500-1250; 6. 1250-1000; 7. 1000-750; 8. 750-500; 9. 500-250; 10. < 250; 11. Elevation point. Hydrography. 12. Aude-WS boundary; 13. Aude R.; 14. Main tributaries; 15. River numbering [1- Upper Aude R., 2- Middle Aude R., 3- Lower Aude R., 4- Fresquel R., 5- Trapel R., 6- Orbiel R., 7- Rieu Sec B. and its WS, 8- Clamoux R., 9- Rivassel R., 10- Argent Double R., 11- Ognon R., 12- Répudre R., 13- Cesse R., 14- Sals R., 15- Lauquet R., 16- Orbieu R.]; 16. Municipality.

Fig. 3 – Localisation de la zone d'étude. *A : le bassin de l'Aude (1) en France ; B : les principaux sous-bassins versants du bassin de l'Aude. Altitude (en m NGF) ; C : caractéristiques hydro-géomorphologiques des lits de rivière et enjeux sociétaux.*

1. > 2250 ; 2. 2250-2000 ; 3. 2000-1750 ; 4. 1750-1500 ; 5. 1500-1250 ; 6. 1250-1000 ; 7. 1000-750 ; 8. 750-500 ; 9. 500-250 ; 10. < 250 ; 11. Point coté. Hydrographie. 12. Limite du bassin de l'Aude ; 13. Fleuve Aude ; 14. Principaux affluents ; 15. Numérotation des cours d'eau [1- Aude amont, 2- Aude moyenne, 3- Aude aval 4- Fresquel, 5- Trapel, 6- Orbiel, 7- Rieu Sec et son bassin-versant, 8- Clamoux, 9- Rivassel, 10- Argent Double, 11- Ognon, 12- Répudre, 13- Cesse, 14- Sals, 15- Lauquet, 16- Orbieu] ; 16. Commune.

flood-management documents such as PPRI [flood risk prevention plans] and PAPI [flood prevention action program] (32 %), expert reports commissioned by local institutions (28 %), papers published in scientific journals dealing with climatology, hydrology, social impact of floods or land-use planning (25 %), unpublished research reports dealing with hydraulics (10 %), and national reports commissioned by the government (5 %). Furthermore, we included (*i*) press reviews from local daily newspapers (*La Dépêche du Midi*; *L'Écho du Languedoc*; *L'Indépendant*; *Midi Libre*) and (*ii*) information obtained from discussions with local managers and residents.

3.3. At the Rieu Sec-sub-watershed scale

3.3.1. Hydraulics, morphometry and sediment transport

Quantitative methods served as the foundation for the measurements and estimates proposed across various fields. In the area of hydraulics, substantial data (flow rates, water levels, *etc.*) is available on the Banque Hydro/Hydroportail websites. However, this data is often inconsistent, necessitating extensive bibliographic and web research to standardize the information, alongside fieldwork to gather data that is unavailable elsewhere. Specifically, we reconstructed cross-sections to estimate specific stream power (ω in W/m^2) determined by multiplying water density, gravitational acceleration, river discharge, and water slope) and W = channel width (in m). Gradients were measured using GIS tools or in the field with a laser meter and DGPS, while channel width was gauged with a laser meter. Riverbed incision was measured using a decameter and compared with image processing data (aerial photography and LiDAR). Specific discharge (in $m^3.s^{-1}.km^{-2}$), was calculated manually. The drainage density (D_d in km/km^2, *i.e.*, the ratio of the hydrographic network length in km to the WS area in km^2) was calculated automatically using GIS tools. The evaluation of the confluence ratio (R_c) within a WS was based on the Horton-Strahler stream order classification. In this study, Strahler order was also calculated manually to include all drains, including temporary ones. The confluence ratio (R_c, a ratio of rank x drains to rank x+1 drains) and the count of major tributaries were similarly calculated manually. WS morphometry was assessed through the Gravelius compactness index (K_c), which is calculated as the ratio of the WS perimeter (in km) to the circumference of a circle (in km) whose area (in km^2) matches that of the drainage basin (in km^2). The relief ratio (R_h) was determined by dividing the total relief (or relative relief) of the WS (in km) by the WS length (in km). We additionally calculated the width ratio (R_w), defined as the ratio of the active-channel width after the flood event to the active-channel width before the flood event. Sedimentary facies of alluvial deposits supplied by the Oct. 14-15, 2018 flood event on the channel bottom, such as plane beds or pools/bars/riffles, or in the flood plain, including hydraulic dunes and ripples, provided valuable insights into flow dynamics and the equilibrium between sediment supply and transport capacity (Buffington and Montgomery, 1997).

3.3.2. Sediment budget and forest uprooted by the flood

Sediment budget and forest balance were calculated for the Rieu Sec floodplain and the tributaries. Before quantifying these balances, it was essential to delineate the WS and the riverbeds. The Rieu Sec WS was manually delineated using QGIS. To ensure maximum accuracy, two geographic data sources were utilized. (*i*) the hydrographic network from the BDCarto database, accessible through the IGN Géoservices site, and (*ii*) the RGE Alti digital terrain model from 2024 with a 1-m resolution, also sourced from IGN Géoservices. This model was processed to extract slope exposure and contour lines at 1-m intervals. These data points were crucial for identifying ridgelines, allowing for precise manual definition of the WS boundaries. Riverbeds were also delineated manually using high-resolution airborne LiDAR data (30 cm in both x and y directions, and 15 cm in z), collected on Dec. 29, 2019. The raw LiDAR data were initially presented as a dense point cloud, necessitating conversion into a Digital Terrain Model (DTM). The conversion process occurred in two stages. (*i*) Point classification. Utilizing the CloudCompare open-source software, points corresponding to the ground were isolated to exclude vegetation and manmade structures; (*ii*) DTM generation. Interpolation of the filtered points was performed to create an accurate and homogeneous DTM. This resultant DTM was integrated into QGIS for the manual delineation of the Rieu Sec riverbed and its tributaries. To enhance this delineation, a network of segments perpendicular to the main channel was generated. Analyzing the elevation points recorded on these segments allowed for alignment of elevations across opposite banks, ensuring accurate topographical contours.

The sediment budget (Trimble, 1983) for the flood event of Oct. 14-15, 2018, was determined in the Rieu Sec WS by comparing a DTM from May 5, 2017, provided by the Aude DDTM (departmental directorate of territories and the sea), with a resolution of 5 m × 5 m per pixel, and a DTM derived from a LiDAR survey collected on Dec. 29, 2019, originally at a resolution of 1 m x 1 m per pixel. Given the differing resolutions, the 2019 DTM was resampled to 5 m x 5 m to match that of the 2017 DTM. The models were then aligned to ensure perfect pixel correspondence. During this alignment process, neighboring pixel values were averaged to facilitate a seamless transition and optimize data consistency. Following alignment, pixel values were subtracted (DTM 2019 - DTM 2017) to identify morphological changes. positive values indicated an increase in sediment volume, reflecting bed aggradation, while zero values signified no topographical modification. A tolerance margin of -0.5 m to +0.5 m was applied due to data resolution; negative values indicated a decrease in sediment volume, correlating to bed incision. To enhance interpretation of the results, an optimized symbology was used to clearly distinguish variations in riverbed aggradation and incision. The Raster Surface Volume tool quantified the sediment volumes (in m^3) mobilized between 2017 and 2019. Subsequently, the sediment budget for the Oct. 2018 flood was established at the WS scale and then analyzed in three specific zones (A = upstream; B = midstream; C = downstream) by separating the riverbed of the Rieu Sec from its tributaries. We consistently refined the values obtained from image processing through field observations and our understanding of the studied WS. Unfortunately, we were unable to use the results of image processing to quantify the sediment budget on the slopes, as the images produced outputs that were completely anomalous and inconsistent with reality, possibly due to the vegetation covering the slopes. Therefore, we reconstructed the sediment budget by directly observing and quantifying erosion and accumulation patterns in the field. This approach enabled us to effectively account for the effects of gullying and landslides in the sediment budget at the WS scale.

The impact of the Oct. 14-15, 2018 flood on forest cover was assessed by comparing two datasets. aerial photographs from the IGN taken on Jul. 4, 2018, three months prior to the flood, and those taken on Jul. 18, 2020, which is twenty months after the flood. These datasets were employed to map forest cover in the Rieu Sec WS. Forested areas were manually digitized from orthophotographs. The areas of forest uprooted by the flood, expressed in m^2, were analyzed to establish the overall forest removal for the period from Jul. 2018 to Jul. 2020. This analysis highlighted the impact of the Oct. 2018 flood at the WS scale, further refining the assessment into the three specific zones (A = upstream; B = midstream; C = downstream) by distinguishing the Rieu Sec riverbed from its tributaries.

3.3.3. Stratigraphic surveys, sediment-facies analysis, and radiocarbon dating

A series of natural, stratigraphic sections was studied along the Rieu Sec active channel, a right-bank tributary of the Orbiel R. Each stratigraphic section was drawn, contextualized within its hydro-geomorphological setting, analyzed for stratigraphic units, sampled (one to three samples per stratigraphic unit depending on sedimentary facies diversity), and interpreted in terms of sedimentary environments. Sediment sampling adhered to strict precautions (gloves, masks, cleaning of clothing and equipment, protection of samples, and careful laboratory practices), given that the Orbiel WS, particularly the Rieu Sec B., is heavily contaminated with heavy metals and arsenic (Delplace et al., 2022).

Sediment structure was analyzed using the methodology of Pettijohn and Potter (1964), supplemented by Pierson (2005) for hyper-concentrated flows. Sediment texture was analyzed according to Wentworth's (1922) particle-size classification. Particle sizes were determined through three methods. *In situ* measurement of b-axes for particles larger than 6 mm, dry sieving for particles between 6 mm and 1 mm, and laser particle sizing for particles smaller than 1 mm. The proportion of each fraction was calculated as a percentage of the original sample weight. For the Oct. 2018 alluvial deposits (E1 and E2), we employed 1 m quadrats for sampling to align more closely with the grain sizes obtained from the stratigraphic sections. We extracted the respective percentages of gravel, sand, silt, and clay, alongside median particle size (D_{50}), coarsest percentile (D_{99}), and the Inclusive Graphic Standard Deviation (σ_I; Folk and Ward, 1957) from each cumulative frequency particle-size curve.

In addition to sedimentology, N. Limondin-Lozouet (UMR 8591 LGP) analyzed from field photographs the malacological content of SU6 to characterize the ecological conditions of the sedimentary environment in the valley bottom before the Oct. 14-15, 2018, flood event.

Fossil wood identified in the stratigraphic sections was cut cleanly in the field, and the unpolluted core sample was subsequently sent to the Beta Analytic laboratory in Miami (USA) for AMS (Accelerator Mass Spectrometry) radiocarbon dating (fig. 10E, F). The ^{14}C dates obtained were corrected for $\delta^{13}C$ and calibrated to calendar years using the BetaCal4.20. HPD method. INTCAL20 (Reimer et al., 2020). All measurements passed acceptance tests, and the laboratory provided two probability intervals (95.4 % and 68.2 %). We opted to consider only the first interval (±2 σ), which has a 95.4 % probability of encompassing the true conventional age (Bronk Ramsey, 2009). The age of the trees at the time of death was determined via dendrochronology (counting annual growth rings), while the tree species (*Alnus glutinosa*) was identified by M. Dupuis (SMMAR) and É. Grésillon (UMR 7533 LADYSS). Our review of past flood events, categorized into three classes (frequent floods; remarkable floods; historical floods), is based on a comprehensive compilation of data from various sources (Rousseau, 1875; Pardé, 1930a, 1930b, 1933a, 1933b, 1934a, 1934b, 1941; LeRoy Ladurie, 1967; Verdeil, 1999; Antoine et al., 2001; Vinet, 2003; Payrastre et al., 2006; SRTM, 2017; Larguier, 2018; MétéoFrance; flood markers; PPRIs for relevant WSs).

4. Results

4.1. Systemic analysis of the October 2018 flood event in the Aude watershed

Systemic analysis compels us to define and prioritize three groups of factors (predisposing, triggering, aggravating/mitigating) that contributed to the catastrophic flood event of Oct. 14-15, 2018, which resulted in 15 fatalities, 99 injuries, and declared 257 municipalities as being in a state of natural disaster ("Cat-Nat" compensation scheme in France), including 204 in the Aude department alone, leading to damages totaling 256 million euros (fig. 4).

4.1.1. Predisposing factors

Natural, predisposing factors refer to a set of physical characteristics, on a regional scale, that make the area under study vulnerable to flooding. In the Aude WS, these physical characteristics can be classified into three categories.

(*i*) Climate. The WSs of the left-bank tributaries of the Aude R. (rivers Fresquel, Trapel, Orbiel, Rivassel, Argent Double, Ognon, Répudre, and Cesse), situated on the southern slopes of the Montagne Noire and its piedmont (Minervois), are particularly vulnerable to atmospheric low-pressure areas moving from the Mediterranean toward the continent. This phenomenon is characteristic of cyclogenesis affecting the northwestern part of the Mediterranean basin (Béranger, 1960).

(*ii*) Hydrography. The hydrographic basins facilitate the flow of rivers toward the southeast, while atmospheric depressions move in the opposite direction, toward the northwest. The runoff that reaches the downstream areas of these basins, initially originating from rainfall upstream, is enhanced and replenished by additional rainfall occurring in the downstream sections of the basins (Chorley et al., 1984).

(*iii*) Geomorphology. There is a contrast between the mountain massifs primarily composed of schist (Montagne Noire), characterized by steep slopes, confined high-energy riverbeds, and a substantial supply of debris from the surrounding slopes and rivers, and the foothills (Minervois) composed of sedimentary rock (Tertiary molasse). The latter features gentle slopes and naturally wandering rivers, creating conditions conducive to debris accumulation along the margins of active channels, especially during flood events (Arnaud-Fassetta et al., 2002, 2024). These naturally wandering rivers have been artificially narrowed since the beginning of the Modern Era.

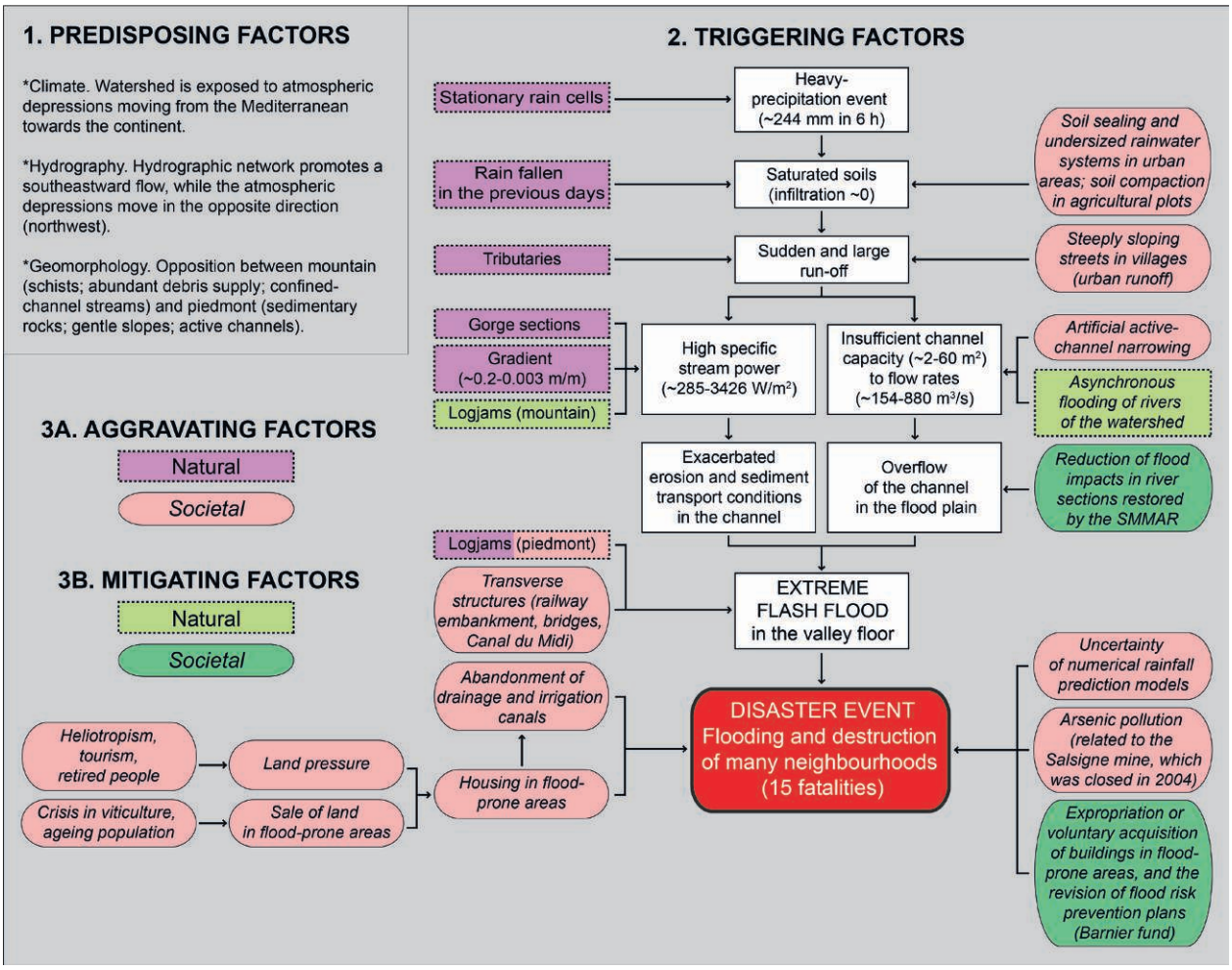

Fig. 4 – Systemic analysis of the October 14-15, 2018, flood event in the Aude department.

Fig. 4 – Analyse systémique de la crue des 14-15 octobre 2018 dans le département de l'Aude.

4.1.2. Triggering factors

On the night of Oct. 14 to 15, 2018, a Mediterranean HPE occurred in the departments of Pyrénées-Orientales, Aude (the most affected), and Hérault. During the previous week (Oct. 10-15, 2018), the Balearic Islands were hit by very heavy rains, ravaging (13 deaths) the east coast of Mallorca on the night of Oct. 9, 2018 (Lorenzo-Lacruz et al., 2019). The synoptic situation on Oct. 14 and 15, 2018, was defined by a complex system of upper-level low pressure that extended from the northern Iberian Peninsula to Brittany (Kreitz et al., 2020; Caumont et al., 2021; Mandement and Caumont, 2021). This setup generated a highly dynamic trough axis over the eastern Pyrenees, leading to substantial uplift over the Aude department during the latter part of the night. In the upper troposphere, this arrangement produced notable diffluence, evidenced by the simultaneous left-exit and right-entry of two branches of the jet stream. One centered over Catalonia and the other extending from Aquitaine to southern England. Against this dynamic backdrop, an undulating cold front spanned from the Balearic Islands to Brittany, traversing the Aude WS during the night of Oct. 14-15. A moderately deep surface low (1002 hPa at 00.00 UTC on Oct. 15) momentarily settled over Catalonia, intensifying the low-level jet that had developed along its northeastern edge. This corridor of strong winds subsequently reached the surface. Significant convergence occurred between the ESE winds flowing from the Gulf of Lion and the westerly winds advancing from the west of Roussillon. It was in this zone of intense humid convergence that the most substantial and prolonged rainfall took place, lasting nearly ten hours and primarily impacting the central region of the Aude département. The intensity of the precipitation was further heightened by the instability of the air mass, which was heavily enriched with moisture from the Mediterranean.

The rain began to intensify significantly around 23.30 UTC on Sunday, Oct. 14, fairly simultaneously along the entire precipitation axis, from the southern slopes of the Montagne Noire to the western slopes of the Corbières massif. They became very intense by 01.00 UTC on Oct. 15. The floods began a little later on Oct. 15 for the right-bank tributaries of the Aude R. in the Corbières massif (at 01.00 UTC in the Upper Orbieu R., at 01.30 UTC in the Salz R., and at 03.00 UTC in the Lauquet R.). The period of heaviest rainfall extended from 01.00 to 06.00 UTC on Oct. 15. The most affected area (Montagne Noire, Cabardès, east of Carcassonne, Val de Dagne) is a climate transition zone between the Atlantic and Mediterranean influences and is therefore usually somewhat sheltered from the most violent episodes. The area that experienced rainfall totals exceeding 150 mm on Oct. 14-15, 2018, covers approximately

600 km², indicating that the rainfall was intense but geographically concentrated. The near-stationarity of the rain axis for nearly 9 h resulted in very high rainfall totals, with extreme values recorded at 300 mm in 24 h in Conques-sur-Orbiel on Oct. 14-15, 2018 (fig. 5A). While it seems that we are far from the 551 mm in 24 h measured in Lézignan-Corbières on Nov. 12-13, 1999, these values could, however, have been greatly exceeded. Indeed, the radar in Opoul (MétéoFrance) was out of service during the HPE in Oct. 2018, leading to a lack of rainfall data in the Montagne Noire area and a significant underestimation of rainfall in the Corbières and Carcassonne regions. Supporting the notion of an underestimation of daily totals in Oct. 2018 provided by MétéoFrance, rainfall totals measured by winegrowers (in agricultural trailer bin) reached 800 mm in Aragon (Rieu Sec and Vallouvière WSs) on Oct. 14-15, 2018. The hourly rainfall intensities were high (57 mm in 1 h in Caunes-Minervois at 04.00 UTC on Oct. 15, 2018), but not exceptional (on Nov. 12-13, 1999, the Lézignan-Corbières station recorded an hourly total of more than 106 mm). It was primarily the rainfall totals over 3 h, 6 h (244 mm in Trèbes), and 12 h that were exceptional on Oct. 15, 2018. The RI was often exceeded by a factor of about two (213 mm in 6 h at Villegailhenc for a centennial total of 101 mm). The consequences were catastrophic near the precipitation maximum because most of the rain fell in 7 to 9 h (Ayphassorho et al., 2019). The maximum rainfall amounts were located in the Trapel WS, on the west side of the Orbiel WS, to the northeast of the Fresquel WS, and on many WSs (Bazalac, Bretonne) south-east of Carcassonne.

The first rises in flooding occur on the left-bank tributaries of the Aude R. in the Minervois during the early hours of Oct. 15, with flood peaks being reached 2 to 3 h later. Flooding begins a little later for the right-bank tributaries of the Aude R. in the Corbières massif. This led to spectacular flash floods (Lebouc et al., 2019). The rivers Orbiel, Rieu Sec, and Trapel devastated the municipalities of Aragon, Villegailhenc, Villemoustaussou, Villalier, and Conques-sur-Orbiel. In Villedubert, just upstream from Trèbes and the confluence with the Aude R., the Orbiel R. rose by 6 m in less than 4 h; In the Corbières massif, the Lauquet R. surged by 6 m in 2 h at Saint-Hilaire; Significant flooding occurred in the tributaries (Dure, Rougeanne) of the Fresquel R. originating from the Montagne Noire, as well as on the Sor B. (a tributary of the Agout R.) on the Atlantic side of the Montagne Noire. Further downstream, other tributaries (Argent Double, Rivassel, Ognon, Répudre, Cesse, Orbieu) of the Aude R. experienced more moderate flood intensities. Between Carcassonne (Fresquel R.) and the Orbieu R., the flood of Oct. 2018 in the Aude R. is significantly greater than that of Nov. 1999 and at least equivalent to that of Oct. 1891, if not locally greater, fueled by exceptional discharges of the tributaries (Lebouc et al., 2019b): Trapel R. (WS: 60 km²), 240 m³/s; Orbiel R. upstream of the confluence (WS: 252 km²), 770 m³/s (100-yr RI peak flow: 984 m³/s) according to DDTM, 2024; Vallouvière B. (WS: 16 km²): 125-130 m³/s; Rieu Sec B. (WS: 33.3 km²): 250 m³/s (350 m³/s according to DDTM, 2024). The Lauquet R., a right-bank tributary of the Aude R., reaches 880 m³/s before the confluence (WS. 190 km²). The set of these values corresponds to maximum specific discharges of around 8 $m^3.s^{-1}.km^{-2}$ (fig. 5B).

The hydrometeorological event of Oct. 2018 generated extreme morphogenesis in the affected WSs.

(*i*) In the upstream part of the WSs (mountains), the rainfall contributed to concentrated runoff, which resulted in gully erosion of the non-forested slopes. The heads of the streams experienced hyper-concentrated flows, successively feeding the midstream part of the WSs.

(*ii*) In the midstream part of the WSs, the riverbeds were incised down to the geological substrate (fig. 6A). Large volumes of runoff water caused the streams and rivers to rise rapidly, with very quick response times. In the Salz R., water level increased by +1 m in 5 min. The channel capacity at bankfull stage was quickly exceeded, leading to floodwaters overflowing outside of ordinary riverbeds. The insufficient channel capacity also resulted in a significant active-channel widening (fig. 6D, E) and meander cutoffs (fig. 6B) as well as avulsions (fig. 6F). In the floodplain areas, the channel pattern characterizing the rivers before the floods (*i.e.*, narrow channels a few meters wide and sinuous) evolved towards a channel pattern with multiple wandering or braided channels (fig. 6C).

(*iii*) In the downstream parts of the WSs and in the Aude plain downstream of Carcassonne, widespread flooding was observed in the valley floor (fig. 6G), with water levels reaching 7.67 m (Aude R. in Trèbes on Oct. 15, 2018, at 07.00 UTC, comparable to the 7.95 m water level from the reference flood of Oct. 25, 1891) and 6.64 m (Aude R. in Puichéric on Oct. 15, 2018, comparable to the 6.61 m water level from the reference flood of Oct. 25, 1891; fig. 6H). The peak flood flow of the Aude R. on Oct. 15, 2018, reached 1660 m³/s in Moussan (and possibly even 3000 m³/s), while it was only 950 m³/s in Carcassonne. The contributions from the left-bank tributaries of the Aude R. in the Montagne Noire/Minervois piedmont clearly played a major role in the unfolding of the extreme flood of Oct. 2018.

4.1.3. Aggravating and mitigating factors

Regarding the aggravating factors, five natural factors can be identified.

(*i*) Stationarity of rain cells. The rain cells remained stationary for several hours over certain WSs. In particular, the WSs of the Vallouvière B., a left-bank tributary of the Trapel R., and the Rieu Sec B., a right-bank tributary of the Orbiel R., were entirely situated within the maximum rainfall zone for 7 to 9 h.

(*ii*) Rain fallen in the previous days. An initial rainstorm (60-80 mm) had affected the area five days prior, leading to significant soil saturation. The daily Soil Wetness Index reported by MétéoFrance indicated a shift from a deficit of 20-30 % on Oct. 8 to a surplus of 10-20 % from the 9th to the day before the event, with localized areas in the Corbières massif and the Middle Aude R. (in the vicinity of La Redorte) reaching 50-60 % saturation (Kreitz et al., 2020).

(*iii*) Tributaries. The contributions of water and sediment from the tributaries were substantial, significantly influencing the morphogenesis of the main rivers. In the Orbiel WS, the Rieu Sec B. appears to have been the primary contributor to downstream flooding, delivering up to 250-350 m³/s at its confluence with the Orbiel R. The Upper Orbiel R. contributed between 130 and 150 m³/s downstream of Lastours, while the Clamoux R. contributed approximately 75-243 m³/s upstream of the confluence with the Orbiel R. These values align closely with the 490-770 m³/s recorded at the Bouilhonnac station on the Lower Orbiel R. In the Lauquet WS, located south of Carcassonne, the estimated upstream contributions to the Lauquet flood are around 300 m³/s from the Lauquette B., 140 m³/s from the Alberte B., and 275 m³/s from Upper

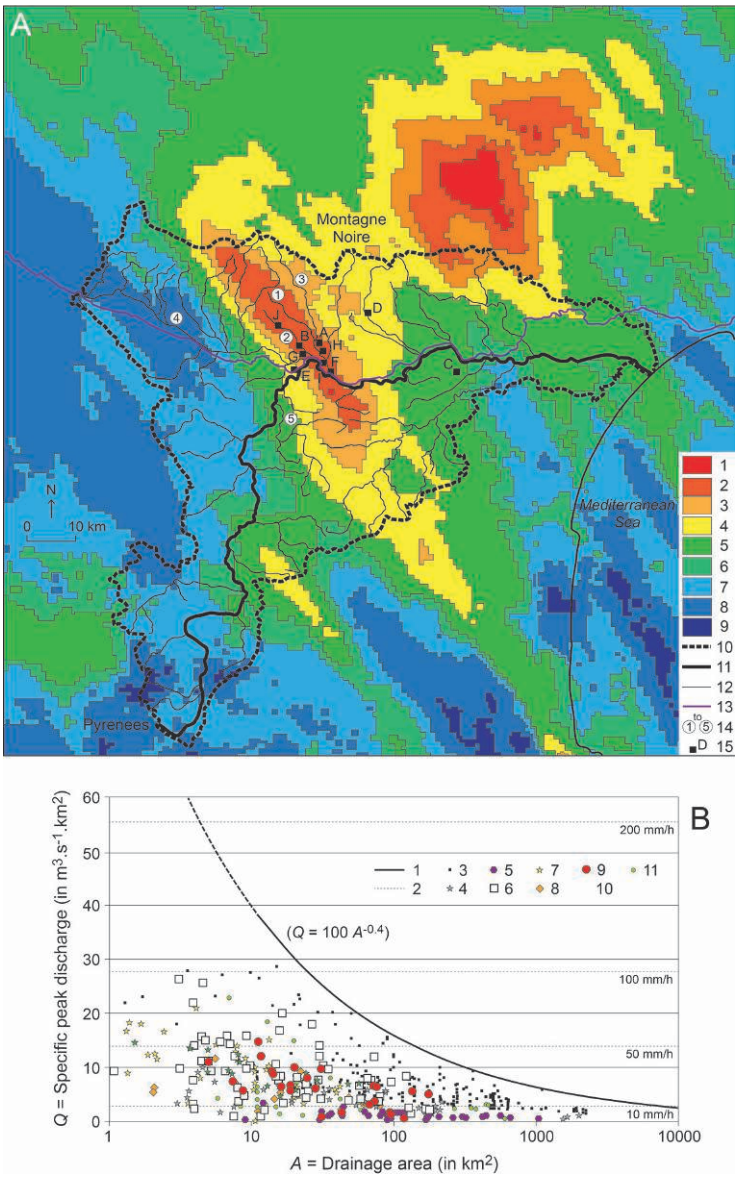

Fig. 5 – Rainfall on October 14-15, 2018 and hydrological response in the Aude department.

A: cumulative rainfall (in mm) recorded by the Antilope radar from Oct. 14 at 19.00 UTC to Oct. 15 at 06.00 UTC (MétéoFrance data).

1. 400-300; 2. 300-250; 3. 250-200; 4. 200-150; 5. 150-100; 6. 100-80; 7. 80-60; 8. 60-40; 9. 40-20; 10. Aude-WS boundary; 11. Aude R.; 12. Main tributaries; 13. Canal du Midi; 14. River numbering [1- Rieu Sec B., 2- Trapel R., 3- Orbiel R., 4- Fresquel R., 5- Lauquet R., 15. Municipality. A- Conques-sur-Orbiel, B- Villegailhenc, C- Lézignan-Corbières, D- Caunes-Minervois, E- Carcassonne; F- Trèbes, G- Villemoustaussou, H- Villalier, I- Villedubert, J- Aragon].

B: specific flows reached by rivers in the Aude département in Oct. 2018, compared with specific flows of other rivers during flash floods in southern France.

1. HYDRATE envelope curve (Gaume et al., 2009); 2. Hourly rainfall intensity limits; 3. Maximum values known in France (2009; Lebouc et al., 2019b); 4. Jun. 2010 (Var departement; rivers Argens, Florieye, Réal, Nartuby and Aille ; Payrastre et al., 2012); 5. Jun. 2013 (Pyrenees massif ; Payrastre et al., 2014); 6. Sep./Oct. 2015 (Gard and Hérault departments; rivers Orb, Hérault, Vidourle, Gardons, Cèze, Chassezac, Lez, Mosson and Ardèche ; Payrastre, 2015); 7. Oct. 2015 (Alpes Maritimes department. rivers Brague, Grande Frayère and Riou de l'Argentière; Lebouc and Payrastre, 2017); 8. Aug. 2018 (Ardèche and Gard departments; rivers Ardèche and Cèze; Lebouc et al, 2019a); 9. Oct. 2018 (Aude department; rivers Orbiel and tributaries, Trapel and Lauquet; Lebouc et al., 2019b); 10. Nov./Dec. 2019 (Var and Alpes Maritimes departments; Riou de l'Argentière and tributaries, rivers Agay, Reyran, and Argens tributaries. Grande Garonne, Endre; Lebouc and Payrastre, 2020); 11. Oct. 2020 (Alpes-Maritimes department; rivers Roya, Tinée and Vésubie; Payrastre and Nicolle, 2021).

Fig. 5 – La pluie des 14-15 octobre 2018 et la réponse hydrologique dans le département de l'Aude.

A : lame d'eau ou cumul de précipitations (en mm) relevé par le radar Antilope du 14 oct. à 19.00 TU au 15 oct. à 06.00 TU (données MétéoFrance).

1. 400-300 ; 2. 300-250 ; 3. 250-200 ; 4. 200-150 ; 5. 150-100 ; 6. 100-80 ; 7. 80-60 ; 8. 60-40 ; 9. 40-20 ; 10. Limite du bassin de l'Aude ; 11. Fleuve Aude ; 12. Principaux affluents ; 13. Canal du Midi ; 14. Numérotation des cours d'eau [1- Rieu Sec, 2- Trapel, 3- Orbiel, 4- Fresquel, 5- Lauquet, 15. Commune. A- Conques-sur-Orbiel, B- Villegailhenc, C- Lézignan-Corbières, D- Caunes-Minervois, E- Carcassonne, F- Trèbes, G- Villemoustaussou, H- Villalier, I- Villedubert, J- Aragon].

B. débits spécifiques atteints par les rivières du département de l'Aude en oct. 2018 et comparaison avec les débits spécifiques d'autres cours d'eau lors de crues brutales dans le sud de la France.

1. Courbe enveloppe HYDRATE (Gaume et al., 2009) ; 2. Limites des intensités de pluie horaires ; 3. Maximums connus en France (2009 ; Lebouc et al., 2019b) ; 4. Juin 2010 (département du Var ; rivières Argens, Florieye, Réal, Nartuby et Aille ; Payrastre et al., 2012) ; 5. Juin 2013 (Pyrénées ; Payrastre et al., 2014) ; 6. Sep./oct. 2015 (départements du Gard et de l'Hérault ; rivières Orb, Hérault, Vidourle, Gardons, Cèze, Chassezac, Lez, Mosson, Ardèche ; Payrastre, 2015) ; 7. Oct. 2015 (département des Alpes Maritimes. rivières Brague, Grande Frayère et Riou de l'Argentière ; Lebouc et Payrastre, 2017) ; 8. Août 2018 (départements de l'Ardèche et du Gard ; rivières Ardèche et Cèze ; Lebouc et al., 2019a) ; 9. Oct. 2018 (département de l'Aude ; rivières Orbiel et ses affluents, Trapel et Lauquet ; Lebouc et al., 2019b) ; 10. Nov./déc. 2019 (départements du Var et des Alpes Maritimes ; rivières Riou de l'Argentière et ses affluents, Agay, Reyran, affluents de l'Argens. Grande Garonne, Endre ; Lebouc et Payrastre, 2020) ; 11. Oct. 2020 (département des Alpes-Maritimes ; rivières Roya, Tinée et Vésubie ; Payrastre et Nicolle, 2021).

Fig. 6 – The triggering factors of the October 14-15, 2018, flood event in the Aude watershed and their hydro-geomorphological impacts. A: incision (-3 m) of the Upper Rieu Sec riverbed to the geological substratum (WS zone A; © M. Dupuis, 2018/10/22); B: chute cutoff observed downstream of the Rieu Sec B. (© M. Dupuis, 2018/10/22); C: transition in the channel pattern of the Lower Rieu Sec B., shifting from a sub-rectilinear single-channel configuration to a wandering multi-channel form (© M. Dupuis, 2018/10/22); D: widening of the Orbiel channel (Conques-sur-Orbiel) due to bank undercutting on the concave side (© M. Dupuis, 2018/10/18); E: active-channel widening of the Trapel R. as it passes through Villegailhenc, which resulted in the flooding of 870 buildings, the destruction of the D118 bridge, and four fatalities (AFP – S. Thomas, 2018/10/15); F: avulsion of the Orbiel R. in Villalier, occurring on the concave bank of a meander, likely exacerbated by the presence of an under-calibrated bridge (this shift caused the Orbiel channel to abruptly move 200 m, resulting in the death of a heavy goods vehicle driver; © IRMA – S. Gominet, 2018/10/15); G: flooding of the Aude valley floor in the Puichéric area (© AFP – S. Thomas, 2918/10/15); H: flood-water markers within the village of Puichéric demonstrate that the 2018 event is the most significant flood in over a century (notably surpassing the levels seen in 1891, which is not marked in the image; © IRMA – S. Gominet, 2018).

Fig. 6 – Les facteurs déclenchants de la crue des 14-15 octobre 2018 dans le bassin de l'Aude et leurs impacts hydro-géomorphologiques. *A : incision (-3 m) du lit du Rieu Sec amont jusqu'au substrat géologique (zone A du bassin-versant ; © M. Dupuis, 22/10/2018) ; B : recoupement de sinuosité (Rieu Sec aval ; © M. Dupuis, 22/10/2018) ; C : changement de style fluvial du Rieu Sec aval (passage d'un style subrectiligne à chenal unique à un style divagant à chenaux multiples ; © M. Dupuis, 22/10/2018) ; D : élargissement du chenal de l'Orbiel (Conques-sur-Orbiel) par sapement de berge en rive concave (© M. Dupuis, 18/10/2018) ; E : élargissement de la bande active du Trapel dans sa traversée de Villegailhenc (© AFP – S. Thomas, 15/10/2018) ; F : défluviation de l'Orbiel à Villalier, mise en place sur la rive concave d'un méandre et certainement aggravée par la présence d'un pont sous-calibré (le chenal de l'Orbiel s'est déplacé brutalement de 200 m, entraînant le décès d'un chauffeur de poids lourd ; © IRMA – S. Gominet, 15/10/2018) ; G : inondation du fond de vallée de l'Aude dans le secteur de Puichéric (© AFP – S. Thomas, 15/10/2018) ; H : repères de crue indiqués dans le village de Puichéric montrant que l'événement de 2018 est le plus important depuis plus de 100 ans (si l'on considère que 2018 a dépassé 1891, non indiqué sur l'image ; © IRMA – S. Gominet, 2018).*

Lauquet R. These estimates are consistent with further downstream measurements, which indicate flows of approximately 750 m^3/s upstream of Saint Hilaire and 880 m^3/s upstream of Verzeille (Ayphassorho et al., 2019).

(*iv*) Gorge sections. In mountainous areas, gorge sections lead to the narrowing of riverbeds and an increase in specific stream power downstream.

(*v*) Slope values. River sections with steep gradient were conducive to accelerated flow velocities, which in turn enhanced river energy, intensifying erosion processes and increasing sediment transport.

Alongside these natural factors, there are eight additional societal factors.

(*vi*) Soil sealing and under-calibration of stormwater drainage systems. In the piedmont region, soil sealing was observed on the interfluves and flood plains, both in urban areas (settlement and asphalt surfaces) and in agricultural zones where mechanized viticulture and fruit tree farming compact the soil. In urban areas, stormwater drainage systems were often under-sized, which hampers the control of surface runoff management.

(*vii*) Urban runoff. The contribution of rainwater runoff, which was significant in villages characterized by steep lanes oriented towards the riverbed, locally increased the river flows. Moreover, urban runoff posed a risk in itself, given the steep lanes and considerable amounts of water runoff.

(*viii*) Artificial channel narrowing. Most riverbeds were narrowed from the 18th to 19th century, which made them more prone to flooding due to reduced capacity, and increased specific stream power (fig. 7A, C). Channelization has been accompanied by an increase in sinuosity, thereby increasing the chances of meander cutoff and avulsions during floods.

(*ix*) Barriers to water flow in riverbeds. Flood flows in the channel have been partially obstructed by transverse structures, such as undersized road bridges (in Trèbes, Conques-sur-Orbeil, Villehailhenc, Villeneuve-Minervois, and Caunes-Minervois) and canal bridges (along the Canal du Midi; fig. 7B). These obstructions have contributed to rising water levels in the channel and resulted in flooding of the valley floor upstream (Hocini et al., 2020; fig. 7C).

(*x*) Logjams (in the piedmont). This phenomenon is influenced by both natural factors, such as the biological process of tree growth, and societal factors, since logjams primarily occur due to undersized bridges, leading to a rise in water levels upstream. Overall, there were fewer logjams in Oct. 2018 compared to Nov. 1999, with many of these logjams observed in the Lauquet channel (fig. 7A). This decrease is likely a result of improved river management by the SMMAR.

(*xi*) Housing in flood-prone area. In the Aude department, the Oct. 2018 flood event claimed the lives of 15 individuals, including 6 in Trèbes, 4 in Villegailhenc, 2 in Villalier, and 1 each in Villardonnel, Carcassonne, and Saint-Couat-d'Aude. Over half of the victims were elderly. The disaster affected 19,000 buildings and approximately 5700 vehicles, many of which were swept away. On Oct. 15, more than 10,000 residents were left without access to drinking water, and over 6000 ENEDIS customers experienced power outages. Additionally, more than 1000 km of departmental roads were rendered impassable, including 50 that were completely closed. Four road bridges were destroyed, while five others sustained damage. Several railway lines were also impacted and temporarily shut down. One of the primary factors contributing to this disaster was the presence of housing in flood-prone areas (fig. 7D). In the Aude department, which had a population of 372,806 in 2018, 390 out of 436 communes are identified as vulnerable to flooding according to the Aude departmental major risk file. Among the communes most severely affected by the Oct. 2018 floods, Conques-sur-Orbiel saw 53 % of its population (approximately 1374 buildings) located in flooding areas, while Trèbes had 60 % of its population (about 2077 buildings) situated in similar vulnerable areas. Tragically, 53 % of the flood victims died in their homes, including one individual who drowned on the first floor of his house when the water rose to 4 m. There were also fatalities on the roads, such as a truck driver who was swept away by the floodwaters in Villalier (fig. 6F).

(*xii*) Uncertainties in numerical rainfall forecasting models. During the Oct. 2018 HPE in the Aude department, MétéoFrance forecasting models experienced significant variability (in terms of intensity and fine-scale localization), both among themselves and across different networks. The post-event analysis revealed that the 'correct' scenario for the HPE only emerged from the AROME model on Oct. 14 at 12.00 UTC, just a few hours before the onset of the HPE (Kreitz et al., 2020).

(*xiii*) Arsenic pollution. Heavy rainfall, through runoff and the resurgence of groundwater, released three to five tons of arsenic (As) within 24 h that had been stored in the area of the former gold mine in Salsigne and the Orbiel valley along with its tributaries (Grésillou and Rieu Sec; fig. 7E). The concentration levels of As in suspended matter samples collected from the brooks Grésillou and Rieu Sec indicates very high values, reaching 870 mg/kg and 143-631 mg/kg, respectively (Delplace et al., 2022). This pollution factor transforms the natural disaster of Oct. 2018 into an industrial and technological catastrophe.

The primary natural factor mitigating the Oct. 2018 flood in the Aude WS is hydrological.

(*xiv*) Successive arrival of floods in the sub-WSs. Fortunately, the downstream hydraulic propagation of the four flood waves was delayed. The Middle Aude R. (Trèbes) reached its flood peak at 07.30 UTC on Oct. 15, well ahead of the Upper Aude R., which peaked at 11.00 UTC. This time lag in the arrival of the four flood waves in the Lower Aude R. – first from the Cesse R., then from the Orbieu R., followed by the Middle Aude R., and finally from the Upper Aude R. – helped avert a more severe disaster.

(*xv*) Logjams (in the mountain). Driftwood carried by the river has accumulated on the valley floor, where it has been obstructed by trees that were not uprooted by the flood. These natural dams reduce flow energy and discharge, as illustrated in the Rieu Sec B. (fig. 9E).

There are also two societal factors that mitigated the impact of the floods, related to the restoration of riverbeds and the zoning of flood-prone areas.

(*xvi*) River sections restored by SMMAR. These restored river sections, resulting from SMMAR's acquisition of land within the designated freedom space of the active channels, exhibit a substantial ability to dissipate flood flow energy and more effectively retain sediment as gravely bars (fig. 7F), particularly in river sections upstream of urbanized areas that concentrate most of the material and human stakes present in the floodplain (Arnaud-Fassetta et al., 2024).

Fig. 7 – The aggravating or mitigating factors of the October 14-15, 2018, flood event in the Aude watershed. A: logjam of trees and debris in the narrow channel of the Lauquet R. (© France 3 – LR, 2018/10); B: overflow of the Orbiel R. onto the Canal du Midi in Trèbes (© VNF, 2018/10/15, 07.45 UTC); C: flooding in Villegailhenc caused by the Trapel R., resulting in 870 buildings inundated, the D118 bridge washed away, and four fatalities (© IRMA – S. Gominet, 2018/10/17); D: flooding in Trèbes from the Orbiel R., Aude R., and Canal du Midi, leading to six deaths (© RGLR – C. Tignard, 2018/10/15); E: arsenic contamination downstream of Salsigne, in the Gourg Peyris B., a left-bank tributary of the Rieu Sec B. in the Orbiel WS (© O. Saint-Hilaire, 2018/10); F: section of the Clamoux R. (a left-bank tributary of the Orbiel R.) restored by the SMMAR, where the widened active channel now aids in flood attenuation and sediment storage upstream of critical areas like Villegly (© G. Arnaud-Fassetta, 2018/11/22); G and H: the Montplaisir district in Conques-sur-Orbiel, located within the Orbiel flood plain, before (G; © G. Arnaud-Fassetta, 2021/10/11) and after (H; © G. Arnaud-Fassetta, 2022/4/15) the demolition of homes that were repeatedly impacted by flooding.

Fig. 7 – Les facteurs aggravants ou atténuants de la crue des 14-15 octobre 2018 dans le bassin de l'Aude. *A : embâcle d'arbres et autres déchets dans le chenal étroit (corsetage) du Lauquet (© France 3 – LR) ; B : surverse de l'Orbiel par-dessus le Canal du Midi à Trèbes (© VNF, 15/10/2018, 07.45 TU) ; C : inondation de Villegailhenc par le Trapel (870 bâtiments inondés, pont de la D118 emporté, 4 morts ; © IRMA – S. Gominet, 17/10/2018) ; D : inondation de Trèbes par l'Orbiel, l'Aude et le Canal du Midi (6 morts ; © RGLR – C. Tignard) ; E : pollution à l'arsenic en aval de Salsigne, dans le bassin du ruisseau du Gourg Peyris, affluent du ruisseau du Rieu Sec, bassin de l'Orbiel (© O. Saint-Hilaire, 10/2018) ; F : tronçon de la Clamoux (affluent de l'Orbiel) restauré par le SMMAR (la large bande active permet désormais une atténuation de la puissance des crues et le stockage sédimentaire en amont des zones à enjeux comme Villegly ; © G. Arnaud-Fassetta, 22/11/2018) ; G et H : quartier Montplaisir (Conques-sur-Orbiel) dans la plaine d'inondation de l'Orbiel, avant la destruction par l'État des maisons maintes fois touchées par les inondations (G ; © G. Arnaud-Fassetta, 11/10/2021) et après (H ; © G. Arnaud-Fassetta, 15/4/2022).*

(*xvii*) Expropriations, amicable acquisitions, and revision of flood risk prevention plans (PPRI). In response to the repeated exposure of certain buildings to flood risk in the Aude WS, the French government has identified 170 structures deemed too dangerous. These buildings may be acquired through negotiated settlements or expropriated via the Barnier fund. The societal impacts of such changes are manifold (Larive and Marshall, 2022). The areas most affected include Trèbes (52 buildings), Villegailhenc (29 buildings), Couffoulens (20 buildings), and Conques-sur-Orbiel (18 buildings, including 15 houses in the Montplaisir district; fig. 7G, H). Following the Oct. 2018 flood event, the DDTM, in collaboration with the SMMAR, has determined that the PPRI (flood risk prevention plan) needs to be revised for approximately one hundred municipalities.

4.2. Bio-geomorphological impacts, sediment budget, and recurrence interval of the October 2018 flash-flood event in the Rieu Sec watershed

4.2.1. Geomorphological impacts of hydrometeorological event

According to MétéoFrance radar, between Oct. 14 at 19.00 UTC and Oct. 15 at 06.00 UTC, the Rieu Sec WS received between 250 and 300 mm of rain overall, with Conques-sur-Orbiel recording as much as 319 mm in just 11 h. However, this estimate is likely underestimated, as personal observations suggest the local total may have reached 800 mm. The orientation and position of the rain convergence line were precisely aligned with the Rieu Sec and Trapel valleys (fig. 8A). Rain fell continuously for 6 to 8 h across the entire length of the WS, with rainfall cells moving upstream in a WS elongated along the airflow direction. The small size of the WS (33.3 km^2) resulted in a rapid concentration of runoff, which was somewhat mitigated by two factors. (*i*) the elongated shape of the basin (K_c = 1.62), which helped attenuate the peak of the flood hydrograph at the beginning of the event, and (*ii*) the geology of the WS, particularly the permeability of the substrate (faults and joints), as evidenced by the resurgence of arsenic-laden water from Salsigne at the foot of the slopes (fig. 8B). However, given the intensity and volume of rainfall in the WS, infiltration remained modest, leading to a rapid Hortonian flow response. The steep slopes (with gradients of up to 80 %) and very high connectivity (97 %) between the slopes and the channel further facilitated the concentration of runoff and the conveyance of water to the valley floor. Overall, the effective hydro-morphological response time was extremely rapid, occurring within 1 to 2 h. Here, we define effective hydro-morphological response as the point at which the channel bed experiences significant changes. from plane bed channel stability to incision; the onset of floodplain deposition due to overflow; and a shift in channel pattern towards meandering or channel splitting.

We now analyze the hydro-morphological response in three distinct zones (A = upstream; B = midstream; C = downstream), consistent with the systemic analysis of the WS as defined by A. Surell (1841).

- Upstream Zone (A). It accounts for 33.9 % of the WS and is characterized by a rounded basin shape combined with significant relief (R_h = 0.1) and a high drainage density (D_d = 2.46). The confluence of five brooks (Sauzil; Pré de la Ferrière; Galiberne; Bagnadous; and Lacalm) each exhibiting steep gradients (11-21.4 %, Strahler orders 1 and 2), contributes to extremely rapid hydrological response times. Zone A is a major source of sediment due to the exposure of schist formations, which release substantial quantities of clay through weathering. This zone is predominantly characterized by erosion phenomena, including gullying on the slopes cut into schists, landslides at the base of the slopes, and incision in torrential channels. In the Rieu Sec riverbed, the presence of plane-bed facies indicates a balance between upstream sediment supply and downstream evacuation. In the channels, the average incision reached -2.8 m, and many ancient weirs were breached during the Oct. 2018 flood (fig. 9B). Energy is conserved in the confined channels (12 m wide), allowing specific stream power to reach maximum values of 8676 W/m^2. The fine sediment load in the brooks enabled the rapid transport of coarse debris downstream, facilitating the development of hyper-concentrated flows.

- Midstream Zone (B). Covering 64.6 % of the WS, it experiences a decrease in relief (R_h = 0.03) while displaying an increase in drainage density (D_d = 3.64), primarily due to the presence of impermeable rocks in the Tertiary molasses, and confluence ratios (fig. 8C). As a result, lower-order drains on steep slopes (8.8-15.2 %), primarily located on the left bank except in the downstream section, have reinforced the hyper-concentrated flows from Zone A. These hyper-concentrated flows are particularly evident in the Malabau riverbed, characterized by coarsening upward sequences, with metric boulders on the surface and sandy gravels at the base (fig. 9A). The Rieu Sec riverbed, which was 2 to 3 m wide before the flood, now exhibits active channels widened by an average of 21.6 m (ranging from 8.5 to 55.4 m; fig. 9C, D), enhanced avulsions (fig. 9G), and increased meander cutoffs. The already substantial sediment supply from upstream (Zone A) is further amplified by the near-complete erosion of the active channel, which exposes the geological substrate through floodplain erosion (fig. 9F, 10A). In some cases, the excavation of the alluvial floor has been extensive enough to expose ancient roads or hydraulic structures (fig. 10B-D) and old riparian vegetation (fig. 10E, F). This incision phenomenon, averaging -1.4 m, indicates sediment export that is partially balanced by inflows from tributaries (Malabau, Pech Agut, Sagnes, Gourg Peyris). In the Rieu Sec B., the mode of sediment transport operates at the interface between torrential bedload and hyper-concentrated flow. *In situ* observations of the deposits reveal a lack of distinct organization, particularly the absence of imbricated pebbles or coarsening upward sequence; instead, coarse particles on the surface seem to result from an armoring effect due to the leaching of fine particles at the end of the flood event (fig. 11A). Particle-size analyses (samples E1 and E2) show that the proportion of fine matrix (< 2 mm) varies from 16 % to 42 %, with the granulometric median (D_{50}) ranging from 8.5 mm to 13.9 mm, and the coarsest percentile (D_{99}) from 230 mm to 350 mm (fig. 11B). The deposits are poorly sorted ($1 < \sigma_I < 1.2$). These are almost certainly deposits that occur at the end of a flood, when energy levels decrease and the erosion process shifts to aggradation along the margins of the active channel or within the convexities. In wider active channels, the characteristic sedimentary facies include pools, bars, and riffles, clearly indicating the diversity of flow velocities in the lower gradient channel sections. The dissipation of energy in these low-gradient sections leads to flooding of the valley floor, alternating with the narrowing of the bedrock sections, which, in turn, results in homogenized flow velocities and high specific stream powers.

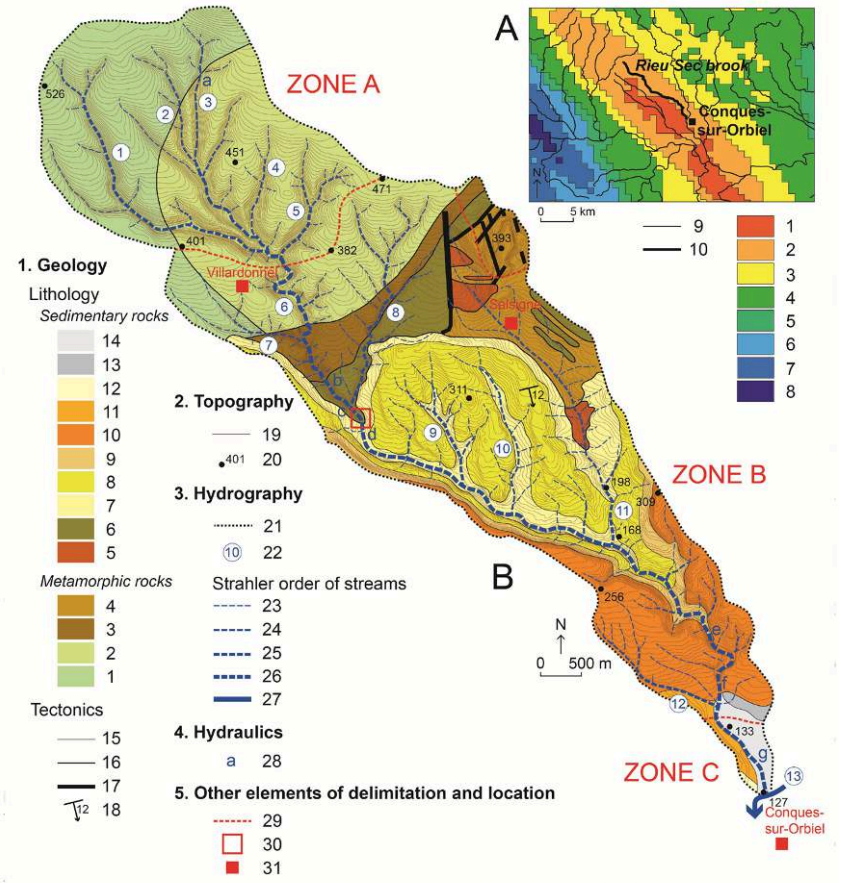

C

Rieu Sec watershed								Rieu Sec brook							Rieu Sec tributaries		
	Gravelius compactness index	Relief ratio	Drainage density (in km/km²)	Confluence ratio				Channel slope (in %)	Mean channel width (in m)		Width ratio (post-2018 flood / pre-2018 flood)	Mean channel incision (in m)	Specific stream power (in W/m²)		Channel slope (in %)		
	K_c	R_h	D_d	R_c Order 1 / Order 2	R_c Order 2 / Order 3	R_c Order 3 / Order 4	R_c Order 4 / Order 5	s	Before 2018 flood W_{BEF}	After 2018 flood W_{AFT}	R_w	I_{2018}	ω_{2018} Sites / values		s Order 1	s Order 2	s Order 3
ZONE A	1.62	0.1	2.46	4.8	3	3	0	6.7	2.7	12	4.5	-2.8	a	8676	21.4	11	5.1
ZONE B		0.03	3.64	6.1	4.2	5	0	1.5	4	21.6	5.4	-1.4	b	2384	15.2	8.8	4
								2					c	2119			
								1.2					d	2119			
								1					e	1423			
								1.3					f	612			
ZONE C		0.02	2.6	0	0	0	1	0.5	5	12.3	2.5	-0.8	g	54	-	-	-

Fig. 8 – The Rieu Sec brook, a right-bank tributary of the Orbiel River, which is itself a left-bank tributary of the Aude River in the Minervois region.

A: cumulative rainfall (in mm), as obtained via radar, from Oct. 14 at 19.00 UTC to Oct. 15 at 06.00 UTC, overlaid on rivers descending from the Montagne Noire (MétéoFrance data).

1. 300-250; 2. 250-200; 3. 200-150; 4. 150-100; 5. 100-80; 6. 80-60; 7. 60-50; 8. 50-40; 9. River; 10. Rieu Sec B.

B: map of the Rieu Sec WS (geological data. BRGM).

1. Algonkian or Cambrian (metamorphic rocks); 2. Algonkian or Cambrian (schists); 3. Sandtone-schist complex; 4. Middle or Lower Georgian (sandstone-schist complex, with alternating sandstone and limestone at the top); 5. Upper Georgian (varied limestones); 6. Gothlandian (Silurian) and Upper Devonian (compact limestones overlaid with slab limestones); 7. Montian (rusty clays, sands, sandstones, and conglomerates); 8. Thanetian (Montolieu limestone); 9. Sparnacian (red clays, sands, and white sandstones); 10. Lower Lutetian and Ypresian (marls and limestones); 11. Middle Lutetian (Vintenac limestone); 12. Upper Lutetian (varied molasses alternating with conglomerates); 13. Ancient alluvium; 14. Modern alluvium; 15. Normal contact between rocks; 16. Abnormal contact (angular unconformity); 17. Abnormal contact (fault); 18. Dip (direction and angle of layer inclination); 19. Isohypse (equidistance. 5 m); 20. Point with elevation (in m a.s.l.); 21. Stream name [1- Sauzil B., 2- Pré de la Ferrière B., 3- Galiberne B., 4- Bagnadous B., 5- Lacalm B., 6- Rieu Sec B., 7- Rivals B., 8- Malabau B., 9- Pech Agut B., 10- Sagnes B., 11- Gourg Peyris B., 12- Garrigue B., 13- Orbiel R.]; 22. Strahler order 1 (intermittent stream); 23. Strahler order 2 (intermittent stream); 24. Strahler order 3 (intermittent stream); 25. Strahler order 4 (intermittent stream); 26. Strahler order 5 (perennial river); 27. Location of cross-sections for the estimation of specific stream powers; 28. Subdivision of the WS in three zones (A, B, C); 29. Location of the studied stratigraphic sections; 30. Municipality.

C: physical characteristics of the Rieu Sec WS.

Fig. 8 – Le ruisseau de Rieu Sec, affluent de rive droite de l'Orbiel, lui-même affluent de rive gauche de l'Aude dans le Minervois.

A : cumul de précipitations (en mm) obtenu par radar du 14 oct. à 19.00 TU au 15 oct. à 06.00 TU superposé aux cours d'eau descendant de la Montagne Noire (données MétéoFrance).

1. 300-250 ; 2. 250-200 ; 3. 200-150 ; 4. 150-100 ; 5. 100-80 ; 6. 80-60 ; 7. 60-50 ; 8. 50-40 ; 9. Cours d'eau ; 10. Rieu Sec.

B : cartographie du bassin-versant du Rieu Sec (données géologiques. BRGM).

1. Algonkien ou Cambrien (roches métamorphiques) ; 2. Algonkien ou Cambrien (schistes) ; 3. Complexe gréso-schisteux ; 4. Géorgien moyen ou inférieur (complexe gréso-schisteux avec alternance de grès et de calcaires au sommet) ; 5. Géorgien supérieur (calcaires variés) ; 6. Gothlandien (Silurien) et Dévonien supérieur (calcaires compacts surmontés de calcaires en plaquettes) ; 7. Montien (argiles rutilantes, sables, grès et conglomérats) ; 8. Thanétien (Calcaire de Montolieu) ; 9. Sparnacien (argiles rouges, sables et grès blancs) ; 10. Lutétien inférieur et Yprésien (marnes et calcaires) ; 11. Lutétien moyen (Calcaire de Vintenac) ; 12. Lutétien supérieur (molasses variées alternant avec des conglomérats) ; 13. Alluvions anciennes ; 14. Alluvions modernes ; 15. Contact normal entre les couches ; 16. Contact anormal (discordance angulaire) ; 17. Contact anormal (faille) ; 18. Pendage (direction du pendage et angle d'inclinaison de la couche) ; 19. Isohypse (équidistance. 5 m) ; 20. Point coté (en m NGF) ; 21. Nom du cours d'eau [1- ruisseau de Sauzil, 2- ruisseau du Pré de la Ferrière, 3- ruisseau de la Galiberne, 4- ruisseau des Bagnadous, 5- ruisseau de Lacalm, 6- ruisseau de Rieu Sec, 7- ruisseau de Rivals, 8- ruisseau de Malabau, 9- ruisseau de Pech Agut, 10- ruisseau des Sagnes, 11- ruisseau du Gourg Peyris, 12- ruisseau de la Garrigue, 13- Orbiel] ; 22. cours d'eau temporaire d'ordre 1 (Strahler) ; 23. cours d'eau temporaire d'ordre 2 (Strahler) ; 24. cours d'eau temporaire d'ordre 3 (Strahler) ; 25. cours d'eau temporaire d'ordre 4 (Strahler) ; 26. cours d'eau pérenne d'ordre 5 (Strahler) ; 27. Localisation des sections en travers pour l'estimation des puissances spécifiques ; 28. Subdivision du bassin-versant en trois zones (A, B, C) ; 29. Localisation des coupes stratigraphiques étudiées ; 30. Commune.

C : caractéristiques physiques du bassin-versant du Rieu Sec.

Specific stream power values vary from 2384 to 612 W/m², decreasing from upstream to downstream in accordance with the reduction in channel gradient (fig. 8C).

- Downstream Zone (C). It covers only 1.5 % of the WS. Relief is minimal (R_h = 0.02) and drainage density is also low (D_d = 2.6), corresponding to the Rieu Sec alluvial fan. The channel features an average width of 12.3 m, a gentle slope of 0.5 %, and a specific stream power of 54 W/m², providing a relatively stable transport corridor for gravelly bedload. In the downstream part of Zone B, sediment and driftwood accumulate in the channel sinuosities and structural constrictions of the valley, which reduces the debris load entering the Orbiel R. via Zone C. The channel capacity of the Rieu Sec B. was significantly less than the volume of water and sediment that needed to be transported to the Orbiel R., leading to overflow into the flood plain (fig. 9H). This flood plain is characterized by the predominance of sand and clay, which spreads into the

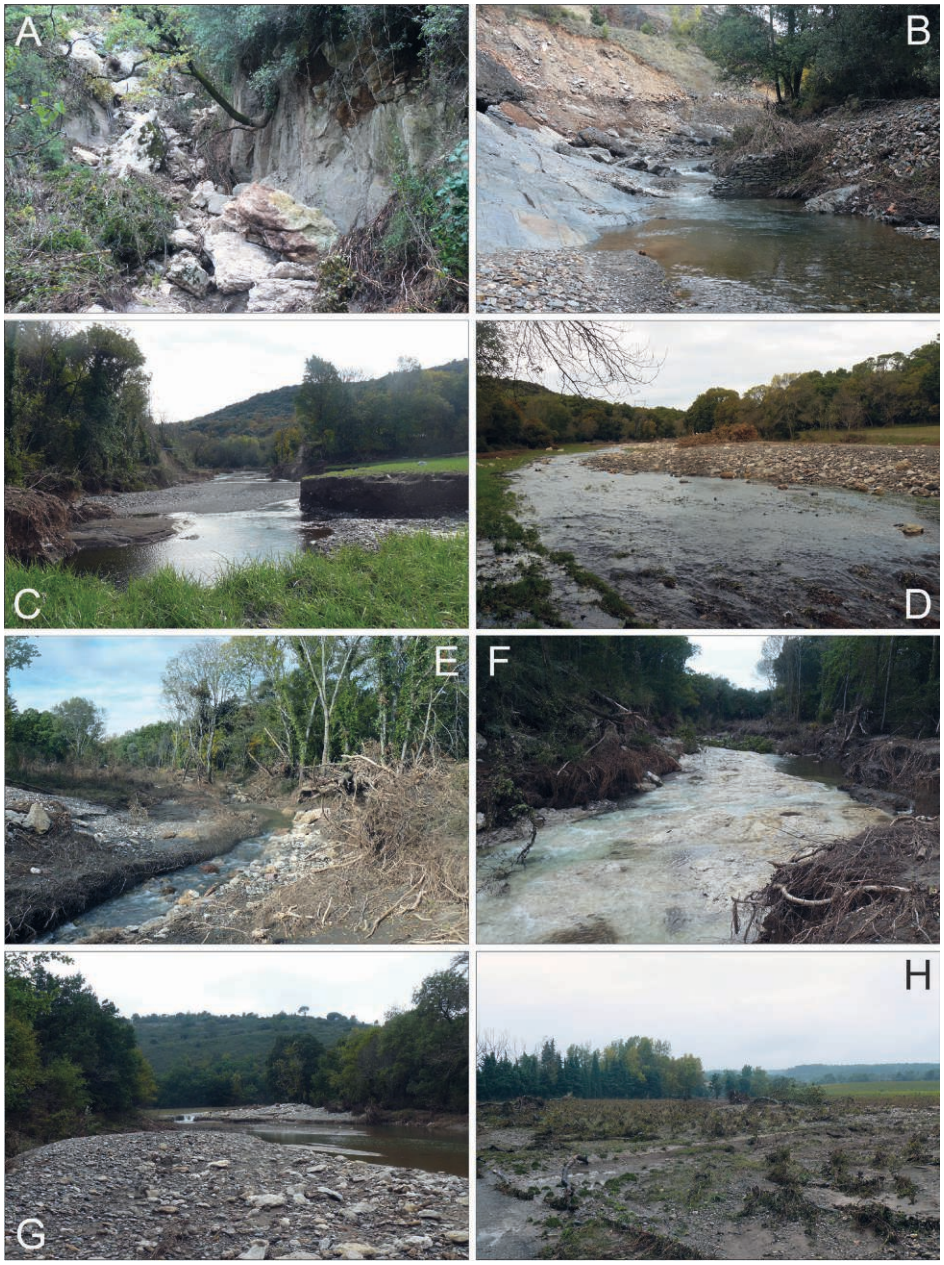

Fig. 9 – Hydro-geomorphological impacts of the October 14-15, 2018 flood event in the Rieu Sec watershed (Orbiel tributary). A: remnant of debris flow from the Malabau B., a left-bank tributary of the Rieu Sec B. (Zone B; © M. Dupuis, 2018/10/22); B: undercutting at the base of the slope and incision (-2 m) of the Upper Rieu Sec channel (Zone A), reaching down to the geological substratum (an old dry-stone weir has collapsed; © M. Dupuis, 2018/10/22); C: channel incision (-3 m) and widening (20-30 m) of the Rieu Sec B. (Zone B; © M. Dupuis, 2018/10/22); D: slope reduction (Zone B) in the Rieu Sec floodplain that is favorable for bedload deposition, forming an alluvial bar now bypassed by the channel (avulsion; © M. Dupuis, 2018/10/22); E: the presence of a dense alluvial forest in the Rieu Sec valley floor (Zone B) contributes to logjams, thereby slowing down the water flow (© M. Dupuis, 2018/10/22); F: scouring of the entire Rieu Sec valley floor by floodwaters, resulting in a channel incision of -2 m and widening of 15-25 m (© M. Dupuis, 2018/10/22); G: the reduction in slope promotes bedload deposition (alluvial bar), which impedes the flow of the Rieu Sec B. (Zone B) and forces it to carve out a new channel (avulsion) in what was previously the flood plain (© M. Dupuis, 2018/10/22); H: at the WS outlet (Zone C), bedload deposition occurs near the channel, and suspended matter (sand) accumulates in the flood plain, which was covered with vineyards that have been severely damaged or destroyed by the flood (© M. Dupuis, 2018/10/22).

Fig. 9 – Impacts hydro-géomorphologiques de la crue des 14-15 octobre 2018 dans le bassin du Rieu Sec (affluent de l'Orbiel). *A : reste d'un dépôt de lave torrentielle provenant d'un affluent (Malabau B.) du Rieu Sec (© M. Dupuis, 22/10/2018) ; B : sapement de pied de versant et incision (-2 m) du chenal du Rieu Sec amont (Zone A) jusqu'au substrat géologique (un vieux seuil en pierres sèches a cédé ; © M. Dupuis, 22/10/2018) ; C : incision (-3 m) du fond du lit et élargissement (20-30 m) du Rieu Sec (Zone B ; © M. Dupuis, 22/10/2018) ; D : secteur de réduction de pente (Zone B), favorable au dépôt de la charge de fond, contourné désormais par le chenal (défluviation ; © M. Dupuis, 22/10/2018) ; E : la présence d'une forêt alluviale dense dans le fond de vallée du Rieu Sec (Zone B) est favorable aux embâcles, donc à un ralentissement des eaux d'écoulement (© M. Dupuis, 22/10/2018) ; F : décapage de tout le fond de vallée du Rieu Sec par la crue (incision : 2 m ; élargissement : 15-25 m ; © M. Dupuis, 22/10/2018) ; G : la réduction de la pente est favorable au dépôt de la charge de fond, qui gêne l'écoulement du Rieu Sec (Zone B) et le pousse à creuser son nouveau chenal (défluviation) dans ce qui était auparavant la plaine d'inondation (© M. Dupuis, 22/10/2018) ; H : à l'exutoire du bassin-versant (Zone C), dépôt de la charge de fond près du chenal et de matières en suspension (sables) dans la plaine d'inondation recouverte de vignobles (très endommagées ou détruites par la crue (© M. Dupuis, 22/10/2018).*

vineyards and occasionally erodes in areas most susceptible to tractive currents (proximal flood plain).

In conclusion, the 2018 Oct. flood resulted in a significant widening of the Rieu Sec active channel. On average, the channel-width ratio (R_w) was 4.84 along the 17 km stretch of the Rieu Sec, with Zone B (11.1 km long) reaching a value of 5.36. R_w oscillates between 1.27 (minimum value) and 14 (maximum value). Channel In the Rieu Sec WS, the disproportionate extent of Zone B (64.6 % of the WS) emphasizes the significant sediment purging the valley floor has experienced, manifested in the widening and deepening of the active channels, which will affect the overall sediment budget.

4.2.2. Sediment budget

The quantification of sediment budgets through image processing corroborates field observations (fig. 12). Following the flood of Oct. 14-15, 2018, sediment budgets were calculated for the slopes, tributaries, and riverbed of the Rieu Sec in three WS zones (A, B, and C). Overall, the flood was erosive at the WS scale, resulting in a sediment budget deficit of -386,259 m^3, or -11,599 m^3/km^2 in less than 24 h. Zone B was the hardest hit by erosion, with a total of -305,618 m^3 (or 79 % of the overall erosion). All systems (slopes and rivers) consequently eroded more than they stored, except for Zone C, which had a surplus of 25,183 m^3.

On the slopes, gullying contributed to an erosion of -183,928 m^3, and landslides, primarily located at the foot of the slopes in zones A and B, accounted for an additional -30,000 m^3. Only a small amount of sediment remained stored in the WS, estimated at 15,328 m^3 for deposits related to upstream gully erosion, and 10,000 m^3 for remnants of landslides that were not removed by the rivers. In fact, most of the erosion products resulting from gullying and landslides have contributed to the hyper-concentrated flows of the rivers, primarily the Rieu Sec tributaries.

The tributaries of the Rieu Sec did not significantly contribute to sediment mobilization, except in the vicinity of confluences. The tributary that supplied the most coarse debris to the Rieu Sec B. is the Malabau B. (Zone B), which flows through the contact zone between schists and limestone. In contrast, the dense forest cover in the other tributaries has likely acted as a barrier against erosion. Ultimately, of the 34,597 m^3 of sediment mobilized in the tributaries, only a small portion (2203 m^3) became trapped in the riverbeds, while nearly all (32,394 m^3) of the sediment load was transported to the Rieu Sec B.

The reworking of the Rieu Sec floodplain was the primary source of input to the system. The widening and incision of the Rieu Sec active channel contributed 294,750 m^3 of sediment, with 44 % (129,445 m^3) remaining trapped in the floodplain. Zone B was the main contributor of sediment, accounting for 249,750 m^3 (85 %). In contrast, Zone C only stored 34,225 m^3 (14 %), indicating that a significant portion of the sediment load eroded from zones A and B was transported downstream to the Orbiel R., totaling 386,259 m^3.

The sediment budget will help determine whether the tributaries can compensate or not for the erosion occurring in the main valley floor. Collectively, the tributaries contributed 32,394 m^3 of alluvium to the Rieu Sec riverbed. This amount is less than the volume of sediment removed from the WS by the Rieu Sec B., which totaled 165,265 m^3. This indicates that nearly 81 % of the sediment removed originated from the reworking of the main valley floor (zones A and B) and was not compensated for by the tributaries. The complete purging of sediment from the valley floor following the flood reinforces this point and highlights the role of major flood events as long-term agents of incision, raising questions about the mechanisms of alluvial terrace formation (see Section 4.2.4 below).

In conclusion, while Surell's (1841) simplified model has been expanded, our findings illustrate that Zone A exhibits dominant erosion (-105,824 m^3), Zone C is characterized by dominant accumulation (25,183 m^3), and Zone B is primarily eroded (-305,618 m^3), showing evidence of significant (though unquantified) sediment transport processes. Sediment transport was equally effective in zones A and B; however, the narrowing of the valley downstream, coupled with final meander configurations and anthropogenic structures such as plane tree hedges, limited sediment transport to the Orbiel R. (Zone C), potentially influencing driftwood transport as well.

4.2.3. Assessment of the riparian forest

The impact of Oct. 14-15, 2018, flood event on riparian forest was analyzed in the valley bottoms, distinguishing between the riverbed of the Rieu Sec (17 km long) and that of its tributaries. The results are presented by zone (A = upstream; B = midstream; C = downstream) at the WS scale. The flood had a significant impact on the riparian forest, with 8.9 % (or 13.855 ha) of the forest in the riverbeds affected (fig. 12 C-F). In contrast, only 3.2 % of the forest was removed from the riverbeds of the Rieu Sec tributaries, with the Malabau B. accounting for 26 % of this loss. The brooks Gourg Peyris (20 %), Pré de la Ferrière (18 %), and Galiberne (18 %) contributed to a lesser extent. Overall, 96.8 % of the riparian vegetation was removed from the valley floor of the Rieu Sec B. Among the three notable zones where the riparian forest was cleared, the furthest downstream zone (between 9.6 and 14.4 km) experienced the most significant changes, with the greatest active-channel widening (fig. 12C). In Zone A, 1067 ha of riparian forest were cleared, representing 8.1 % of the valley-floor forest. This loss is greater than that in Zone C, where very few trees were uprooted due to the lower specific stream power of the Rieu Sec B. downstream. However, it is notably less than the impact in Zone B, where 12.153 ha of trees were uprooted by the flood, amounting to 13.7 % of the valley floor forest. In Zone B, this corresponds to an average uprooting width of 11 m along the 11.1 km stretch of the Rieu Sec. During this same stretch, the Rieu Sec active channel widened by an average of 21.6 m.

The Rieu Sec WS was predisposed to the extraordinary uprooting of trees from the valley floor due to floodwaters. Prior to the flood, the valley floor was densely forested (fig. 12E). The valley is narrow in relation to the volume of water that falls and runs off during severe hydro-meteorological events (such as intense downpours). The downstream funnel shape of the WS is created by structural constrictions that favor the accumulation of debris and driftwood in the meandering sections. Although specific stream powers are very high in the valley bottoms, discharge (and water height, reaching up to 5 m) is greater in the Rieu Sec bed. In addition, the two main tree species present in the valley floor exhibit varying adaptations to resist uprooting during floods. The black poplar (*Populus nigra*) is significantly better adapted than the common alder (*Alnus glutinosa*) due to its deep root system, which allows it to endure the hydraulic stresses associated with flooding.

Tree removal was primarily driven by bank erosion, which resulted from the widening and incision of the active channel,

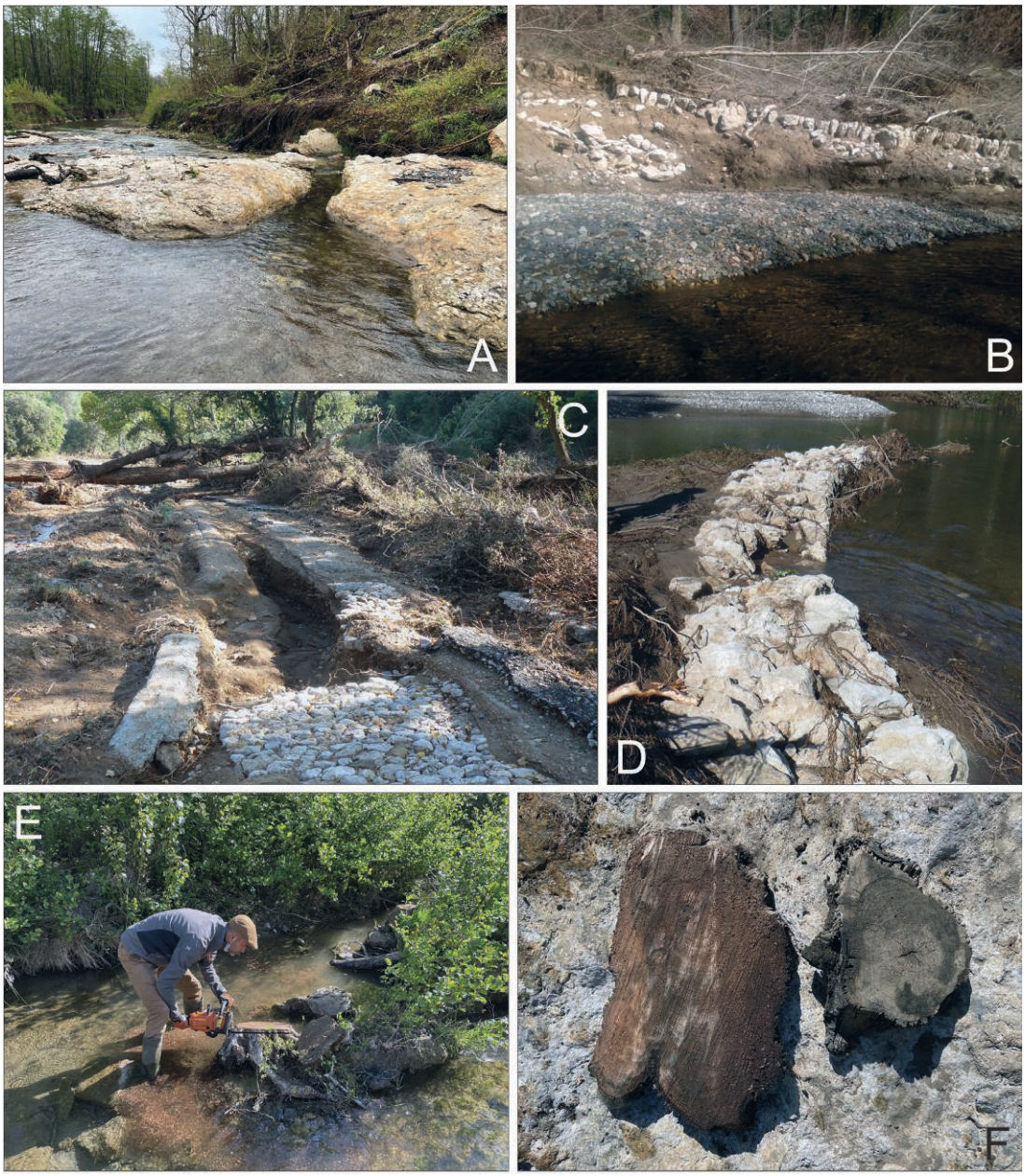

Fig. 10 – Exhumation, following the significant incision (at an average depth of 1 to 2 m) of the channel during the October 14-15, 2018, of bedrock, ancient tree trunks in a living position, and ancient structures that had been buried for centuries under the alluvial deposits of the Rieu Sec brook (Orbiel tributary). A: exhumation of the bedrock at the bottom of the Rieu Sec channel (longitudinal abrasion grooves, 30-40 cm wide and deep, cut into the bedrock by torrential flows, are polyphasic); B: remains of an old road partly eroded by the channel widening of the Rieu Sec B. during the flood (© T. Bellon, 2019/2/20); C: exposure of an old road by sediment stripping on the active-channel margin of the Rieu Sec B. during the flood (© M. Dupuis, 2018/10/22); D: remains of a dry-stone wall or (more likely) an old road (ford?) that were unearthed in the axis of the 2018 active channel (© M. Dupuis, 2018/10/22); E: sampling of the fossil trunk (section c, fig. 14) exhumed by the Oct. 14-15, 2018, flood event in the Rieu Sec active channel (© G. Arnaud-Fassetta, 2021/4/14); F: detail of two of the three fossil wood slices sent to the Beta Analytic laboratory (Miami) for radiocarbon dating (left slice. section c/fig. 14, age of tree determined by dendrochronology = 25 yrs; ^{14}C dating of wood = 220 ± 30 BP/Beta-521320; right slice = section b/fig. 14, age of tree determined by dendrochronology = 17 yrs; ^{14}C dating of wood = 220 ± 30 BP/Beta-59086; © G. Arnaud-Fassetta, 2021/4/14).

Fig. 10 – Exhumation, suite à l'incision conséquente (1 à 2 m en moyenne) du chenal les 14-15 octobre 2018, du lit rocheux, de vieux troncs d'arbre en position de vie et d'anciennes structures qui étaient enfouis depuis des siècles sous les alluvions du Rieu Sec (affluent de l'Orbiel). *A : exhumation du lit rocheux au fond du chenal du Rieu Sec (les cannelures d'abrasion longitudinales, de 30-40 cm de largeur et de profondeur, taillées dans le substratum par les écoulements torrentiels, sont polyphasées) ; B : restes d'une ancienne route en partie érodée par l'élargissement du lit du Rieu Sec durant la crue (© T. Belon, 2/2019) ; C : mise à jour d'une ancienne route par décapage des sédiments sur la marge de la bande active du Rieu Sec lors de la crue (© M. Dupuis, 22/10/2018) ; D : restes d'un mur en pierres sèches ou (plus probable) d'une ancienne route (passage à gué ?) qui ont été exhumés dans l'axe de la bande active de 2018 (© M. Dupuis, 22/10/2018) ; E : échantillonnage du tronc fossile (coupe c, fig. 14) exhumé par la crue des 14-15 oct. 2018 dans le lit du Rieu Sec (© G. Arnaud-Fassetta, 14/4/2021) ; F : détail de deux des trois rondelles de bois fossiles envoyées au laboratoire Beta Analytic (Miami) pour datation radiocarbone (rondelle de gauche. coupe c/fig. 14, âge de l'arbre déterminé par dendrochronologie = 25 ans ; datation ^{14}C du bois = 220 ± 30 BP/Beta-521320 ; rondelle de droite = coupe b/fig. 14, âge de l'arbre déterminé par dendrochronologie = 17 ans ; datation ^{14}C du bois = 220 ± 30 BP/Beta-590869 ; © G. Arnaud-Fassetta, 14/4/2021).*

Site	Sample	% (weight) - Wentworth (1922) grain-size classification					D_{50}	D_{99}	Inclusive Graphic Standard
		Gravel	Total S+Z+C	Sand	Silt	Clay	(in mm)	(in mm)	Folk and Ward (1957)
		G		S	Z	C			σ_1
Cross section a	SU 6	11	89	77	9	3	1.1	40	0.9
	SU 5	66	34	30	3	1	7.8	80	1
	SU 2	19	81	69	9	3	2.6	40	0.8
Cross section b	SU 6	12	88	75	10	3	1.2	50	0.9
	SU 5 (iii)	60	40	35	4	1	8.1	100	1
	SU 5 (ii)	20	80	70	8	2	2.8	50	0.9
	SU 5 (i)	50	50	41	7	2	24.1	260	1.8
	SU 2	18	82	67	11	4	2.4	90	0.9
Cross section c	SU 6	15	85	73	10	2	1.7	30	0.8
	SU 3	45	55	44	9	2	15.9	100	1.3
	SU 2	9	91	79	9	3	0.6	30	0.7
Cross section d	SU 6	17	83	72	9	2	1.9	30	0.8
	US 5 (iii)	55	45	38	6	1	9.7	120	1
	SU 5 (ii)	15	85	73	9	3	1.7	20	0.9
	US 5 (i)	49	51	41	8	2	20.1	180	1.7
	SU 4	19	81	69	10	2	2.2	20	0.9
	SU 3	47	53	43	8	2	17.2	100	1.2
	SU 2	7	93	80	10	3	0.6	20	0.7
	SU 1	59	41	25	13	3	19.5	380	1.3
October 14-15, 2018, deposit B	E1	84	16	12	3	1	13.9	350	1.2
	E1 (bed surface layer - armor)	100	-	-	-	-	32.4	550	-
	E2	58	42	38	3	1	8.5	230	1
	E2 (bed surface layer - armor)	100	-	-	-	-	15.9	450	-

Fig. 11 – Sedimentology of alluvial deposits observed on stratigraphic sections and in the Rieu Sec active channel. A: E2 sediment deposited along the margin of the Rieu Sec active-channel during the Oct. 15, 2018, river recession phase (© G. Arnaud-Fassetta, 2019/2/19). The image illustrates (a) the massive structure of the poorly sorted sediment and the significant proportion of fine matrix interspersed within the gravelly debris, as well as (b) the surface armoring; B: particle-size analysis.

Fig. 11 – Sédimentologie des dépôts alluviaux observés sur les coupes stratigraphiques et dans la bande active du Rieu Sec. *A : dépôt E2 mis en place en bordure du lit du Rieu Sec lors de la décrue du 15 oct. 2018 (© G. Arnaud-Fassetta, 19/2/2019). On observe (a) la disposition en vrac du matériel et le pourcentage élevé de matrice fine emballant les débris graveleux ainsi que (b) le pavage sommital ; B : analyse texturale des sédiments.*

and stripping process in the proximal flood plain. Torn-off tree trunks formed noticeable logjams, especially in Zone B. In the more confined areas of the floodplain, (*i*) where the riverbed did not deepen or widen excessively, logjams came to rest on the trees that had withstood uprooting (fig. 13A). In these instances, black poplars played a crucial role, being the most resistant to erosion (fig. 13B). (*ii*) When the riverbed suddenly dropped by up to 3 m, this created a disconnection between the calmer margins of the active channel and the proximal flood plain, where driftwood accumulated and pressed against the resilient trees, particularly the black poplars (fig. 13C, D). In the broader sections of the floodplain, often characterized by channel avulsion, (*iii*) trees were able to lean laterally against those that remained anchored, as the flows were poorly channeled (i.e., not deeply incised; fig. 13E). Conversely, (*iv*) downstream, where flows were strongly channeled due to the structural narrowing of the valley, trees accumulated in the center of the channel, obstructing a substantial portion of the sediment load traveling downstream (fig. 13F). These structural constrictions are thought to exacerbate logjams locally while mitigating their severity downstream. In Zone C, structures such as plane tree hedges (fig. 13G), with strong root systems oriented perpendicular to flood flows on the floodplain, acted as natural jam traps, restricting the supply of trees to Zone C and, further downstream, to the Orbiel R. and other high-risk areas (Conques-sur-Orbiel, Villalier, Trèbes).

In conclusion, the volume of driftwood that reached the Orbiel R. is considered negligible, which is quite extraordinary given that 13.855 ha of forest were removed from the upstream riverbeds in the WS. For instance, the passage beneath the bridge over the Rieu Sec

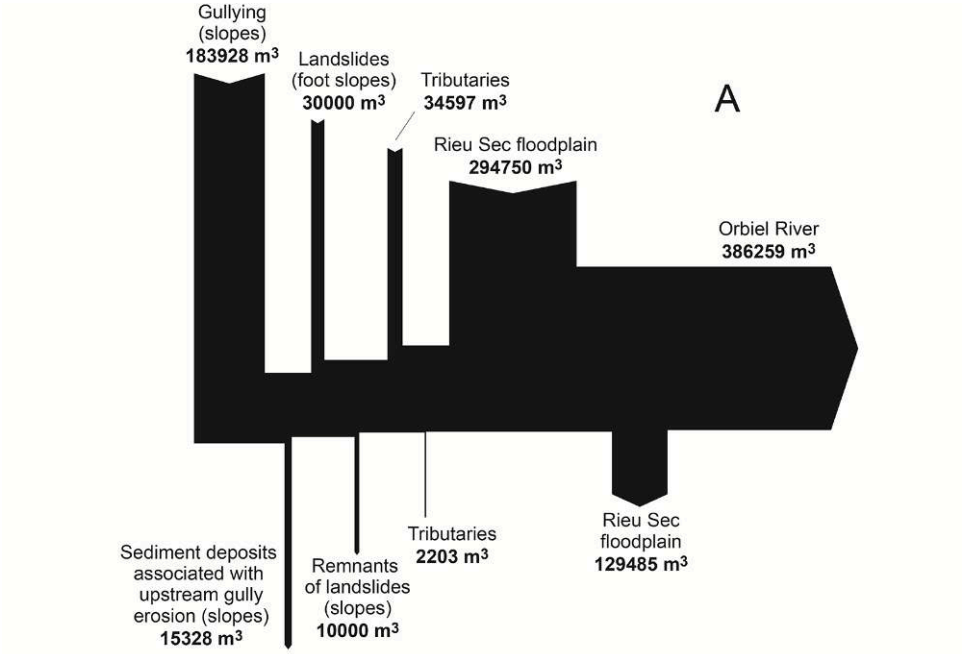

B

	Slopes							Rieu Sec tributaries			Rieu Sec riverbed			Rieu Sec watershed		
	Gullying			Landslides			Total									
	E	Ag	SB	E	Ac	SB	SB	E	Ag	SB	E	Ag	SB	E	Ag	SB
Zone A	-66466	5539	-60927	-15000	5000	-10000	-70927	-11840	943	-10897	-36000	12000	-24000	-129306	23482	-105824
Zone B	-117405	9784	-107621	-15000	5000	-10000	-117621	-22757	1260	-21497	-249750	83250	-166500	-404912	99294	-305618
Zone C	-57	5	-52	-	-	-	-52	-	-	-	-9000	34235	25235	-9057	34240	25183
Total	-183928	15328	**-168600**	-30000	10000	**-20000**	**-188600**	-34597	2203	**-32394**	-294750	129485	**-165265**	-543275	157016	**-386259**

E = Erosion (in m^3); Ag = Aggradation (in m^3); Ac = Accumulation (in m^3); SB = Sediment budget (in m^3)

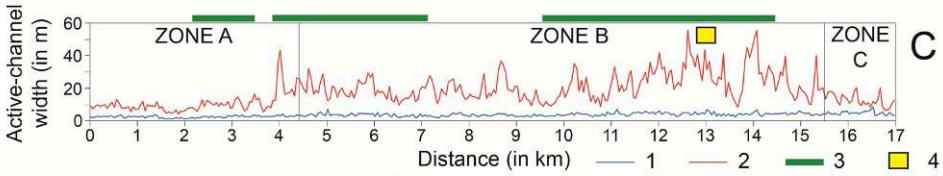

D

		Rieu Sec riverbed				Rieu Sec tributaries				Rieu Sec watershed			
		1. Forest removal		2. Area	Specific forest balance	1. Forest removal		2. Area	Specific forest balance	1. Forest removal		2. Area	Specific forest balance
		(in ha)	(in ha)	(in m^2)	(1/2, in %)	(in m^2)	(in ha)	(in m^2)	(1/2, in %)	(in m^2)	(in ha)	(in m^2)	(1/2, in %)
Zone A		10668	1.067	132200	-8.1	1887	0.189	90100	-2.1	12555	1.256	222300	-5.6
Zone B		121531	12.153	884200	-13.7	2521	0.252	1088300	-0.2	124052	12.405	1972500	-6.3
Zone C		1939	0.194	490300	-0.4	-	-	-	-	1939	0.194	490300	-0.4
Total	(in m^2 or ha)	134138	13.414	1506700	-	4408	0.441	1178400	-	138546	13.855	2685100	-
	(in %)	96.8		56.1	-8.9	3.2		43.9	-0.4	-		-	-5.2

Fig. 12 – Sediment budget and forest balance of the October 2018 flood event in the Rieu Sec watershed (Orbiel tributary). A: sediment budget of the Rieu Sec WS; B: detailed numerical sediment budget of the Rieu Sec WS; C: downstream evolution of the active-channel width of the Rieu Sec B; D: forest balance in the Rieu Sec WS. E: zoom on the active channel of the Rieu Sec B. at kilometer point 13 before the flood (2018/7/4); F: zoom on the active channel of the Rieu Sec B. at kilometer point 13 after the flood (2020/7/18), showing the uprooting of the riparian forest due to the flood impact. Photos E and F. IGN data.

1. Before the flood (2018/7/4); 2. After the flood (2020/7/18); 3. Area of tree uprooting in the riparian forest; 4. Fig. 12E, F.

Fig. 12 – Budget sédimentaire et bilan forestier de la crue d'octobre 2018 dans le bassin du Rieu Sec (affluent de l'Orbiel). *A : budget sédimentaire dans le bassin-versant du Rieu Sec ; B : détail chiffré du budget sédimentaire dans le bassin-versant du Rieu Sec ; C : évolution vers l'aval de la largeur de la bande active du Rieu Sec ; D : bilan forestier dans le bassin-versant du Rieu Sec ; E : zoom sur la bande active du Rieu Sec au point kilométrique 13 avant la crue (4/7/2018) ; F : zoom sur la bande active du Rieu Sec au point kilométrique 13 après la crue (18/7/2020), montrant l'arrachage de la ripisylve par la crue. Photos E et F. données IGN.*

1. Avant la crue (4/7/2018) ; 2. Après la crue (18/7/2020) ; 3. Secteur d'arrachage des arbres de la ripisylve ; 4. Fig. 12E, F.

B. at its confluence with the Orbiel R. was not obstructed by logjams (fig. 13H). The regulation of driftwood transport, primarily through natural processes, such as the role of black poplars in the riparian zone, and somewhat facilitated downstream by plane tree hedges oriented perpendicular to the flow, was remarkably effective in the Rieu Sec B. The amount of wood removed from the riparian forest during the flood of Oct. 14-15, 2018, was exceptional. S. Benaksas and G. Piton (2023) have proposed methods for converting the hectares of uprooted forest into cubic meters, utilizing the approach outlined by M. Quiniou and G. Piton (2022). If we take 1 ha of forest to equal 150-450 m^3 of wood, then the 13.855 ha of forest uprooted in the Rieu Sec WS is equivalent to approximately 2078-6235 m^3 of wood, or 62-187 m^3/km^2 of the WS, and more pertinent, 799-2398 m^3/km^2 of the valley floor. Furthermore, S. Benaksas and G. Piton (2023) propose a method to estimate the volume of logjams, assuming that a driftwood jam consists of 60 % void space. Under this assumption, the logjams that accumulated in the Rieu Sec WS could represent a volume of approximately 6235-15,588 m^3.

4.2.4. Recurrence interval of the flood event deduced from valley-floor dynamics

In the midstream zone (B) of the Rieu Sec WS, the flood that occurred on Oct. 14-15, 2018, resulted in the widening and deepening of the active channel, exposing new sediment outcrops deposited prior to the flood (fig. 14 A-C). During this event, the Rieu Sec B. incised its bed by 1 to 3 m down to the geological substratum, while simultaneously widening by 8.5 to 55 m, thereby revealing ancient sedimentary sequences along its left bank. Four specific stratigraphic sections were surveyed and analyzed (fig. 14D).

Stratigraphic sections, with a thickness of 2 to 3 m, reveal seven stratigraphic units (SU) overlying the bedrock, listed from bottom to top.

- Bedrock (apparent thickness in the field. 2 m). This consists of an outcrop of compact limestone that is overlain by slab limestone dating from the Silurian and Upper Devonian periods (stage 6 in fig. 8B). At the top of the limestone layer, the bed of the Rieu Sec B. exhibits incisions (grooves that are 20 to 40 cm deep and 30 to 60 cm wide) running in the direction of the valley, formed by concentrated runoff. The development of these grooves is multiphase, with average incision depths in the bedrock (limestone) ranging from a few millimeters to several centimeters per flash flood event (Sklar and Dietrich, 2001). Consequently, these grooves had already formed prior to 2018, having been exhumed by the subsequent incision of the Rieu Sec bed.

- SU1 (thickness. 0.5 m). This unit rests in angular unconformity on the bedrock and is only visible in section a downstream (fig. 14D). It consists of a fining-upward sequence (crudely graded flow unit) that is poorly sorted (s_i = 1.3), composed of boulders and cobbles (59 %) loosely arranged without any imbrication, and embedded in an abundant fine matrix (41 %). This channel deposit was formed through torrential flows with high competence (D_{50} = 19.5 mm; D_{99} = 380 mm) and exhibits a significant concentration of suspended solids.

- SU2 (thickness. 0.5-0.6 m). This unit is present in all stratigraphic sections and exhibits a distinct evolution from upstream to downstream. Upstream, it consists of silty-clayey sands (81-82 %) mixed with pebbles and granules (18-19 %), while downstream, the composition shifts to silty-clayey sands (91-93 %) with fewer pebbles and granules (7-9 %). This variation reflects a decreasing hydrodynamic influence as the valley floor widens. The deposits are very moderately sorted ($0.7 < \sigma_I < 0.9$), transported by a poorly selective, low-competence agent ($0.6 < D_{50} < 2.6$ mm). This unit corresponds to a quiet margin of an active channel or a proximal flood plain. Several fossil trunks corresponding to trees *in situ* have been found within this unit, three of which have been analyzed in detail. These trunks belong to *Alnus glutinosa*, a species not known for its longevity (averaging 60-80 yrs, with a maximum of 120 yrs). The ages obtained through dendrochronology range from 17 to 25 yrs, with an average age of 21 yrs, indicating that these are mature trees. Notably, the trunks bear saw marks, suggesting they were artificially truncated. *Alnus glutinosa* has a highly developed root system, but its soft wood is quite fragile. Once dead, it cannot be exposed to the open air for long without disintegrating rapidly. This indicates that these alders were quickly buried by alluvial deposits and preserved in a cold-water alluvial aquifer shortly after being cut. Three trunks were dated using ^{14}C dating method. The resulting ages ranged from 180 ± 30 yrs BP to 220 ± 30 yrs BP (fig. 14D), translating to calibrated ages of 1735-1806 cal. AD (54.9 %) or 1642-1684 cal. AD (45.1 %) for Beta-521320; 1731-1806 cal. AD (57.5 %) or 1640-1687 cal. AD (42.5 %) for Beta-590869; and 1722-1814 cal. AD (71.9 %) or 1656-1698 cal. AD (27.8 %) for Beta-590870. Considering their average age of 21 yrs, the trees likely emerged on the quiet margin of the active channel between AD 1619 and 1793, with a 61 % probability for the interval AD 1701-1793.

- SU3 (thickness. 0.3 m). This unit is present only downstream, specifically in stratigraphic sections c and d, and is in contact with SU2 through a gully unconformity, suggesting emplacement by a vigorous transport agent. The deposit is composed of loose cobbles and pebbles (45-47 %) embedded in an abundant fine matrix (43-44 %). The sediment grains are poorly sorted ($1.2 < \sigma_I < 1.3$) and transported by a highly competent agent ($15.9 < D_{50} < 17.2$ mm; D_{99} = 100 mm). SU3 is interpreted as a channel deposit formed by torrential, high-energy flows with high concentrations of suspended solids. The deposition of SU3 occurred after AD 1640-1814, with a 61 % probability for the interval following AD 1701-1793. This rapid deposition was crucial to preserving the wood of the alders it fossilizes, preventing degradation due to exposure to air.

- SU4 (thickness. 0.2 m). This unit is found only downstream in section d and consists primarily of silty-clayey sands (81 %) with some pebbles and granules (19 %; D_{99} = 20 mm). The deposit is very moderately sorted (Si = 0.9) and was transported by a low-competence agent (D_{50} = 2.2 mm). SU4 corresponds to a quiet margin of an active channel or a proximal flood plain.

- SU5 (thickness. 0.7-1.2 m). This unit is present in sections a, b, and d, but is absent from section c. In the upstream section (a), it is characterized by cobbles and pebbles (66 %; D_{99} = 80 mm) with a moderately abundant fine matrix (34 %). The deposit was formed by a transport agent that is not very selective (s_i = 1) but is highly competent (D_{50} = 7.8 mm). Downstream, the unit exhibits greater diversity, marked by two main assemblages. (i) boulders, cobbles, and pebbles (49-60 %; $100 < D_{99} < 260$ mm) combined with an abundant fine matrix (40-51 %), which is poorly sorted ($1 < \sigma_I < 1.8$), and (ii) silty-clayey sands (80-85 %) containing some gravels and granules (15-20 %; $1.7 < D_{50} < 2.8$ mm), which are very

Fig. 13 – Natural and anthropogenic driftwood trapping in the Rieu Sec watershed (Orbiel tributary) during the October 14-15, 2018, flood. A: blockage, almost in the axis of the Upper Rieu Sec riverbed (zone B), of driftwood by riparian trees that withstood the floodwaters (© M. Dupuis, 2018/10/22); B: a black poplar positioned in the axis of the Middle Rieu Sec riverbed (zone B), which was shaped by the Oct. 2018 floodwaters. This species is exceptionally adapted to strong currents and acts as a natural logjam trap (© G. Arnaud-Fassetta, 2021/4/14); C: Logjam located on the edge of the active channel along the left bank of the Middle Rieu Sec B., zone B (© G. Brousse, 2018/11/22); D: a detailed view of the logjam described in C, reaching almost 4 meters in height (© G. Brousse, 2018/11/22); E: support for logjams formed by riparian trees that resisted the floodwaters at the edge of the active channel of the Middle Rieu Sec B. (zone B) opened in Oct. 2018 (© G. Brousse, 2018/11/22); F: a logjam situated in the axis of the Middle Rieu Sec channel, located downstream of zone B in the last structural constrictions of the valley (© G. Brousse, 2018/11/22); G: a plane tree hedge (chemin de Vic, Conques-sur-Orbiel) functioned as an artificial driftwood trap in the Rieu Sec flood plain, zone C (© G. Arnaud-Fassetta, 2019/10/19). H : the cleared Rieu Sec bridge (Zone C) just upstream of the confluence with the Orbiel R. (© SMAC, 16/10/2018). The arrows indicate the direction of floodwater flow.

Fig. 13 – Piégeages naturels et anthropiques des bois flottés issus de l'arrachage de la ripisylve par la crue des 14-15 octobre 2018 dans le bassin du Rieu Sec (affluent de l'Orbiel). *A : blocage, quasiment dans l'axe du lit du Rieu Sec amont (zone B), des bois flottés par les arbres de la ripisylve ayant résisté aux flots de crue (© M. Dupuis, 22/10/2018) ; B : un peuplier noir dans l'axe du lit du Rieu Sec moyen (zone B) emprunté par la crue d'oct. 2018, une espèce parfaitement adaptée aux écoulements vigoureux et jouant le rôle de piège naturel à embâcles (© G. Arnaud-Fassetta, 14/4/2021) ; C : embâcle sur la marge de la bande active en rive gauche du Rieu sec moyen, zone B (© G. Brousse, 22/11/2018) ; D : détail de l'embâcle en C, accusant près de 4 m de hauteur (© G. Brousse, 22/11/2018) ; E : appui des embâcles sur les arbres de la ripisylve ayant résisté aux flots de crue en marge de la bande active du Rieu Sec moyen (zone B) ouverte en oct. 2018 (© G. Brousse, 22/11/2018) ; F : embâcle dans l'axe du chenal du Rieu Sec moyen dans les derniers resserrements structuraux en aval de la zone B (© G. Brousse, 22/11/2018) ; G : haie de platanes (chemin de Vic, Conques-sur-Orbiel) ayant joué le rôle de piège artificiel aux bois flottés dans la plaine d'inondation, zone C (© G. Arnaud-Fassetta, 17/10/2019). H : le pont du Rieu Sec (zone C) non embâclé en amont immédiat de la confluence avec l'Orbiel (© SMAC, 16/10/2018). Les flèches indiquent le sens d'écoulement des eaux de crue.*

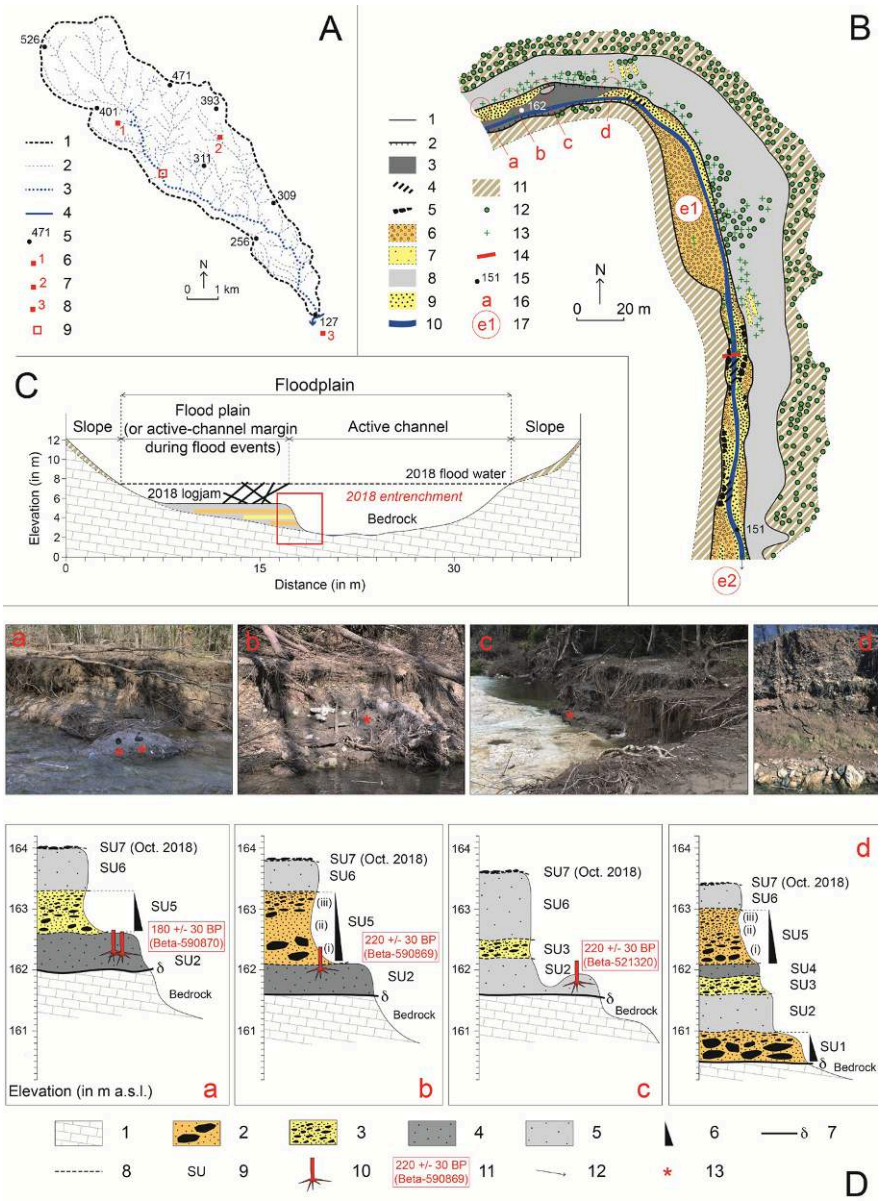

Fig. 14 – Stratigraphic sections in the Rieu Sec watershed (Orbiel tributary).

A: location of stratigraphic sections in the Rieu Sec WS.

1. Rieu Sec WS boundary; 2. Rieu Sec tributaries; 3. Rieu Sec B.; 4. Orbiel R.; 5. Elevation point (in m a.s.l.); 6. Villardonnel; 7. Salsigne; 8. Conques-sur-Orbiel; 9. Location of stratigraphic sections.

B: hydro-geomorphological map showing the impact of the Oct. 14-15, 2018, flood event in the floodplain of the Rieu Sec WS (Zone B). Floodplain.

1. Flood-plain boundary (Oct. 2018 active-channel margin); 2. Active-channel notch (Oct. 2018); 3. Bedrock (Oct. 2018); 4. Pool (Oct. 2018); 5. Large boulders (Oct. 2018); 6. Gravelly bar (Oct. 2018); 7. Sandy hydraulic dune (Oct. 2018); 8. Gravelly-sandy alluvial deposit on active-channel margin (Oct. 2018); 9. Shallow alluvial mat (primarily put in place in Oct. 2018, but more or less reworked after Oct. 2018); 10. Ordinary channel (Feb. 2019); Slopes. 11. Colluvium; Vegetation. 12. Tree; 13. Uprooted tree transported by Oct. 2018 floodwaters (logjam); Hydraulic structures. 14. 1960s concrete weir (destroyed in Oct. 2018); Topography. 15. Elevation point (in m a.s.l.); Other elements. 16. Stratigraphic section opened in Oct. 2018; 17. Alluvial sample collected for grain-size analysis.

C: general morphological context of the studied stratigraphic sections.

D: studied stratigraphic sections.

1. Limestone substratum; 2. Boulders, cobbles and pebbles with abundant fine matrix; 3. Cobbles and pebbles with abundant fine matrix; 4. Silty-clayey sands with some cobbles, pebbles and granules; 5. Silty-clayey sands with some pebbles and granules; 6. Fining-upward sequence (crudely graded flow units); 7. Angular discordance; 8. Erosional discordance; 9. Stratigraphic unit; 10. Fossil tree trunk in a living position; 11. Radiocarbon dating; 12. Direction of stream flow; 13. Location of fossil tree trunks in photos.

Fig. 14 – Coupes stratigraphiques dans le bassin du Rieu Sec (affluent de l'Orbiel).

A : localisation des coupes stratigraphiques dans le bassin-versant du Rieu Sec.

1. Limite du bassin-versant du Rieu Sec ; 2. Affluents du Rieu Sec ; 3. Ruisseau du Rieu Sec ; 4. Orbiel ; 5. Point coté (en m NGF) ; 6. Villardonnel ; 7. Salsigne ; 8. Conques-sur-Orbiel ; 9. Localisation des coupes stratigraphiques.

B : carte hydro-géomorphologique montrant les impacts de la crue des 14-15 oct. 2018 dans la plaine alluviale du bassin du Rieu Sec (zone B). Plaine alluviale.

1. Limite de la plaine d'inondation (marge de la bande active d'oct. 2018) ; 2. Entaille de la bande active (oct. 2018) ; 3. Lit rocheux (oct. 2018) ; 4. Mouille (oct. 2018) ; 5. Gros blocs (oct. 2018) ; 6. Banc graveleux (oct. 2018) ; 7. Dune hydraulique sableuse (oct. 2018) ; 8. Épandage d'alluvions gravelo-sableuses sur la marge de la bande active (oct. 2018) ; 9. Tapis d'alluvions peu épais (essentiellement mis en place en oct. 2018, mais plus ou moins remanié après oct. 2018) ; 10. Chenal ordinaire (fév. 2019) ; Versants. 11. Colluvions ; Végétation. 12. Arbre ; 13. Arbre déraciné et transporté par les flots de crue d'oct. 2018 (embâcle) ; Structures hydrauliques. 14. Seuil des années 1960 (détruit en oct. 2018) ; Topographie. 15. point coté (en m NGF) ; Autres éléments. 16. coupe stratigraphique ouverte en oct. 2018 ; 17. échantillon d'alluvions collecté pour la mesure de la taille des grains.

C : contexte morphologique général des coupes stratigraphiques étudiées.

D : coupes stratigraphiques étudiées.

1. substratum calcaire ; 2. Blocs, galets et graviers à matrice fine abondante ; 3. Galets et graviers à matrice fine abondante ; 4. Sables limono-argileux avec quelques galets, graviers et granules ; 5. Sables limono-argileux avec quelques graviers et granules ; 6. granoclassement normal (unités d'écoulement grossièrement classées) ; 7. Discordance angulaire ; 8. Discordance de ravinement ; 9. Unité stratigraphique ; 10. Tronc d'arbre fossile en position de vie ; 11. Datation radiocarbone ; 12. Sens d'écoulement du ruisseau ; 13. Localisation des troncs d'arbre fossiles sur les photos.

moderately sorted (s_i = 0.9). The competence of the deposit is strong at the base (20.1 < D_{50} < 24.1 mm) and decreases towards the top (8.1 < D_{50} < 9.7 mm), indicative of a fining-upward sequence. Overall, this unit is interpreted as an active-channel deposit characterized by significant hydrodynamic variability.

- SU6 (thickness 0.4-1.1 m). This unit is present in all sections and is characterized by silty-clayey sands (83-89 %) mixed with some very moderately sorted pebbles and granules (11-17 %; 30 < D_{99} < 50 mm) with a sorting coefficient (s_i) ranging from 0.8 to 0.9. It was deposited by a low-competence transport agent (1.1 < D_{50} < 1.9 mm). This unit corresponds to a proximal floodplain or a quiet margin active-channel deposit. A preliminary malacological analysis of the deposit indicates that *Pomatias elegans* (O.F. Müller, 1774) is the most abundant species present. This terrestrial snail is highly calcicolous and commonly found in hedges and undergrowth, typically inhabiting loose or stony soils where it can burrow to hibernate. It primarily feeds on decomposing leaves. In Mediterranean environments, *Pomatias elegans* often serves as

the dominant 'forest' taxon in Holocene fluvial series (Magnin et al., 2024). The deposit also contains a substantial presence of terrestrial *Helicidae* species and several individuals from the genus *Radix*, which are perennial aquatic species that cannot withstand even temporary drying conditions.

- SU7 (thickness: 0.1 m). This unit corresponds to the deposit resulting from the flood that occurred on Oct. 14-15, 2018. It exhibits a highly variable grain size and is very thin, as the flood was predominantly erosive in nature.

In conclusion, the analysis of the stratigraphic sections reveals an alternation between coarse deposits (indicative of high-energy active-channels) and fine deposits (reflecting calm margins of the active channels and proximal flood plains). This pattern suggests the functioning of a river characterized by significant lateral instability, which is marked by a contrasting hydrological regime that alternates between flash floods and periods of hydrological calm, typical of Mediterranean rivers (Arnaud-Fassetta et al., 2002). The formation of high-energy active channels occurs in a dynamic environment situated between torrential and hyper-concentrated flow (Pierson, 2005). These characteristics are evident in contemporary deposits (E1 and E2), which consist of coarse material ($8.5 < D_{50} < 32.4$ mm; $230 < D_{99} < 550$ mm) that are sometimes fining-upward sequences, but mainly consist of bulk material. The proportion of the fine matrix ranges from 16 % to 42 %, and the sorting is generally poor ($1 < \sigma_I < 1.2$).

This succession of floods interspersed with hydrological calms commenced during the Little Ice Age and has persisted to the present day. Chronological milestones established through radiocarbon dating (^{14}C) have enabled the reconstruction of this sequence's rhythm, based on the operational model depicted in fig. 15.

- Before AD 1619-1793 (61 % CI. AD 1701-1793). The valley floor was eroded down to the geological substratum by a high-magnitude, low-frequency flood event, comparable in intensity to the Oct. 2018 flood (fig. 15A).

- Between AD 1619 and 1793 (61 % CI. AD 1701-1793). A riparian forest of *Alnus glutinosa* became established along the calm margin of an active channel. After 21 yrs, these trees were artificially cut, and their remaining stumps were rapidly buried by deposits from a subsequent high-energy flood (fig. 15B-D).

- Between AD 1640-1814 (61 % CI. AD 1722-1814) and Oct. 14-15, 2018. The valley floor was infilled by alternating (*i*) deposits from high-energy but not exceptional floods and (*ii*) deposits associated with calm margins of the active channel or proximal flood plain, which supported thriving riparian vegetation (fig. 15D). Infilling between significant floods may occasionally have been partially anthropogenic, linked to the installation of weirs or leveling actions following floods that led to substantial sediment accumulation.

- On Oct. 14-15, 2018. A flash flood eroded parts of the valley floor deposits by widening and incising the active channel down to the geological substrate, while 13.855 ha of riparian forest were washed away by floodwaters (fig. 15E).

Finally, the long-term operating model of the Rieu Sec WS is characterized by (*i*) high-magnitude/low-frequency flood events that deepen and widen the riverbed while causing significant damage to riparian forest, and (*ii*) ordinary flood events, occasionally assisted by anthropogenic activities, that fill the valley floor and promote the growth of riparian forest (fig. 15F). The initial event (before AD 1619-1793; 61 % CI. AD 1701-1793) that purged the valley was indeed an exceptional flood. However, not every exceptional flood results in such phenomena; the sediment purge in 2018 could have mirrored events in 1999 (the flood of Nov. 12-13) or 1891 (the flood of Oct. 25), yet such purges did not occur. We have compiled a list of all exceptional floods recorded in the Montagne Noire since the 14th century (fig. 16). Radiocarbon dating indicates that the event responsible for the valley's sediment purging occurred prior to AD 1619-1793, with a 61 % probability of having taken place before AD 1701-1793. If we seek exceptional events prior to AD 1793, candidates include AD 1756, 1714, and 1680 floods. Furthermore, for dates before AD 1701, AD 1680 stands out as a notable event. Historical archives make no direct reference to events in the Orbiel WS before AD 1619, as studies primarily focus on flooding of the Aude R. However, an exceptional flood was documented on the Aude department in AD 1320, which seems to have impacted the Montagne Noire, as extensive flood damage was reported in Sallèles-d'Aude (Cesse R.).

5. Discussion

5.1. Evidence for an extraordinary flood event

In terms of spatial extent, the hydro-meteorological event of Oct. 14-15, 2018, was geographically limited to approximately 600 km^2. This is notably less extensive than the hydro-meteorological event of Nov. 12-13, 1999, which covered a much larger area (Fort et al., 2001; Arnaud-Fassetta et al., 2002). However, the Oct. 2018 event was characterized by its exceptionally short duration of less than 12 hours and several other remarkable features.

- Geographic shift. The hydro-meteorological event in 2018 occurred further west compared to 1999, clearly aligning with the boundary between the Mediterranean and Atlantic regions (Kreitz et al., 2020).

- Precipitation volume. Official reports documented up to 300 mm of rainfall in 24 h at Conques-sur-Orbiel, based on extrapolated data from a non-operational MétéoFrance radar system during the event. However, local farmers' observations suggest that actual rainfall amounts were closer to 800 mm within the same timeframe.

- Rapid river level rise. The Orbiel R. experienced a dramatic increase of 6 m in less than 4 h; the Lauquet R. surged by 6 m in just 2 h; and in the Salz R., the water level rose by 1 m within 5 min.

- River discharges. Many rivers reached discharges with a RI of 100 yrs, as the Aude R. between the confluences with the rivers Fresquel and Orbieu, which experienced extraordinary inflows from the rivers Fresquel, Trapel, and Orbiel. Maximum specific discharges reached 8 $m^3.s^{-1}.km^{-2}$, comparable to the extreme flooding events recorded in the south of France between 2015 and 2020 (fig. 5B).

Locally, within the Rieu Sec WS, the Oct. 14-15, 2018, flood reached its peak, exhibiting several significant characteristics.

- Flood RI. Stratigraphic studies suggest that the RI of this event is between 204 and 378 yrs, with a 61 % probability of it falling between 204 and 296 yrs. This is a refinement over previous meteorological and hydrological models, which provided a much broader estimate ranging from 100 to 2000 yrs.

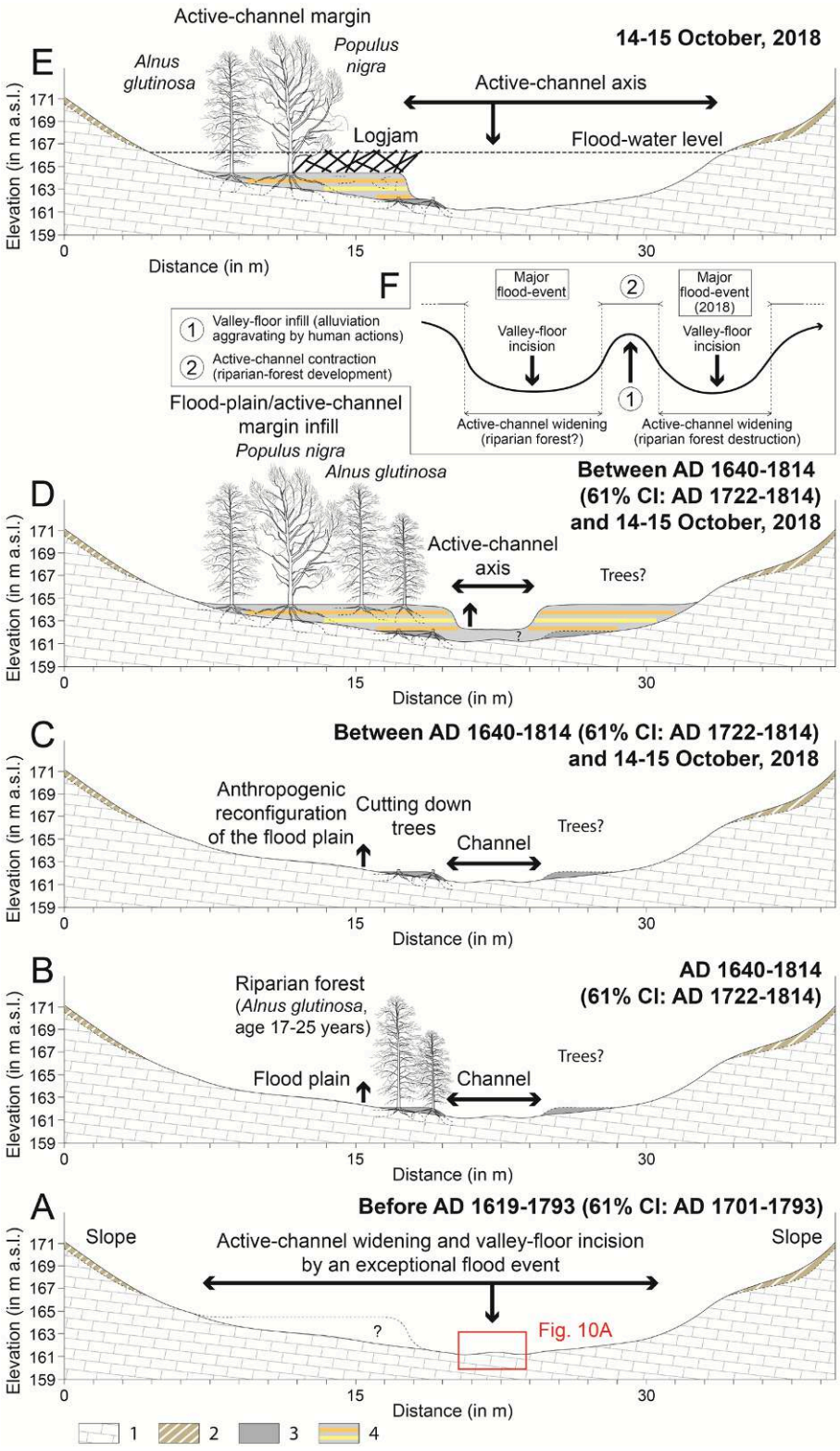

Fig. 15 – Hydro-geomorphological evolution model of valley bottoms in small watersheds of the Montagne Noire.

From A to E: synthetic stratigraphic cross-sections.

1. Limestone substratum; 2. Slope deposit; 3. Flood-plain deposit (silty-clayed sand); 4. Flood-plain/active-channel margin deposit (alternating silty-clayed sand and gravel with abundant, fine matrix).

F: morpho-sedimentary cycle emphasizing the role of major flood events in widening active channels and deepening the valley floor. In contrast, the processes of active-channel infill and contraction are driven by alluviation during small to medium-scale flood events, which are further influenced by human activities such as land leveling and the construction of weirs.

Fig. 15 – Modèle d'évolution hydrogéomorphologique des fonds de vallée dans les petits bassins versants de la Montagne Noire.

De A à E : coupes stratigraphiques de synthèse.

1. Substratum calcaire ; 2. Colluvions ; 3. Dépôt de plaine d'inondation (sables limono-argileux) ; 4. Dépôt de plaine d'inondation/marge de bande active (sables limono-argileux alternant avec des galets/graviers à matrice fine abondante).

F : cycle morpho-sédimentaire mettant en avant le rôle des crues majeures dans l'élargissement de la bande active et l'approfondissement du fond de vallée. En revanche, les processus de remblaiement et de contraction de la bande active sont provoqués par 1) l'alluvionnement lors d'événements de crue de faible à moyenne intensité et 2) aggravés par les activités humaines (nivellement du sol et construction de seuils).

- Hydro-morphological response. The effective hydro-morphological response was estimated to occur in less than 2 h, a duration that can be classified as very rapid.

- Valley floor erosion. In certain areas, the flood eroded the entire valley floor, widening and incising the active channel, and even revealing ancient erosion features and archaeological structures within the geological substrate.

- Channel-width ratio. The average R_w was recorded at an unprecedented 4.84, surpassing previous records. For comparison, R_w observed on the rivers Roya and Vésubie following Storm Alex in 2020 were 3.26 and 4.65, respectively (Liébault et al., 2024). Additionally, the Guil R., a tributary of the Durance R. in the Southern Alps, exhibited a R_w of 2.3 after the flood of 13-14 Jun. 1957 (Arnaud-Fassetta and Fort, 2014),

Fig. 16 – Chronology of flood events in the left-bank tributaries of the Aude River in the Minervois since the 14th century.

1. Frequent flood (RI between 5 and 30 yrs); 2. Remarkable flood (RI between 30 and 80 yrs); 3. Historic flood (RI > 80 yrs). Sources. Rousseau, 1875; Pardé, 1930a, 1930b, 1933a, 1933b, 1934a, 1934b, 1941; LeRoy Ladurie, 1967; Verdeil, 1999; Antoine et al., 2001; Vinet, 2003; Payrastre et al., 2006; SRTM, 2017; Larguier, 2018; MétéoFrance; Flood markers; PPRIs (flood risk prevention plans) for relevant WSs.

Fig. 16 – Chronologie des crues survenues dans les affluents de rive gauche de l'Aude dans le Minervois depuis le XIV^e siècle.

1. Crue fréquente (Q5-Q30) ; 2. Crue remarquable (Q30-Q80) ; 3. Crue historique (> Q80). Sources. Rousseau, 1875 ; Pardé, 1930a, 1930b, 1933a, 1933b, 1934a, 1934b, 1941 ; LeRoy Ladurie, 1967 ; Verdeil, 1999 ; Antoine et al., 2001 ; Vinet, 2003 ; Payrastre et al., 2006 ; SRTM, 2017 ; Larguier, 2018 ; MétéoFrance ; Repères de crue ; PPRI des bassins versants concernés.

which is nearly identical to the 2.32 ratio measured on the Argent Double R. following the flood of Nov. 12-13, 1999 (Arnaud-Fassetta, 2007).

- Sediment budget. A striking 81 % of the sediment discharged from the WS was attributed to the erosion of the floodplain by the Rieu Sec B. (trunk channel). The Oct. 2018 flood resulted in significant erosion throughout the WS, with an estimated volume of sediment exported from the WS reaching -386,259 m^3.

- Specific degradation rate. The specific degradation rate reached an impressive 11,599 m^3/km^2 in less than 12 h across the WS.

- Riparian forest impact. Approximately 9 % (or 14 ha) of riparian trees were uprooted, leading to a specific uprooting rate of 62-187 m^3/km^2 at the WS level, while this rate increased to 799-2398 m^3/km^2 at the scale of the floodplain (including the trunk channel and its tributaries).

- Driftwood transport. The natural regulation of driftwood transport, resulting from uprooted riparian forest, was facilitated by numerous logjams that captured driftwood within the WS. The role of the black poplar, with its strong root system, was essential in this process. In the downstream area of the WS, driftwood was effectively caught by a plane-tree hedge located along a path in the flood plain, positioned perpendicular to the direction of the floodwaters. Very little driftwood exited the WS, in stark contrast to the 2078-6235 m^3 of riparian trees that were removed.

We will conclude by examining the significant changes in the Rieu Sec WS, which can be described as a triple metamorphosis of river, forest, and landscape. However, it is essential to keep in mind the meaning of "fluvial metamorphosis", as articulated by Schumm (1977), which refers to a lasting transformation in a river's channel pattern. The key question revolves around the interpretation of 'lasting'. As geomorphologists, along with Schumm (1977) and Bravard (1998), we believe this concept pertains to "geomorphological time" (ranging from 10^2 to 10^4 yrs). Thus, if a river changes its channel pattern following a flood event, it does not necessarily undergo fluvial metamorphosis if the hydro-bio-morphological changes are temporary and the recovery time for the river spans only a few years. For instance, Arnaud-Fassetta and Fort (2014) demonstrated that the Guil R. reacted by widening its active channel each time a high-magnitude, low-frequency flood occurred (notable examples include June 1957 and June 2000 floods). Between the flood events, the active channel contracted as riparian forest reestablished, suggesting these changes did not constitute 'fluvial metamorphosis'. A similar model was observed in the Aude WS in 1999, when the flood of November 12-13 significantly widened the active channels, particularly in the Argent Double R., a left-bank tributary of the Aude R. in the Minervois region (R_w. 2.32). In the years following the flood (2000-2005), the riverbed and riparian forest gradually reestablished themselves in the areas they had previously occupied, as the managers undertook efforts to restore the channel to its original state (Arnaud-Fassetta and Fort, 2011). In contrast, since 2005, the reopening of riverbeds (initiated by M. Dupuis, SMMAR, in the Clamoux R.) through the removal of longitudinal structures has led many river sections to adopt a new channel pattern. This shift has rapidly and permanently transformed them from a sinuous, single-channel configuration to a more wandering pattern (Arnaud-Fassetta et al., 2024). In this scenario, where the action is irreversible – unless the river's lateral constraints are reconstructed due to anthropogenic factors – we can indeed speak of fluvial metamorphosis. The very idea of a short morphosedimentary cycle (ranging from 10^{-1} to 10^2 yrs) in the floodplain is generally incompatible with the concept of fluvial metamorphosis. Regarding the Rieu Sec WS, given that we observe a morphosedimentary cycle driven by major flood events (which have occurred randomly during the Little Ice Age and the current phase of global warming; fig. 15F) rather than as a result of a specific hydro-climatic period, it is more challenging to define this as fluvial metamorphosis in the sense of Schumm (1977), even though we remain within a multi-century morphosedimentary cycle. The question, however, remains open. Ultimately, it hinges on the WS's recovery time and its capacity to revert to its initial state, as described by Knighton (1998), from hydrographic, geomorphological, ecological, or landscape perspectives. Perhaps we also need to develop the concept, distinguishing between ephemeral and lasting metamorphoses.

5.2. A functional model of high-energy rivers. Confirming the importance of extreme flood events in shaping riverbeds

The study of the flood that occurred on Oct. 14-15, 2018, in the Aude WS, particularly in the Rieu Sec sub-WS in the Montagne Noire, reveals a specific functioning model of high-energy rivers. This model confirms the significance of extreme hydro-meteorological events in shaping riverbeds. In this model, applied to small mountainous WSs (< 40 km^2), it is shown that high-magnitude/low-frequency floods are erosive (in parallel with the active-channel widening) and lead to a sediment deficit at the WS scale. The relative stability of the system between floods, aided or not by human actions (such as the construction of weirs, leveling of the active-channel margins and the proximal flood plain), promotes the development of riparian forest and the alluvial infilling of the valley bottom, in parallel with the active-channel contraction (fig. 15F). The stratigraphic study also illustrates the impact of societies on riparian zones, particularly through deforestation actions over recent centuries.

This 'erosive' (or degrading) functioning model applied to small mountainous WSs is the opposite of what is observed in the piedmont areas, where floods contribute large amounts of sediment while also widening the active channels, whereas, between floods, ordinary flows contribute to the erosion of the main channel (Arnaud-Fassetta et al., 2024). In the Aude WS, an analogue to the 2018 event can be found in 1999, when the flood of Nov. 12-13 in the Rieussec B., a tributary of the Argent Double R. in the Montagne Noire, led to significant erosion of the valley bottom (Fort et al., 2001), while in the piedmont, numerous channel avulsions contributed to the aggradation of the valley bottom (Arnaud-Fassetta et al., 2002). Unfortunately, today, the only natural sources of alluvial replenishment for the piedmont areas are these exceptional floods events and their impacts in the mountains. Most of the time, the lack of renewal of the alluvial stock inherited from the Little Ice Age, the disconnection between the WS and the channel, and the reforestation of the mountainous massif severely limit sediment contributions from the mountain, resulting in alluvial deficits for rivers in the piedmont (Arnaud-Fassetta et al., 2024).

The floods of Oct. 2020 in the Roya and Vésubie WSs demonstrate a functioning model where floods are aggradational while also widening the active channel (Liébault et al., 2024). One can certainly add the Upper Guil R. upstream of Château-Queyras after the Jun. 1957 flood event (Tricart, 1958; Arnaud-Fassetta and Fort, 2014). This apparent dichotomy between 'aggradational' and 'degradational' models is not a true dichotomy. It is important to view these models as complementary within the longitudinal continuum of the WS. The transition from one model to another can be explained by numerous hydro-geomorphological variables, including WS size, sediment supply from the WS and the impacts of erosion within the WS, the position of the studied section within the WS (thus, its Strahler order), the confinement index of the valley bottom, the specific stream power of the river relative to its transport capacity, and local geomorphological configurations. Every aggradational model is preceded upstream by a degradational model, aligning with classical considerations on the functioning of the 'WS' (Surell, 1841; Tricart, 1962; Chorley, 1969; Schumm, 1977; Brierley and Fryirs, 2005; Fort et al., 2025). In all cases, all models emphasize the crucial role of high-magnitude/low-frequency events in shaping riverbeds in Mediterranean regions and allow for discussions on hydro-bio-morphological adjustments between flood events.

5.3. High variability of flood recurrence intervals in the Aude watershed

The study highlights a significant variability in the return frequencies of extreme hydrometeorological events in the Aude WS. This finding is supported both at the event scale and throughout historical data.

The hydrometeorological event of Oct. 2018 demonstrates that, aside from a specific area focused on the Trapel, Orbiel, and Lauquet sub-WSs, where the RI could reach 204-378 yrs (Rieu Sec WS), the remainder of the Aude WS was not significantly impacted by the effects of rainfall (fig. 5A). The hydrometeorological event of Nov. 1999 had a larger geographical footprint and was more prolonged, characterized by higher cumulative rainfall and more variable intensities, at times reaching significant levels and accompanied by thunderstorms. Furthermore, the peak of this event was displaced eastward in comparison to that of 2018; the heaviest rainfall primarily impacted the eastern Corbières, the Minervois, and the eastern Cabardès. The most affected areas were the Orbieu WS on the right bank of the Aude R., as well as the Argent-Double and Clamoux WSs on the left bank, along with the Berre WS, which is located closer to the coast. Among the six monitoring stations (Les Martyrs, Cuxac-Cabardès, Conques-sur-Orbiel, Arquettes-en-Val, Lézignan-Corbières, and Caunes-Minervois) that measure 24-hour rainfall totals (in mm), none recorded the maximum total for both 1999 and 2018, with the 1999 event holding the record for the highest total on four occasions (Kreitz et al., 2020).

In historical terms, chronicles indicate the occurrence of flood events that (*i*) often did not have the same intensity depending on the considered sub-WS, (*ii*) affected only a portion of the sub-WSs, or conversely, (*iii*) were widespread across the entire Aude WS (fig. 16). However, the Aude WS and the Aude department, in particular, are regularly exposed to floods of varying magnitudes. All events are documented in the chronicles with impacts that range from more or less damaging consequences and varying degrees of changes in channel width, erosional phenomena, and the extent of flooding. Additionally, there are damages to homes, infrastructure, crops, and individuals. Therefore, it is very challenging to attribute a generalized RI to a flood event, as its impacts are often distinct even within nearby sub-WSs or within the same sub-WS. What remains to be monitored in the future is the RI of hydrometeorological events in the western part of the Aude WS. To summarize the question was the flood of Oct. 2018 in the Aude WS an isolated phenomenon, or does it mark the beginning of a trend where Mediterranean-type extreme rainfall is shifting toward the Atlantic façade (Dubreuil, 2022)?

5.4. Will climate change lead to more severe catastrophic floods?

The ongoing impacts of climate change and its potential to increase the frequency and severity of hydrological disasters warrants careful consideration. Will we witness a recurrence of extreme events similar to those experienced in the Aude WS on Oct. 14-15, 2018? Are these high-magnitude, low-frequency hydro-meteorological events – often resulting in tragic consequences – indicative of climate change?

In the Aude department, the signs of ongoing climate change are evident in several ways (GIEC and MétéoFrance data) : a significant rise in average annual temperatures (+1.5 °C since the 1970s), with a current increase of +0.3°C per decade; a 20 % increase in the intensity of extreme rainfall events (those exceeding 150 mm), which are now impacting larger areas; a 10 % decrease in rainfall in Carcassonne over the past 50 yrs; and increasingly early and severe low-water levels in rivers. Climatologists predict that this trend will persist at a well-defined rate until 2050. The climate conditions at the end of the century will be directly influenced by the trajectory of greenhouse gas emissions during the current period. Climate projections for Occitanie region up to 2050 indicate greater precipitation variability, with expectations of. stability or a slight decrease (0 to -3 %) in annual accumulated precipitation, though with considerable uncertainty depending on the model (±20 %); a slight increase in winter precipitation (+5 %) coupled with a significant reduction in summer rainfall (-15 %); and a rise in both summer droughts and extreme rainfall events. Based on SIM2 simulations from the Explore2 project, annual river flows are anticipated to decline significantly (-5 to -10 % for the Aude R. in Carcassonne).

Consequently, while the frequency of extreme rainfall may not see a rise, its intensity is expected to increase, resulting in a more virulent flood hazard. In a context of uncontrolled urbanization or heightened urban vulnerability, floods could pose even greater dangers and cause more extensive damage. Effectively managing the escalating intensity of flood phenomena in the near future thus necessitates addressing and mitigating the vulnerability of our territories. Reducing vulnerability has already been implemented in the Orbiel WS, exemplified by the expropriation of an entire housing estate in Conques-sur-Orbiel (Montplaisir district; fig. 7G, H), where detached houses were situated in highly flood-prone and hazardous areas. Similar actions have been taken in Trèbes (Aude

R., Orbiel R., Canal du Midi) and Villegailhenc (Trapel R.). Efforts to reduce the intensity of flooding hazards are also underway, as seen with SMMAR since 2004 and SMAC since 2017, which have focused on riverbed restoration projects designed to slow flows and capture bedload and driftwood (Arnaud-Fassetta et al., 2024).

Lastly, it is important to clarify the historical context of flood events in the Rieu Sec WS over the past few centuries. The last significant flood event prior to Oct. 2018 likely occurred during the Little Ice Age. This paleo-hydro-climatic perspective highlights the challenge of distinguishing between isolated events and broader climatic trends in the Mediterranean region. We argue that neither the initial flood during the Little Ice Age nor the subsequent event in Oct. 2018 should be interpreted as clear signs of climate change. A single event cannot adequately represent a flood-dominated regime (as proposed in G. Arnaud-Fassetta's concept of the 'hydrological crisis', 1998), nor signify climate change, especially in the Mediterranean, where rivers exhibit a markedly contrasting hydrological regime.

6. Conclusions

The fine systemic analysis of the hydrometeorological event of Oct. 14-15, 2018, enabled the identification, for the first time, of all the factors of predisposition, triggering, and aggravation/mitigation that explain the genesis, impacts, and management of the event in the Aude WS. Attention was then focused on one of the parts of the WS that received the highest cumulative precipitation, namely the Rieu Sec WS, a right-bank tributary of the Orbiel R. in the Minervois region. Evidence is presented that the Oct. 2018 event was extraordinary in several respects. a geographic shift towards the west of extreme rains that had previously been concentrated more to the east of the Aude WS; a very significant volume of precipitation (up to 800 mm/12 h) considering the reality of the rainfall; a rapid river level rise (up to 1 m within 5 min); river discharges reaching or even exceeding the centennial RI and maximum specific discharges comparable to the extreme flooding events recorded in southern France between 2015 and 2020; locally, within the Rieu Sec WS, the RI is estimated at 204 and 378 yrs, with a 61 % probability of it falling between 204 and 296 yrs, based on the stratigraphic study; a very rapid hydro-morphological response (less than 2 h); valley floor erosion revealing ancient erosion features and archaeological structures within the geological substratum; a high R_w (4.84); a negative sediment budget (-386,259 m^3), with 81 % of the sediment discharged from the WS attributed to the erosion of the floodplain by the Rieu Sec B. (trunk channel); a specific degradation rate reaching an impressive 11,599 m^3/km^2 in less than 12 h across the WS; approximately 9 % (or 14 ha or 2078-6235 m^3) of riparian trees uprooted, leading to a specific uprooting rate of 62-187 m^3/km^2 at the WS level, while this rate increased to 799-2398 m^3/km^2 at the scale of the floodplain (including the trunk channel and its tributaries); natural regulation of driftwood transport, resulting from uprooted riparian forest, was facilitated by numerous logjams that captured driftwood within the WS. Very little driftwood exited the WS.

All these observations and measurements allowed us to establish a model of the functioning of small mountainous WSs (< 40 km^2), in which high-magnitude/low-frequency floods play a major role in the hydro-bio-geomorphological dynamics of valley floors. The model is degradational/active-channel widening in the mountain during major flood events. An analogue to Oct. 2018 in the Aude WS is the hydrometeorological event that led to the flood of Nov. 1999, but the impacts, duration, spatial extent, and management differ between the two events. In Oct. 2018, while in the mountains the flood caused significant erosion in the WSs (*e.g.*, Rieu Sec), on the piedmont, it instead contributed to refilling the active channels, which is essential in the context of chronic sediment deficit in the sub-WSs, particularly in the Minervois region. We will conclude with the significant variability in rainfall observed from one sub-WS to another, which creates difficulties in managing rains and floods. We will particularly mention MétéoFrance, which had to adapt its rainfall forecasting method in the Aude department, called the "*méthode audoise*". The challenge for the future lies in enhancing flood forecasting and the effective dissemination of these forecasts.

Acknowledgements

The authors would like to express their gratitude to Nicole Limondin-Lozouet, Étienne Grésillon, ADREUC, OFB, SMMAR, SMAC, the editorial committee of the journal, and the anonymous reviewers for their valuable contributions and support.

References

Amaral I. (1968) – As inundações de 25/26 de Novembro de 1967 na região de Lisboa. Finisterra, 3 (5), 80–84. DOI :10.18055/Finis2513

Antoine J.M., Desailly B., Gazelle F. (2001) – Les crues meurtrières, du Roussillon aux Cévennes. Annales de Géographie, 622, 597–623. DOI : 10.3406/geo.2001.1704

Arnaud P., Cantet P., Perrin C., Bourgin F., Thirel G. (2014) – Détermination des incertitudes de la méthode SHYREG calée localement. Propagation des incertitudes de la pluie et rôle du calage du modèle hydrologique sur l'incertitude des débits. Unpublished report, IRSTEA, 20 p.

Arnaud-Fassetta G. (1997) – Évolution du plancher alluvial du Petit Rhône à l'échelle pluriannuelle (delta du Rhône, France du Sud). Géomorphologie : relief, processus, environnement, 3 (3), 237–256. DOI :10.3406/morfo.1997.922

Arnaud-Fassetta G. (1998) – Dynamiques fluviales holocènes dans le delta du Rhône. Thèse de géographie physique, université de Provence (Aix-Marseille 1), 329 p. Atelier National de Reproduction des Thèses, Villeneuve d'Ascq, numéro ANRT 27620, 358 p.

Arnaud-Fassetta G. (2007) – L'hydrogéomorphologie fluviale, des hauts bassins montagnards aux plaines côtières, entre géographie des risques, géoarchéologie et géosciences. Habilitation à diriger des recherches (HDR) en géographie physique, université Paris-Diderot (Paris 7), 3 vol., 35 p., 435 p. et 357 p.

Arnaud-Fassetta G., Fort M. (2011) – Dix ans de recherches hydrogéomorphologiques dans le département de l'Aude et

une question, comment parvenir à réduire le risque de crue en domaine méditerranéen ? In Fort M., Ogé F. (Eds.) Actes du colloque international « Risques naturels en Méditerranée occidentale », 16-21 novembre 2009, Carcassonne, France. Reproduction Héliographique Audoise, Carcassonne, 33–52.

Arnaud-Fassetta G., Fort M. (2014) – Hydro-bio-morphological changes and control factors of an upper Alpine valley bottom since the mid-19th century. Case study of the Guil River, Durance catchment, southern French Alps. In Carozza J.M., Devillers B., Marriner N., Morhange C. (Eds.) The Little Ice Age in the Mediterranean. Méditerranée – Revue géographique des pays méditerranéens (Journal of Mediterranean geography), 122, 159–182. DOI :10.4000/mediterranee.7245

Arnaud-Fassetta G., Ballais J.L., Béguin É., Jorda M., Meffre J.C., Provansal M., Roditis J.C., Suanez S. (1993) – La crue de l'Ouvèze à Vaison-la-Romaine (22 septembre 1992). Ses effets morphodynamiques, sa place dans le fonctionnement d'un géosystème anthropisé. Revue de géomorphologie dynamique, 62 (2), 33–48.

Arnaud-Fassetta G., Beltrando G., Fort M., Plet A., André G., Clément D., Dagan M., Méring C., Quisserne D., Rycx Y. (2002) – La catastrophe hydrologique de novembre 1999 dans le bassin-versant de l'Argent Double (Aude, France), de l'aléa pluviométrique à la gestion des risques pluviaux et fluviaux. Géomorphologie : relief, processus, environnement, 8, 1, 17–34. DOI : 10.3406/morfo.2002.1125

Arnaud-Fassetta G., Brun M., Brousse G., Michler L., Chauvet Y., Dorval I., Flesch C., Gonod B., Magallon N., Pignot K., Thas É., Yvars M., Berthelot P., Tourade F., Cuisenier C., Jouanny J., Krouch M., Espiaut M.A., Fontanieu N., Bellon T., Perrine L., Walentin V., Gros J., Vallin T., Theureaux O., Chabre C., Picot M., Fort M., Melun G., Mercier O., Tomanova S., Corenblit D., Housset F., Dupuis M., Pouillat M. (2024) – Twenty-five years of hydromorphological restoration in high-energy, gravel-bed rivers of southern France. What are the current benefits for bedload dynamics and sediment balance in the left-bank tributaries of the Aude River within the Minervois region? Géomorphologie: relief, processus, environnement, 30 (2), 115–148. DOI : 10.4000/12m3m

Arnaud-Fassetta G., Cossart É., Fort M. (2005) – Hydro-geomorphic hazards and impact of man-made structures during the catastrophic flood of June 2000 in the Upper Guil catchment (Queyras, French Alps). Geomorphology, 66, 41–67. DOI : 10.1016/j.geomorph.2004.03.014

Astrade L., Jacob N., Bravard J.P., Alvarez C. (1999) – Dynamique sédimentaire d'un cours d'eau de montagne court-circuité. La haute vallée de l'Aude à l'aval du barrage de Puyvalador (France). Bulletin de la Société géographique de Liège, 37 (2), 91–109.

Ayphassorho H., Pipien G., Guion de Meritens I., Lacroix D. (2019) – Retour d'expérience des inondations du 14 au 17 octobre 2018 dans l'Aude. Unpublished report CGEDD 012561-P, IGA 18105-RP, 176 p.

Benaksas S., Piton G. (2023) – Action Embâcle. Sources, risques et mesures associés. Outils et recommandations. Rapport final de la Tâche 4. Retour d'expérience sur les pièges à bois flottant. Institut des Géosciences de l'Environnement, 43 p.

Bérenger M. (1960) – Les types de temps en Méditerranée. Revue de météorologie maritime de Météo-France, 29, 23–41.

Bravard J.P. (1998) – Le temps et l'espace dans les systèmes fluviaux, deux dimensions spécifiques de l'approche géomorphologique. Annales de géographie, 599 3–15. DOI : 10.3406/geo.1998.20830

Brierley G.J., Fryirs K.A. (2005) – Geomorphology and river management. Applications of the river styles framework. Blackwell Publishing, Oxford, 398 p. DOI : 10.1002/9780470751367

Bronk Ramsey C. (2009) – Bayesian analysis of radiocarbon dates. Radiocarbon, 51 (1), 337–360. DOI : 10.1017/S0033822200033865

Buffington J.M., Montgomery D.R. (1997) – A systematic analysis of eight decades of incipient motion studies, with special reference to gravel-bedded rivers. Water Resources Research, 33, 1993–2029. DOI : 10.1029/96WR03190

Caloiero D., Mercury T. (1980) – Le alluvioni in Calabria dal 1921 al 1970. CNR-IRPI, Geodata N. 7, 161 p.

Calvet M., Lemartinel B. (2002) – Précipitations exceptionnelles et crues-éclair dans l'aire pyrénéo-méditerranéenne. Géomorphologie : relief, processus, environnement, 8 (1), 35–49. DOI : 10.3406/morfo.2002.1126

Carrega P., Michelot N. (2021) – Une catastrophe hors norme d'origine météorologique le 2 octobre 2020 dans les montagnes des Alpes-Maritimes. Physio-Géo, 16. DOI : 10.4000/physio-geo.12370

Cat Berro D., Mercalli L. (2018) – Le alluvioni di inizio novembre 1968 nel Biellese e nel Monferrato. Nimbus, 80.

Caumont O., Mandement M., Bouttier F., Eeckman J., Lebeaupin Brossier C., Lovat A., Nuissier O., Laurantin O. (2021) – The heavy precipitation event of 14-15 October 2018 in the Aude catchment. A meteorological study based on operational numerical weather prediction systems and standard and personal observations. Natural Hazards and Earth System Sciences, 21, 1135–1157. DOI : 10.5194/nhess-21-1135-2021

Chardon M. (1990) – Les catastrophes naturelles de l'été 1987 en Lombardie. Crues, inondations, écroulement de Val Pola. Revue de géographie alpine, 78 (1-3), 1990, 59–87. DOI : 10.3406/rga.1990.2767

Chorley R.J. (1969) – The drainage basin as the fundamental geomorphic unit. In Chorley R.J. (Ed.) Introduction to Physical Hydrology. Routledge, London, 77–99. DOI : 10.4324/9780429273339

Chorley R.J., Schumm S.A., Sugden D.E. (1984) – Geomorphology. Methuen, London, New York, 607 p. DOI : 10.1017/S0016756800035573

Delplace G., Viers J., Schreck E., Oliva P., Behra P. (2022) – Pedo-geochemical background and sediment contamination of metal(loid)s in the old mining-district of Salsigne (Orbiel valley, France). Chemosphere, 287, 132111. DOI : 10.1016/j.chemosphere.2021.132111

Dubreuil V. (2022) – Le changement climatique en France illustré par la classification de Köppen. La Météorologie, 116, 37–47. DOI : 10.37053/lameteorologie-2022-0012

Folk R.L., Ward, W.C. (1957) – Brazos River Bar. A study in the significance of grain-size parameters. Journal of Sedimentary Petrology, 27, 3–26. DOI : 10.1306/74D70646-2B21-11D7-8648000102C1865D

Fort M., Arnaud-Fassetta G., Beltrando G., Plet A., André G., Mering C. (2001) – Impacts hydromorphologiques des fortes précipitations des 12-13 novembre 1999 sur la retombée méridionale de la Montagne Noire. l'exemple de l'Argent Double (Aude). In Médi-Terra (éd.) Au chevet d'une catastrophe. Les inondations des 12 et

13 novembre 1999 dans le Sud de la France. Actes du colloque de Perpignan, 26-28 juin 2000, Presses Universitaires de Perpignan, Perpignan, 41–52.

Fort M., Bétard F., Arnaud-Fassetta G. (2025) – Géomorphologie dynamique et environnement. Processus et relais dans les bassins versants. Armand Colin, Paris, 2nd edition, 352 p. DOI : 10.3917/arco.fort.2015.01

Gaume E., Bain V., Bernardara P., Newinger O., Barbuc M., Bateman A., Blaškovičová L., Blöschl G., Borga M., Dumitrescu A., Daliakopoulos I., Garcia J., Irimescu A., Kohnova S., Koutroulis A., Marchi L., Matreata S., Medina V., Preciso E., Sempere-Torres D, Stancalie G., Szolgay J., Tsanis I., Velascom D., Viglione A. (2009) – A compilation of data on European flash floods. Journal of Hydrology, 367 (1-2), 70–78. DOI :10.1016/j.jhydrol.2008.12.028

Guigo M. (1973) – Pluie et crue des 7 et 8 octobre 1970 dans la région génoise. Méditerranée – Revue géographique des pays méditerranéens (Journal of Mediterranean geography), 1, 55–80. DOI : 10.3406/medit.1973.1467

Hadžič E., Aronica G.T., Milišić H., Šuvalija S., Ključanin S., Šarić A., Sulejmanović S., Mujić F. (2022) – Development of flood hazard and risk maps in Bosnia and Herzegovina, key study of the Zujevina River. Coupled Systems Mechanics, 11 (6), 505–524. DOI : 10.12989/csm.2022.11.6.505

He K., Yang Q., Shen X., Dimitriou E., Mentzafou A., Papadaki C., Stoumboudi S., Anagnostou E.N. (2024) – Brief communication. Storm Daniel flood impact in Greece in 2023. mapping crop and livestock exposure from synthetic-aperture radar (SAR). Natural Hazards and Earth System Sciences, 24, 2375–2382. DOI: 10.5194/nhess-24-2375-2024

Hocini N., Payrastre O., Bourgin F., Gaume É., Davy P., Lague D., Poinsignon L., Pons F. (2020) – Performance of automated flood inundation mapping methods in a context of flash floods. A comparison of three methods based either on the Height Above Nearest Drainage (HAND) concept, or on 1D/2D shallow water equations. Hydrology and Earth System Sciences, Discussions, 23 p. DOI : 10.5194/hess-2020-597

Knighton D. (1998) – Fluvial forms and processes. A new perspective. Arnold, London, 383 p. DOI : 10.4324/9780203784662

Kreitz M., Calas C., Baille S. (2020) – Inondations de l'Aude du 15 octobre 2018. analyse météorologique, conséquences hydrologiques et prévisibilité. La Météorologie, 110, 46–64. DOI : 10.37053/lameteorologie-2020-0067

Lajournade C., Beaufrère C., Lalanne-Berdouticq G., Martignac F. (1998) – La catastrophe de Biescas du 7 août 1996 ; analyse de la crue torrentielle du rio Aras dans les Pyrénées aragonaises (Espagne). La Houille Blanche, 5-6, 128–137. DOI: 10.1051/lhb/1998073

Lang M., Arnaud P., Carreau J., Deaux N., Dezileau L., Garavaglia F., Latapie A., Neppel L., Paquet E., Renard B. Soubeyroux J.M., Terrier B., Veysseire J.M., Aubert Y., Auffray A., Borchi F., Bernardara P., Carre J.C., Chambon D., Cipriani T., Delgado J.L., Doumenc H., Fantin R., Jourdain S., Kochanek K., Paquier A., Sauquet É., Tramblay Y. (2014) – Résultats du projet ExtraFlo (ANR 2009-2013) sur l'estimation des pluies et crues extrêmes. La Houille Blanche, 2, 5–13. DOI : 10.1051/lhb/2014010

Larguier G. (2018) – Catastrophe naturelle et effets à long terme. l'inondation de 1316 et le changement de lit de l'Aude. Bulletin de la Société d'Études Scientifiques de l'Aude, CXVIII, 79–96.

Larive J., Marshall A. (2022) – D'entre deux eaux. Factory-Résidence 1+2, auto-édition, 20 p.

Lebouc L., Payrastre O. (2017) – Reconstitution et analyse des débits de pointe des crues du 3 octobre 2015 dans les Alpes Maritimes. Convention DGPR-Ifsttar 2016 n°2201030666 du 14 octobre 2016 – Action 14. Institut Français des Sciences et Technologies des Transports, de l'Aménagement et des Réseaux. Unpublished report, 18 p.

Lebouc L., Payrastre O. (2020) – Reconstitution des débits de pointe des crues des 23-24 novembre et 1er décembre 2019 dans les départements du Var et les Alpes-Maritimes. Institut Français des Sciences et Technologies des Transports, de l'Aménagement et des Réseaux. Unpublished report, 13 p.

Lebouc L., Payrastre O., Bourgin F. (2019a) – Reconstitution des débits de pointe des crues du 9 août 2018 dans les bassins de l'Ardèche et la Cèze. Convention DGPR-Ifsttar 2018 n°2201132931 du 22 Mai 2018 – Action 7 appui au SCHAPI. Institut Français des Sciences et Technologies des Transports, de l'Aménagement et des Réseaux. Unpublished report, 13 p.

Lebouc L., Payrastre O., Bourgin F (2019b) – Reconstitution des débits de pointe des crues du 15 octobre 2018 dans le bassin de l'Aude. Convention DGPR-Ifsttar 2018 n°2201132931 du 22 mai 2018 – Action 7 appui au SCHAPI. Institut Français des Sciences et Technologies des Transports, de l'Aménagement et des Réseaux. Unpublished report, 14 p.

Le Roy Ladurie E. (1967) – Histoire du climat depuis l'an mil. Flammarion, Paris, 376 p.

Liébault F., Melun G., Piton G., Chapuis M., Passy P., Tacon, S. (2024) – Channel change during catastrophic flood: Example of storm Alex in the Vésubie and Roya valleys. Geomorphology, 446, 109008. DOI: 10.1016/j-geomorph.2023.109008.

Llasat M.C. (2004) – La vulnérabilité en Catalogne et la perception sociale. La Houille Blanche, 90 (6), 71–75. DOI : 10.1051/lhb.200406009

Lorenzo-Lacruz J., Amengual A., Garcia C., Morán-Tejeda E., Homar V., Maimó-Far A., Hermoso A., Ramis C., Romero R. (2019) – Hydro-meteorological reconstruction and geomorphological impact assessment of the October 2018 catastrophic flash flood at Sant Llorenç, Mallorca (Spain). Natural Hazards and Earth System Sciences, 19, 2597–2617. DOI : 10.5194/nhess-19-2597-2019

Luino F. (1999) – The flood and landslide event of November 4-6 1994 in Piedmont region (Northwestern Italy). Causes and related effects in Tanaro valley. Physics and Chemistry of the Earth, Part A. Solid Earth and Geodesy, 24 (2), 123–129. DOI : 10.1016/S1464-1895(99)00007-1

Magnin F., Martin S., Ollivier V., Sirdeys N. (2024) – What do Lateglacial and Holocene land snail communities tell us about the palaeoenvironments of Mediterranean France? Boreas. DOI : 10.1111/bor.12681

Malguzzi P., Grossi G., Buzzi A., Ranzi R., Buizza R. (2006) – The 1966 "century" flood in Italy. A meteorological and hydrological revisitation. Journal of Geophysical Research, 111, D24106. DOI : 10.1029/2006JD007111

Mandement M., Caumont O. (2021) – A numerical study to investigate the roles of former Hurricane Leslie, orography and evaporative cooling in the 2018 Aude heavy-precipitation event.

Weather and Climate Dynamics, 2, 795–818. DOI : 10.5194/wcd-2-795-2021

Menad W., Douvinet J., Beltrando G., Arnaud-Fassetta G. (2012) – Évaluer l'influence de l'urbanisation face à un aléa météorologique remarquable. les inondations des 9-10 novembre 2001 à Bab-el-Oued (Alger, Algérie). Géomorphologie : relief, processus, environnement, 18 (3), 337–350. DOI :10.4000/geomorphologie.9954

Modica Scala G. (1969) – La grande alluvione. Edizione Voce Libera Di Modica. Tipolito Sgandurra, Siracusa, 269 p.

Molina J.J.C. (1976) – Genesis de las inundaciones de octubre de 1973 en el Sureste de la peninsula iberica. Cuadernos de Geografía, 4, 149–166.

Normand J.C.L., Heggy E. (2024) – Assessing flash flood erosion following storm Daniel in Libya. Nature Communications, 15, 6493. DOI : 10.1038/s41467-024-49699-8

Ortolano F., Spizuoco A. (2009) – Alluvione des messinese del 1 ottobre 2009. La colata fangoso-detritica des Torrente Racinazzo che ha devastato Scaletta Zanclea Marina (ME). Unpublished report, 19 p.

Pacini A. (2023) – Le alluvioni del 1965. Monografie, supplemento online Anno IV n. 2/2023 della rivista Il Vigile del Fuoco. Editoriale Idea Srl, Roma, 19 p.

Pardé M. (1930a) – La crue catastrophique de mars 1930 dans le Sud-Ouest de la France. Revue de géographie alpine, 18 (2), 343–393. DOI : 10.3406/rga.1930.4534

Pardé M. (1930b) – Les inondations du bassin de la Garonne et du Languedoc en mars 1930. Les études rhodaniennes, 6 (2), 135–148. DOI : 10.3406/geoca.1930.6314

Pardé M. (1933a) – Le régime de l'Aude. Revue géographique des Pyrénées et du Sud-Ouest, 4 (1), 5–29. DOI : 10.3406/rgpso.1933.4084

Pardé M. (1933b) – Les crues de décembre 1932 dans le Languedoc et le Roussillon. Revue géographique des Pyrénées et du Sud-Ouest, 4 (4), 499–512. DOI : 10.3406/rgpso.1933.4113

Pardé M. (1934a) – Crues méditerranéennes en septembre et octobre 1933. Revue géographique des Pyrénées et du Sud-Ouest, 5 (3), 328–336. DOI : 10.3406/rgpso.1934.4152

Pardé M. (1934b) – Intempéries méditerranéennes récentes en France. Revue de géographie alpine, 22 (3), 675–703. DOI : 10.3406/rga.1934.5116

Pardé M. (1941) – La formidable crue d'octobre 1940 dans les Pyrénées-Orientales. Revue géographique des Pyrénées et du Sud-Ouest, 12 (3), 237–279. DOI : 10.3406/rgpso.1941.4493

Pardé M. (1963) – Les crues cévenoles catastrophiques de septembre-octobre 1958. Annales de Géographie, 72 (392), 472–477. DOI : 10.3406/geo.1963.16473

Payrastre (2015) – Estimation des débits de pointe des crues de l'automne 2014 dans le Gard et l'Hérault. Convention DGPR-Ifsttar 2016 2014 n°2101388232 du 10 septembre 2014. Institut Français des Sciences et Technologies des Transports, de l'Aménagement et des Réseaux. Unpublished report, 27 p.

Payrastre O., Gaume É., Andrieu H. (2006) – Apport du recueil de données historiques pour l'étude des crues extrêmes de petits cours d'eau. Étude du cas de quatre bassins versants affluents de l'Aude. La Houille Blanche, 6, 1–7. DOI : 10.1051/lhb.2006105

Payrastre O., Naulin J.P., Nguyen C.C., Gaume É. (2012) – Analyse hydrologique des crues de juin 2010 dans le Var. Institut Français des Sciences et Technologies des Transports, de l'Aménagement et des Réseaux. Unpublished report, 33 p.

Payrastre O., Bonnifait L., Le Boursicaud R., Gaume É., Gasset R., Busseuil G. (2014) – Estimation des débits des crues de juin 2013 dans les Pyrénées. Institut Français des Sciences et Technologies des Transports, de l'Aménagement et des Réseaux. Unpublished report, 15 p.

Payrastre O., Nicolle P. (2021) – Estimation des débits de pointe atteints par les petits cours d'eau des Alpes Maritimes lors de la tempête Alex, le 2 octobre 2020. Action 8.2. Institut Français des Sciences et Technologies des Transports, de l'Aménagement et des Réseaux. Unpublished report, 18 p.

Pech P. (1990) – Les crues du 7 août 1978 dans l'Ossola. Revue de géographie alpine, 78 (1-3), 89–101. DOI : 10.3406/rga.1990.2768

Pettijohn F.J., Potter P.E. (1964) – Atlas and glossary of primary sedimentary structures. Springer-Verlag, Berlin, 370 p. DOI : 10.1180/minmag.1966.035.274.15

Pierson T.C. (2005) – Hyperconcentrated flow — transitional process between water flow and debris flow. In Jakob M., Hungr O. (Eds.) Debris-flow Hazards and Related Phenomena. Praxis, Springer, Berlin, Heidelberg, 159–202.

Pinna S., Grava M. (2016) – Le piogge alluvionali dell'ottobre 1951 in Sardegna. Considerazioni climatologiche e rappresentazioni cartografiche. Bollettino della Associazione italiana di cartografia, 157, 72–81. DOI : 10.13137/2282-572X/14030

Quiniou M., Piton G. (2022) – Embâcles. concilier gestion des risques et qualité des milieux. Guide de diagnostic et de recommandations. Rapport de synthèse, ISL, INRAE, 135 p.

Regione Piemonte (1994) – Primo rapporto sull'evento alluvionale verificatosi in Piemonte il 4-6 novembre 1994. Unpublished report, 74 p.

Reimer P.J., Austin W.E.N., Bard E., Bayliss A., Blackwell P.G., Bronk Ramsey C., Butzin M., Cheng H., Edwards R.L., Friedrich M., Grootes P.M., Guilderson T.P., Hajdas I., Heaton T.J., Hogg A.G., Hughen K.A., Kromer B., Manning S.W., Muscheler R., Palmer J.G., Pearson C., van der Plicht J., Reimer R.W., Richards D.A., Scott E.M., Southon J.R., Turney C.S.M., Wacker L., Adolph F., Büntgen U., Capano M., Fahrni S.M., Fogtmann-Schulz A., Friedrich R., Köhler P., Kudsk S., Miyake F., Olsen J., Reinig F., Sakamoto M., Sookdeo A., Talamo S. (2020) – The INTCAL20 Northern Hemisphere Radiocarbon age calibration curve (0-55 cal kBP). Radiocarbon, 62 (4), 725–757. DOI :10.1017/RDC.2020.41

Ricard D., Ducrocq V., Auger L. (2012) – A climatology of the mesoscale environment associated with heavily precipitating events over a northwestern Mediterranean area. Journal of Applied Meteorology and Climatology, 51, 468–488. DOI : 10.1175/JAMC-D-11-017.1

Rinaldi M., Amponsah W., Benvenuti M., Borga M., Comiti F., Lucía A., Marchi L., Nardi L., Righini M., Surian N. (2016) – An integrated approach for investigating geomorphic response to extreme events. Methodological framework and application to the October 2011 flood in the Magra River catchment, Italy. Earth Surface Processes and Landforms, 41, 835–846. DOI : 10.1002/esp.3902

Rode S. (2022) – Recomposer les territoires pour les adapter aux effets de la crise climatique. l'après-catastrophe comme opportunité pour une meilleure habitabilité ? Sud-Ouest européen, 54. DOI : 10.4000/12g5d

Rosso R. (2017) – Bombe d'acqua. Alluvioni d'Italia dall'Unità al terzo millennio. Marsilio, Venezzia, 280 p.

Rousseau T. (1875) – Étude générale sur le régime des cours d'eau du département de l'Aude. Imprimerie Sirven, Toulouse, 86 p.

Schumm S.A. (1973) – Geomorphic thresholds and complex response of drainage systems. In Morisawa M. (Ed.) Fluvial Geomorphology. Binghamton, New York, 299–310.

Schumm S.A (1977) – The fluvial system. Wiley, New-York, 338 p.

Service de Restauration des Terrains en Montagne des Pyrénées Orientales et de l'Aude (2017) – Étude du risque torrentiel en bassin versant domanial. Argent Double. Communes de Caunes-Minervois, Citou et Lespinassière. Unpublished report, 313 p.

Sklar L.S., Dietrich W.E. (2001) – Sediment and rock strength control on river incision into bedrock. Geology, 29 (12), 1087–1090. DOI : 10.1130/0091-7613(2001)029< 1087.SARSCO> 2.0.CO;2

Soutadé G. (1993) – Les inondations d'octobre 1940 dans les Pyrénées Orientales. Conseil Général, Direction des Archives départementales, Perpignan, 351 p.

Speis P.D., Andreadakis E., Diakakis M., Daidassi E., Sarigiannis G. (2019) – Psychosocial vulnerability and demographic characteristics in extreme flash floods. The case of Mandra 2017 flood in Greece. International Journal of Disaster Risk Reduction, 41, 101285. DOI : 10.1016/j.ijdrr.2019.101285

Stuckmann G. (1970) – Les effets morphologiques des inondations de septembre-octobre 1969 dans le centre et le sud de la Tunisie. UNESCO, Paris, 35 p.

Surell A. (1841) – Études sur les torrents des Hautes-Alpes. Carilian-Gœury et Vor Dalmont (Eds.), 284 p.

Tricart J. (1958) – La crue de la mi-juin 1957 sur le Guil, l'Ubaye et la Cerveyrette. Revue de géographie alpine, 46 (4), 565–627. DOI : 10.3406/rga.1958.1846

Tricart J. (1962) – Les discontinuités dans les phénomènes d'érosion. Publications of the International Association of Hydrological Sciences, 59, 233–243.

Trimble S.W. (1983) – A sediment budget for Coon Creek basin in the Driftless Area, Wisconsin, 1853-1977. American Journal of Science, 283, 454–474. DOI : 10.2475/ajs.283.5.454

Valle C. (1953) – Le alluvioni del 1951 in Italia e le loro cause. Bollettino Della Società Geografica Italiana, 135–141.

Verdeil P. (1999) – Les crues de l'Aude au cours des temps. Spele Aude, 8, 34–45.

Vinet F. (2003) – Crues et inondations dans la France méditerranéenne. Les crues torrentielles des 12 et 13 novembre 1999 (Aude, Tarn, Pyrénées-Orientales, Hérault). Éditions du Temps, Nantes, 224 p.

Wentworth C.K. (1922) – A scale of grade and class terms for clastic sediments. Journal of Geology, 30, 377–392. DOI : 10.1086/622910

Zorn M., Zrc Sazu M. (2014) – Obsežne poplave v Bosni in Hercegovini, Srbiji ter na Hrvaškem maja 2014. Geografki obzornik, 61, 4, 22–25.

Version française abrégée

Chaque année, en moyenne, entre 3 et 6 événements fortement précipitants (> 150 mm/24 h) se produisent autour de la mer Méditerranée, avec une concentration plus forte dans la partie nord-ouest (fig. 1). L'article propose l'étude du dernier en date qui s'est produit dans le département de l'Aude les 14-15 oct. 2018 (15 décès ; 256 M€ de dégâts ; gros impacts hydro-bio-morphologiques). Les études n'ont pas réussi à parvenir à un consensus sur la fréquence de retour de l'événement, les estimations variant considérablement selon les auteurs (de 100 ans à 2000 ans). Cet article va démontrer, données géomorphologiques et stratigraphiques à l'appui, que l'événement hydrométéorologique des 14-15 oct. 2018 a une période de retour de 204-378 ans. L'objectif de l'article est de formaliser un retour d'expérience sur ce qui s'est produit dans le bassin-versant de l'Aude les 14-15 oct. 2018 selon une approche systémique, quantifier les impacts de la crue par l'établissement d'un budget sédimentaire et mettre en avant le rôle de la forêt riveraine dans le contrôle des flux de crue dans la plaine alluviale.

Le fleuve Aude (225,6 km de long ; ordre de Strahler. 7) prend sa source dans le massif du Carlit à une altitude de 2172 m, et se jette dans la mer Méditerranée par le Grau de Vendres (fig. 3). Son lit, dont la largeur moyenne à pleins bords varie entre 21 et 58 m, s'élargit progressivement vers l'aval. Le bassin-versant (6074 km^2) est situé entre la Montagne Noire au nord et les Pyrénées et les Corbières au sud. Le fleuve draine le bassin aquitain (Atlantique) à l'ouest et le bassin languedocien (Méditerranée) à l'est. À partir de Carcassonne, le fleuve Aude est soutenu par les apports de puissants affluents (w_{PB}. 2225-556 W/m^2). Leur débit moyen dépasse rarement quelques mètres cubes et la plupart d'entre eux sont à sec pendant plusieurs mois (été, automne). Cependant, ils peuvent également produire des crues éclair d'une rare intensité, entraînant des débits de plusieurs centaines de mètres cubes en seulement quelques heures. Les forêts riveraines posent des défis importants en matière de gestion des bois morts alors que les villages situés le long des affluents sont confrontés à un risque inondation élevé. L'un des principaux gestionnaires du bassin versant de l'Aude est le SMMAR (Syndicat mixte des milieux aquatiques et des rivières), créé en 2002 pour répondre aux besoins d'une gestion coordonnée de la ressource en eau et de la prévention des inondations à l'échelle du bassin-versant, avec la restauration des lits torrentiels comme objectif spécifique.

À la suite de l'événement hydrométéorologique des 14-15 oct. 2018, 18 missions de terrain couplées au traitement d'images et à la littérature existante nous ont permis de produire une analyse à deux niveaux scalaires. À l'échelle du bassin-versant de l'Aude, nous avons intégré les informations provenant d'une synthèse bibliographique, en plus de nos propres observations de terrain, pour proposer une lecture systémique du déroulé de la crue d'oct. 2018 et de ses impacts. À l'échelle du sous-bassin-versant du Rieu Sec (affluent de l'Orbiel), situé dans la zone qui a reçu les plus forts cumuls de précipitations, nous avons reconstitué les conditions physiques (morphométrie, hydraulique, érosion) du bassin permettant de comprendre l'incidence des forts abats d'eau sur la morphogenèse du fond de vallée. Un budget sédimentaire a été produit à l'échelle du bassin-versant en comparant le MNT du 5 mai 2017 avec le MNT dérivé d'un relevé LiDAR du 29 déc. 2019. Nous avons constamment affiné les valeurs obtenues à partir du traitement d'images grâce à

nos observations sur le terrain et notre compréhension des processus dans le bassin-versant. La comparaison des photographies aériennes de l'IGN prises le 4 juil. 2018 avec celles prises le 18 juil. 2020 a permis de quantifier l'impact de la crue des 14-15 oct. 2018 sur la ripisylve (surfaces d'arbres arrachés ; cartographie des bois flottés). Enfin, une série de coupes stratigraphiques naturelles a été étudiée (sédimentologie, malacologie, datation radiocarbone) le long de la bande active du Rieu Sec afin de reconstituer l'histoire des crues dans le bassin-versant et déterminer l'intervalle de récurrence de la crue de 2018.

Les résultats de l'étude sont les suivants. (*i*) À l'échelle du bassin-versant de l'Aude, l'analyse systémique de la crue d'oct. 2018 a permis d'identifier trois groupes de facteurs (prédisposants, déclenchants, aggravants/atténuants) ayant abouti à la catastrophe hydrologique. La crue a produit une morphogenèse extrême dans les bassins versants touchés. Les contributions des affluents de rive gauche de l'Aude ont clairement joué un rôle majeur dans le déroulement de la crue. (*ii*) Les impacts géomorphologiques ont été conséquents dans le bassin-versant du Rieu Sec, un affluent de rive droite de l'Orbiel. La réponse hydro-morphologique est analysée spécifiquement dans les trois zones distinctes (A = amont ; B = médiane ; C = aval) de ce bassin-versant. L'étendue disproportionnée de la zone B (64,6 % du bassin-versant) souligne l'importance des alluvions purgées dans le fond de vallée, se manifestant par l'élargissement et l'approfondissement de la bande active du Rieu Sec. La quantification du budget sédimentaire corrobore ces observations de terrain (fig. 12). Dans l'ensemble, la crue a été érosive (-386 259 m^3, soit -11 599 m^3/km^2 en moins de 24 h) à l'échelle du bassin-versant. La zone B a été la plus touchée par l'érosion, avec un total de -305 618 m^3 (79 % de l'érosion totale), plus que la zone A en amont (-105 824 m^3). Tous les sous-systèmes (versants et chenaux) ont érodé plus qu'ils n'ont stocké, sauf pour la zone C, faiblement pentue, qui a enregistré un surplus de 25 183 m^3. L'impact de la crue sur la forêt riveraine a été analysé dans les fonds de vallée (Rieu Sec et affluents). Les surfaces d'arbres arrachés par la crue représentent 8,9 % (soit 13,855 ha) de la ripisylve présente dans les fonds de vallée avant la crue (fig. 12 C-F). La quasi-totalité (96,8 %) des arbres a été arrachée dans la plaine alluviale du Rieu Sec, mais seulement 3,2 % dans le lit des affluents. Le peuplier noir (*Populus nigra*) s'est avéré être nettement mieux adapté que l'aulne commun (*Alnus glutinosa*) pour résister aux flux de crue en raison de son système racinaire profond. La quantité de troncs d'arbres arrachés par la crue a été exceptionnelle (6235-15 588 m^3). Pourtant, le volume de bois flotté qui a atteint l'Orbiel est négligeable. Cela s'explique par la régulation du transport de bois flotté, principalement par des processus naturels et accentuée en aval par les haies de platanes orientées perpendiculairement à l'écoulement. Enfin, l'étude de quatre coupes stratigraphiques (fig. 14D) révèle une alternance de phases de creusement et de remblaiement du fond de vallée, lui-même marqué par la succession d'unités sédimentaires soit grossières (chenaux actifs de haute énergie) soit fines (marge des chenaux actifs ou plaine d'inondation proximale). Des jalons chronologiques établis grâce à la datation radiocarbone ont permis de reconstituer le rythme morpho-sédimentaire du fond de vallée (fig. 15). Ils attestent que le précédent événement hydrométéorologique (avant celui de 2018) responsable de la purge sédimentaire du fond de vallée s'est produit avant 1619-1793, avec une probabilité de 61 % qu'il ait eu lieu avant 1701-1793. La crue d'octobre 2018 dans le bassin du Rieu Sec a donc un intervalle de récurrence de 204-378 ans.

Plusieurs éléments sont discutés, à commencer par ce qui constitue les preuves d'un événement de crue extraordinaire (étendue spatiale ; déplacement géographique vers l'ouest des pluies extrêmes ; volume de précipitations ; débits de rivière ; réponse hydro-morphologique ; budget sédimentaire ; taux de dégradation spécifique ; impact sur la forêt riveraine ; transport de bois flotté ; intervalle de récurrence de la crue). La proposition d'un modèle fonctionnel des rivières à haute énergie est également discutée, avec confirmation de l'importance des événements hydrométéorologiques extrêmes dans la morphogénèse des fonds de vallée. La grande variabilité des intervalles de récurrence des crues dans le bassin-versant de l'Aude est aussi discutée, avant la question du changement climatique et de ses impacts sur l'hydromorphologie régionale. Le défi pour l'avenir réside dans l'amélioration des prévisions de crue et la diffusion effective de ces prévisions.